UNIVERSIDADE FEDERAL DO RIO GRANDE DO SUL
INSTITUTO DE GEOCIÊNCIAS
PROGRAMA DE PÓS-GRADUAÇÃO EM GEOCIÊNCIAS

ANÁLISE PETROLÓGICA E SÍSMICA DOS CONTROLES SOBRE A DEPOSIÇÃO DOS SISTEMAS ARENOSOS DE ÁGUAS PROFUNDAS DA BACIA DE CAMPOS

Marcos Roberto Fetter Lopes

ORIENTADORES

Prof. Dr. Luiz Fernando De Ros – UFRGS-IG

Dr. Carlos Henrique Lima Bruhn – Petrobras E&P

BANCA EXAMINADORA

Prof. Dr. Marcus Vinicius Dorneles Remus - UFRGS-IG

Dr. José Antonio Cupertino – Petrobras E&P

Dr. Guilherme Pederneiras Raja Gabaglia – Universidade Petrobras

Tese de Doutorado apresentada como requisito parcial para a obtenção do Título de Doutor em Ciências.

Porto Alegre – 2007

Lopes, Marcos Roberto Fetter
Análise petrológica e sísmica dos controles sobre a deposição dos sistemas arenosos de águas profundas da Bacia de Campos. / Marcos Roberto Fetter Lopes. – Porto Alegre : IGEO/UFRGS, 2007.
[148 f.]. il.

Tese (Doutorado) - Universidade Federal do Rio Grande do Sul. Instituto de Geociências. Programa de Pós-Graduação em Geociências, Porto Alegre, RS - BR, 2007.

1. Estratigrafia. 2. Sedimentologia. 3. Proveniência. 4. Reservatórios. 5. Arenitos. 6. Bacia de Campos. I. Título.

_____

Catalogação na Publicação
Biblioteca do Instituto de Geociências - UFRGS
Renata Cristina Grun CRB 10/1113

SUMÁRIO

Estrutura da Tese

Esta tese foi organizada na forma de três artigos, presentemente submetidos para publicação em periódicos internacionais conceituados, que serão, daqui para frente, designados pelos respectivos algarismos romanos:

I. An active divergent margin: petrographic and seismic evidence on the geodinamically-controlled deposition of Campos Basin giant turbidite reservoirs, southeastern Brazil.

Artigo submetido à revista Geology, no qual é discutido o suprimento de areia em águas profundas em margens continentais divergentes e é definido o controle geodinâmico da deposição dos sistemas siliciclásticos arenosos de águas profundas durante o Cretáceo Superior na Bacia de Campos.

II. The role of basement tectonic reactivation on the structural evolution of Campos Basin, offshore Brazil: evidence from 3D seismic analysis and section restoration.

Artigo submetido à revista Marine and Petroleum Geology, no qual é discutida a evolução geodinâmica da Bacia de Campos, com ênfase no papel relevante da tectônica de embasamento, previamente considerada pouco importante.

III. Petrographic and seismic evidence for the depositional setting of giant turbidite reservoirs and the paleogeographic evolution of Campos Basin, offshore Brazil.

Artigo submetido à revista Earth Science Reviews, no qual são apresentados os resultados da petrografia quantitativa dos principais sistemas siliciclásticos arenosos de águas profundas da Bacia de Campos, e da análise estrutural de padrões envolvendo reativação do embasamento. Com base nestes dados são estabelecidos os controles da deposição destes sistemas, através da reconstrução paleogeográfica do sistema fonte-bacia durante a fase de margem continental divergente, desde o Albiano até o Mioceno.

Introdução

O objetivo deste projeto de doutorado foi a definição dos controles que determinaram a deposição dos sistemas arenosos de águas profundas formados desde o Albiano até o Mioceno, durante a fase de margem divergente da Bacia de Campos, na costa sudeste do Brasil (ver Figuras 1 e 2 do Artigo III). Os arenitos de águas profundas, designados genericamente como turbiditos, em função de seu processo deposicional a partir de correntes de turbidez, apresentam grande relevância econômica por constituírem excelentes reservatórios de petróleo. Os turbiditos da Bacia de Campos, especificamente, comportam cerca de 80% das reservas e da produção brasileiras de hidrocarbonetos (Bruhn et al., 2003) e estão diretamente relacionados com a recentemente atingida auto-suficiência de petróleo do Brasil.

As margens continentais divergentes, contexto geológico geral no qual se insere a Bacia de Campos, são ainda encaradas como ambientes tectonicamente passivos, cuja evolução geodinâmica do tipo recuo de escarpa se restringe a processos de epirogênese, subsidência térmica, erosão, sedimentação e ajustes isostáticos (Ollier, 1985; Weissel e Karner, 1989; Gilchrist e Summerfield, 1990; Beaumont et al., 2000). A deformação observada nas bacias sedimentares das margens divergentes tem sido em grande parte atribuída aos processos gravitacionais da tectônica salífera rasa (Cobbold e Szatmari, 1991). Com estas condições de contorno o registro estratigráfico destas *margens passivas* seria totalmente controlado pelas variações eustáticas do nível do mar, conforme o paradigma clássico da Estratigrafia de Seqüências (Vail et al., 1977), que têm sido junto à Sedimentologia (abordagem ES&S) as disciplinas mais utilizadas no estudo dos sistemas arenosos de águas profundas em todos os tipos de bacias sedimentares (Mutti et al., 2003; Catuneanu, 2006). Mesmo considerando os importantes avanços obtidos na compreensão dos ambientes sedimentares de águas profundas da Bacia de Campos com base nestas disciplinas (Azambuja Filho, 1990; Bruhn, 1993; Peres, 1993; Scarton, 1993; Pereira, 1994; Souza Cruz, 1995; Souza Jr., 1997), importantes aspectos das condições genéticas desta sedimentação ainda não foram adequadamente esclarecidos. A abordagem convencional da estratigrafia de seqüências assume que o suprimento de areias para os sistemas de águas profundas durante a fase de margem divergente da Bacia de Campos tenha sido essencialmente relacionado com períodos de queda acentuada do nível do mar, com retrabalhamento sedimentar na plataforma continental, o que parece não ter ocorrido. Além disso, a evolução de uma margem continental passiva deveria corresponder a um gradual

rebaixamento do relevo, e a um aumento progressivo da maturidade composicional e textural dos turbiditos, o que também não se verifica, uma vez que expressivos sistemas turbidíticos arenosos caracterizados por imaturidade composicional e textural foram recorrentemente depositados na Bacia de Campos (Scarton, 1993; Bruhn e Walker, 1995; Caddah et al., 1998; Artigos I e III).

Mais recentemente, em trabalhos que seguem uma abordagem geodinâmica, foi sugerido que a sedimentação nas bacias da margem continental sudeste do Brasil, incluindo a Bacia de Campos, poderia ter sido controlada por reativações tectônicas do embasamento (Pereira, 1994; Lima, 1999; Cobbold et al., 2001; Lima, 2003; Artigos I e III), e pela passagem da margem sobre uma pluma do manto durante a transição Cretáceo-Terciário (Thomaz Filho et al., 2005; Zalán e Oliveira, 2005; Artigo III). Paralelamente, o soerguimento da margem continental sudeste do Brasil também vem sendo evidenciado por estudos de traços de fissão em apatitas (Gallagher e Brown, 1999; Saenz et al., 2003). Embora em linhas gerais tanto o rejuvenescimento tectônico do relevo quanto a atividade magmática e o soerguimento dinâmico causados pela pluma do manto sejam coerentes com a imaturidade dos sistemas arenosos de águas profundas, não foram apresentadas ainda evidências científicas sobre o sincronismo do tectonismo e da atividade da pluma com a formação dos vários sistemas turbidíticos da Bacia de Campos.

Nesta perspectiva, o presente projeto de pesquisa foi proposto para analisar as relações entre os principais eventos geodinâmicos e a deposição dos sistemas arenosos de águas profundas da Bacia de Campos. Para isso uma abordagem integrando petrografia sedimentar quantitativa e tectônica (PS&T), já utilizada com sucesso em bacias de margens convergentes e tectonicamente ativas (Valloni e Zuffa, 1984; Fontana et al., 1989; Critelli, 1993; Marchesini et al., 2000; Cibin et al., 2001), foi adaptada para a margem divergente da Bacia de Campos. A metodologia proposta corresponde a uma abordagem da evolução tectônica e paleogeográfica da Bacia de Campos através da integração, até agora não explorada na análise de margens divergentes, de três técnicas individualmente já bastante difundidas: (1) a petrografia quantitativa dos arenitos turbidíticos (Artigos I e III); (2) a análise estrutural de dados sísmicos, com ênfase na deformação produzida pela tectônica de embasamento (Artigos II e III); (3) a restauração seqüencial de seções geológicas (Artigo II). Com esta nova abordagem foi possível estabelecer um conjunto robusto de evidências que indicam uma alternância de controles distintos para o registro estratigráfico de águas profundas da Bacia de

Campos. Estes controles são estabelecidos pela evolução do peso relativo dos processos geodinâmicos, eustáticos e climáticos, cíclicos ou episódicos, durante a fase de margem divergente da bacia, desde o Albiano até o Mioceno (Artigo III).

Metodologia

Bioestratigrafia

A primeira demanda metodológica deste projeto foi a definição de um arcabouço cronogeológico padrão para todas as análises, uma vez que o tema central da pesquisa envolve a investigação da hipótese de sincronismo do processo de sedimentação em águas profundas com os processos geodinâmicos e eustáticos na Bacia de Campos. Este arcabouço se faz necessário não apenas para garantir a uniformidade das correlações entre eventos, mas também para verificar se a resolução temporal está adequada para as correlações estabelecidas.

Todas as datações citadas no presente trabalho estão baseadas no zoneamento de nanofósseis calcários estabelecido para as bacias da margem continental do Brasil por Antunes et al. (2004), com equivalência cronométrica absoluta baseada na Carta Estratigráfica Internacional da Comissão Internacional em Estratigrafia – ICS (http://www.stratigraphy.org/cheu.pdf; Gradstein et al., 2004). Para a fase de margem divergente da Bacia de Campos, o referido zoneamento bioestratigráfico corresponde a 18 biozonas no Período Cretáceo, entre as Idades Albiano e Maastrichtiano, com uma resolução em torno de 2,6 Ma, e a 35 biozonas na Era Cenozóica, entre os Períodos Paleogeno e Quaternário, o que equivale a uma resolução aproximada de 1,8 Ma. Cabe ressaltar que o nível de resolução temporal do arcabouço cronogeológico adotado mostrou-se adequado tanto para a datação da formação dos sistemas turbidíticos arenosos analisados na petrografia quantitativa (Artigos I e III), quanto para a interpretação dos eventos tectônicos indicados pela análise estrutural (Artigos II e III).

Petrografia Quantitativa

A contagem de pontos em lâminas delgadas foi a técnica utilizada no presente projeto para a análise petrográfica quantitativa dos arenitos de águas profundas da Bacia de Campos. A contagem foi feita através do método Gazzi-Dickinson (Gazzi, 1966; Dickinson, 1970; Ingersoll et al., 1984), conforme adaptações sugeridas por Zuffa (Zuffa, 1980; Zuffa, 1985; Zuffa, 1991). Esta metodologia foi escolhida pela sua praticidade e robustez de resultados já amplamente comprovados (Dickinson e Suczec, 1979; Dickinson et al., 1983; Dickinson, 1985; Zuffa, 1987; Dickinson, 1988; Zuffa et al., 1995; Zuffa et al., 2000).

A petrografia quantitativa foi aplicada a onze sistemas turbidíticos da fase de margem divergente da Bacia de Campos, com idades entre o Albiano e o Mioceno (ver

Figura 4 do Artigo III). Foram contados 300 pontos por lâmina em 117 lâminas delgadas correspondentes a 990 m de testemunhos dos sistemas turbidíticos estudados (ver Tabela 1 do Artigo III).

Os parâmetros petrográficos composicionais e texturais e os resultados brutos da contagem de pontos estão registrados nas planilhas em anexo (ver CD em anexo). Também estão discriminadas nas planilhas as totalizações composicionais para os principais diagramas ternários convencionalmente utilizados neste tipo de análise petrográfica (Figuras 5, 6 e 7 do Artigo III). Mesmo não sendo adequadas para análise quantitativa, foram descritas qualitativamente 4 lâminas delgadas de conglomerados do sistema turbidítico do Eoceno Médio (ver CD em anexo), por apresentarem um significado paleogeográfico importante (Artigo III).

Análise Estrutural de Dados Sísmicos

A utilização do método sísmico na análise de bacias sedimentares tem experimentado um grande crescimento nas últimas décadas em função dos progressos tecnológicos e da redução dos custos de aquisição e processamento dos dados sísmicos. Atualmente a maior parte das grandes províncias de hidrocarbonetos do mundo, como a Bacia de Campos, está coberta com sísmica 3D de boa qualidade, de modo que os dados sísmicos já são apontados como um novo marco tecnológico na evolução das Ciências da Terra (Cartwright e Huuse, 2005). Este potencial têm se evidenciado bastante nas áreas de Geologia Estrutural e Tectônica, uma vez que a visualização tridimensional e detalhada das feições estruturais em volumes sísmicos possibilita um entendimento dos sistemas esforço-deformação muitas vezes até melhor do que o que pode ser obtido pelos métodos tradicionais de análise estrutural através de estudo de afloramentos, mapeamento de superfície e sensoreamento remoto. No caso das bacias submersas nas margens continentais, o método sísmico constitui a única ferramenta disponível para o desenvolvimento de análises estruturais de detalhe.

Mais recentemente esta vantagem tecnológica tem sido ampliada pelo estudo de atributos sísmicos voltados especificamente para a interpretação estrutural. Trata-se dos chamados atributos sísmicos geométricos entre os quais se destacam a coerência, inverso da variância (Bahorich e Farmer, 1995), e os atributos obtidos pela aplicação da geometria diferencial aos volumes sísmicos, tais como o gradiente e a curvatura, respectivamente a primeira e a segunda derivadas da estrutura em um referencial tridimensional cartesiano (Chopra e Marfurt, 2006 e 2007).

A análise estrutural de dados sísmicos segue o mesmo fluxo de trabalho da análise estrutural convencional, com a classificação espacial e temporal da deformação quanto ao estilo estrutural, ao padrão cinemático e ao condicionamento dinâmico das estruturas (Davis e Reynolds, 1996). Neste trabalho foi desenvolvida uma análise estrutural de quatro volumes sísmicos regionais da Bacia de Campos. Foram identificadas nestes volumes seis áreas correspondentes aos principais sistemas esforço-deformação produzidos pela tectônica de embasamento. Nestas áreas a análise estrutural de detalhe foi sustentada pela consistência espacial de atributos sísmicos geométricos (Artigos II e III). Todos os volumes sísmicos utilizados, originalmente adquiridos com a coordenada vertical em tempo de trânsito, foram convertidos para profundidade com um único modelo regional de velocidades sísmicas calibradas com um conjunto de tabelas tempo-profundidade medidas em poços. Adicionalmente todos os horizontes sísmicos que fundamentaram o estudo da deformação foram ajustados a marcadores bioestratigráficos.

Através da análise estrutural foi possível caracterizar os principais eventos de deformação relacionados com a tectônica de embasamento durante a fase de margem continental divergente da Bacia de Campos (Artigos II e III). Previamente todos os trabalhos de análise estrutural da fase de margem divergente da bacia haviam sido voltados para o estudo da deformação associada à tectônica salífera (Cobbold e Szatmari, 1991; Demercian et al., 1993). Neste sentido os resultados do presente projeto constituem uma contribuição inédita sobre a Geologia Estrutural e a Tectônica da Bacia de Campos.

Restauração de Seções

A técnica de restauração ou balanceamento de seções geológicas vem sendo utilizada pelo menos desde o início do século passado nos estudos de Geologia Estrutural (Chamberlin, 1910). O princípio básico do método é a restauração de todas as unidades geológicas de uma seção deformada à sua geometria original, com preservação de comprimentos, áreas e volumes, de acordo com a hipótese de um estado plano de deformação. Deste modo, se a restauração não for possível, a estrutura expressa na seção não é viável, ou porque a interpretação não está correta, ou porque houve deformação significativa fora do plano da seção (Dahlstrom, 1969).

Durante muito tempo a restauração foi utilizada apenas para o estudo da deformação compressiva em faixas de cavalgamento, em seções definidas através de mapeamento de superfície (Chamberlin, 1910; Dahlstrom, 1969; Hossack, 1979). Com o uso crescente

do método sísmico, particularmente nas bacias de margem divergente, a restauração de seções passou a ser usada também para o estudo da tectônica distensional de embasamento e da tectônica salífera (Gibbs, 1983; Schultz-Ela, 1991; Rowan, 1993).

Uma importante característica do balanceamento de seções é o fato de que se a restauração é possível, além da definição de interpretações estruturais viáveis, também podem ser feitas inferências e estimativas sobre o processo de deformação (Chamberlin, 1910; Dahlstrom, 1969; Hossack, 1979; Gibbs, 1983; Nunns, 1991; Schultz-Ela, 1992). Particularmente, se as unidades restauradas estiverem ajustadas a um arcabouço geocronológico, podem ser computadas, além das medidas absolutas, as taxas temporais de deformação.

No presente projeto foram restauradas cinco seções extraídas de volumes sísmicos no domínio proximal-distensional da área deformada por tectônica salífera na Bacia de Campos (Artigo II). Todas as seções foram convertidas de tempo para profundidade com o mesmo modelo regional de velocidades citado anteriormente e são transversais a falhas normais lístricas de grande rejeito, que representam adequadamente o processo de tectônica salífera distencional que tem atuado durante a fase de margem divergente da Bacia de Campos. O objetivo deste trabalho foi estudar as taxas de deformação associadas ao processo de deslizamento gravitacional sobre o descolamento definido pelo sal Aptiano, para verificar o possível sincronismo entre a tectônica salífera e as reativações de embasamento (Artigo II).

A restauração de seções foi realizada com o aplicativo RECON desenvolvido pelo Grupo TecGraf da PUC-RJ (http://www.tecgraf.puc-rio.br) em convênio com a Petrobras. Foi adotado o procedimento padrão para restauração seqüencial de seções em zonas de tectônica salífera distencional, com ajuste isostático e descompactação (Schultz-Ela, 1991 e 1992; Rowan, 1993). Em todas as seções os falhamentos normais foram restaurados através do algoritmo de movimento sobre falha, com cisalhamento antitético no bloco baixo. Foi assumido o descolamento totalmente desacoplado no sal Aptiano, de modo que as sucessões pré-Aptianas da fase distencional não foram restauradas. Esta hipótese foi assumida para garantir o valor lógico de uma eventual correlação entre pulsos de tectônica salífera e reativações de embasamento (Artigo II).

Foram restaurados em cada seção nove horizontes da fase de margem divergente da Bacia de Campos, ajustados a marcadores bioestratigráficos com idades entre o Albiano e o Recente (Fundo do Mar). Os resultados geometricamente compatíveis em todas as etapas da restauração das cinco seções indicaram que, em linhas gerais, a hipótese de

descolamento constitui uma aproximação razoável para o processo de deformação do domínio distencional da tectônica salífera na Bacia de Campos (Artigo II).

Resultados Obtidos

A petrografia quantitativa pelo método Gazzi-Dickinson evidenciou a existência de duas classes de turbiditos durante a fase de margem divergente da Bacia de Campos, em função da maturidade petrográfica. Estas duas classes ficaram bem discriminadas no gráfico dos parâmetros médios tamanho de grão *versus* razão quartzo-feldspato – Q/F (Figura 1). Os turbiditos relativamente maturos apresentam granulometria areia fina e igual proporção de quartzo e feldspato (Q/F = 1). Os turbiditos imaturos são definidos pela granulometria areia média e pela maior proporção de feldspatos do que de quartzo (Q/F = 0.75).

Estas duas classes de turbiditos são caracterizadas também por padrões distintos de variação interna dos principais parâmetros petrográficos. Nos sistemas turbidíticos relativamente maturos os parâmetros petrográficos apresentam ou uma organização interna cíclica (Figuras 9 e 20 do Artigo III), ou uma tendência bem definida (Figura 22 do Artigo III). Por sua vez os sistemas imaturos, caracterizados por uma ausência de organização interna dos parâmetros petrográficos, mostram uma correlação direta entre a proporção de quartzo (Q/F) e o tamanho de grão (Figura 12 do Artigo III).

Outro resultado importante da petrografia quantitativa foi a definição das principais tendências dos parâmetros petrográficos médios dos sistemas turbidíticos da fase de margem divergente da Bacia de Campos: (1) a progressiva redução no conteúdo de micas foi interpretada como resultado do final da exumação da Faixa Orogênica Ribeira, do Proterozóico Superior, que aflora na margem da Bacia de Campos (Figura 30 do Artigo III); (2) o aumento significativo da contribuição de fragmentos vulcânicos na transição Cretáceo-Paleógeno foi interpretada como efeito da passagem da margem continental sobre a pluma do manto de Trindade (Figuras 26 e 39 do Artigo III); (3) a redução da proporção de quartzo (Q/F), e o aumento da granulometria foram interpretados como conseqüências do rejuvenescimento do relevo nas margens da bacia, associado com reativações tectônicas de embasamento e com o soerguimento dinâmico causado pela pluma do manto; (4) o aumento da contribuição de intraclastos foi interpretado como efeito conjunto do aumento da energia das correntes de fundo e de reconfigurações da fisiografia do talude continental; (5) o aumento da contribuição de glauconita implica na existência de uma plataforma continental bem desenvolvida e adicionalmente em mudanças nas trajetórias das correntes de fundo através desta plataforma; (6) a contribuição de carbonato intrabacial (CI) também está diretamente relacionada com a existência de uma plataforma rasa na bacia, neste sentido a

significativa redução do parâmetro CI durante o Cretáceo Superior evidencia muito bem a destruição da plataforma Albiana na Bacia de Campos (Figura 27 do Artigo III).

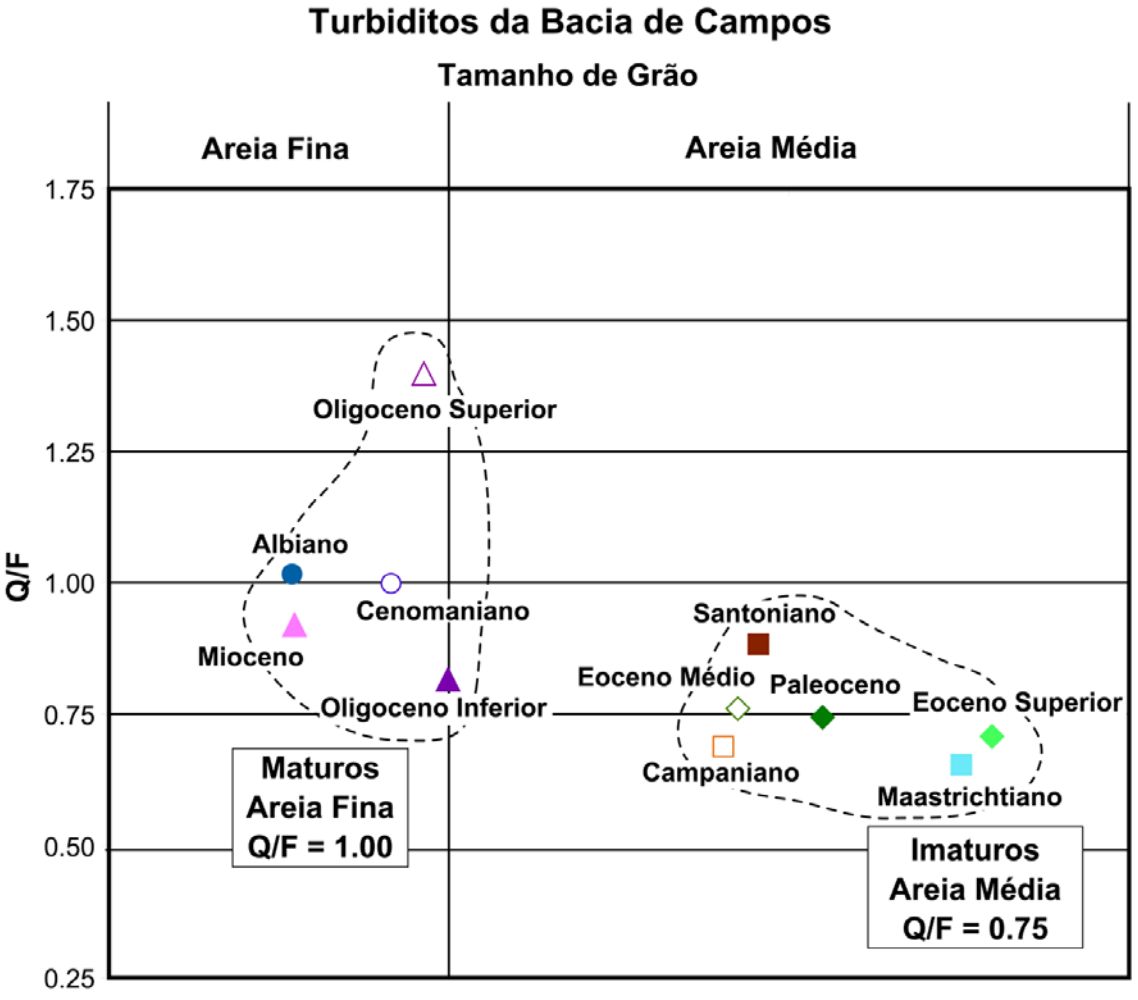

Figura 1 – Classificação dos turbiditos da fase de margem divergente da Bacia de Campos segundo os parâmetros petrográficos médios de maturidade composicional (Q/F – razão quartzo-feldspato) e textural (tamanho de grão).

A análise estrutural de dados sísmicos permitiu a definição de quatro fases principais de reativação tectônica do embasamento durante o estágio de margem divergente da Bacia de Campos: duas fases no Cretáceo, uma no Paleogeno e uma no Neogeno (Tabela 1 do Artigo II e Tabela 3 do Artigo III). A deformação tem estilo estrutural e padrão cinemático transcorrentes e está concentrada junto aos altos estruturais do embasamento, configurando um contexto geodinâmico de tectônica de blocos, com reativação seletiva de estruturas, típicos do ambiente intraplaca (Ziegler et al., 1995; Sibson, 1995; Storti et al., 2003). Cabe ressaltar que os principais altos internos do embasamento da Bacia de Campos controlam, além da deformação transcorrente localizada, feições regionais expressivas, tais como os domínios da tectônica salífera e a frente de progradação do Neogeno (Artigo II).

Através da restauração de seções foi possível definir a natureza episódica da tectônica salífera distencional durante a fase de margem divergente da Bacia de Campos (Figuras 14 e 15 do Artigo II). Adicionalmente observou-se uma boa correlação entre os pulsos da tectônica salífera computados com base na restauração de seções e os eventos de reativação do embasamento definidos com base na análise estrutural de atributos sísmicos (Artigo II). Esta correlação sugere que, na Bacia de Campos, a tectônica salífera tem sido controlada pela tectônica de embasamento.

A integração dos resultados obtidos permitiu o estabelecimento de uma associação entre a evolução geodinâmica, as tendências dos parâmetros petrográficos médios e as duas classes de maturidade dos turbiditos da Bacia de Campos (Figura 2). A evolução da fase de margem passiva da bacia corresponde a uma interação de três processos geodinâmicos (Artigo III): (1) recuo de escarpa em regime tectonicamente passivo; (2) reativações tectônicas de embasamento; (3) soerguimento dinâmico e magmatismo relacionados com pluma de Trindade.

Durante os períodos de recuo de escarpa, no Albiano-Cenomaniano e posteriormente a partir do Oligoceno, foram depositados sistemas turbidíticos relativamente maturos (Figuras 1 e 2). Estes sistemas são caracterizados por proporção mais alta de quartzo (Q/F) e granulometria mais fina (Artigo III). O sistema Cenomaniano tem uma expressiva contribuição de intraclastos e é mais imaturo que o sistema Albiano, já evidenciando algum controle tectônico na sedimentação. O sistema do Mioceno apresenta uma baixa proporção de quartzo (Q/F) e uma contribuição significativa de glauconita em função do rejuvescimento fisiográfico da costa e da plataforma causado pelo evento tectônico do Neogeno.

Por outro lado, durante as fases de reativação tectônica e de soerguimento dinâmico, do Santoniano até o Eoceno, foram depositados sistemas arenosos imaturos nas águas profundas da Bacia de Campos (Figuras 1 e 2). Estes sistemas caracterizam-se por baixa proporção de quartzo, granulometria mais grossa e contribuição significativa de intraclastos (Artigo III). A partir do Paleogeno, com a reconstrução da plataforma continental, também se observa um conteúdo maior de glauconita. Os turbiditos do Maastrichtiano apresentam uma contribuição vulcânica expressiva em função do intenso magmatismo na borda da bacia que estava posicionada exatamente sobre a pluma do manto ao final do Cretáceo.

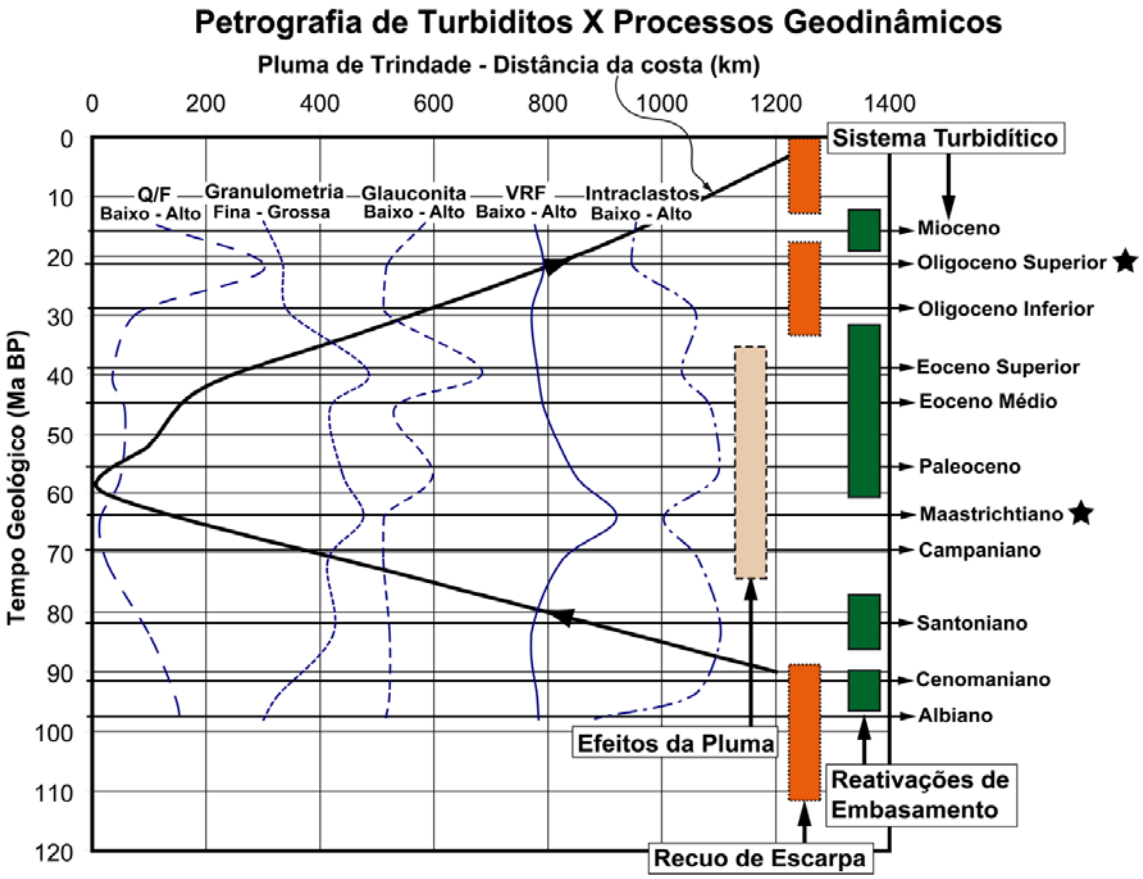

Figura 2 – Correlação entre os processos geodinâmicos atuantes e os valores médios dos parâmetros petrográficos dos sistemas arenosos de águas profundas depositados durante a fase de margem divergente da Bacia de Campos. Q/F - razão quartzo-feldspato. VRF – fragmentos de rocha vulcânica.

A metodologia integrada utilizada permitiu estabelecer um quadro evolutivo do controle da sedimentação em águas profundas durante a fase de margem divergente da Bacia de Campos (Tabela 1). Este quadro está associado à proposição de um modelo coerente de evolução geodinâmica e paleogeográfica para a margem continental sudeste do Brasil. Em linhas gerais a sedimentação de águas profundas na Bacia de Campos evidencia uma alternância entre controle eustático e controle geodinâmico. O controle eustático, associado com ciclicidade climática de alta freqüência, ocorre durante as fases de calma tectônica e recuo de escarpa com deposição de sedimentos maturos no trato de mar baixo através de uma plataforma continental bem desenvolvida. Por sua vez, o controle geodinâmico é associado com episódios climáticos de precipitação pluvial intensa e inundação fluvial capazes de carrear sedimentos aluviais imaturos diretamente para águas profundas durante as fases de rejuvenescimento do relevo causado por reativação tectônica ou por efeito da pluma do manto (Artigo III).

Sistema turbidítico	Análise petrograf.	Padrão interno	Processo geodinâmico	Controle estratigráfico	Relevo da margem	Plataforma continental
Mioceno	Relativam. Maturo	Tendência	Reativação Tectônica	Variação do Nível do Mar	Moderado	Ampla
Oligoceno Superior	Relativam. Maturo	Cíclico/ Tendência	Recuo de Escarpa	Variação do Nível do Mar	Baixo	Ampla
Oligoceno Inferior	Relativam. Maturo	Episódico	Recuo de Escarpa	Variação do Nível do Mar	Moderado	Estreita
Eoceno Superior	Imaturo	Episódico	Reativação Tectônica	Relevo/ Regime Pluvial	Alto	Estreita
Eoceno Médio	Imaturo	Episódico	Reativação Tectônica	Relevo/ Regime Pluvial	Alto	Estreita
Paleoceno	Imaturo	Episódico	Reativação Tectônica	Relevo/ Regime Pluvial	Alto	Estreita
Maastricht.	Imaturo	Episódico	Soerguimento Dinâmico	Relevo/ Regime Pluvial	Alto	Muito Estreita
Campaniano	Imaturo	Episódico	Soerguimento Dinâmico	Relevo/ Regime Pluvial	Alto	Muito Estreita
Santoniano	Imaturo	Episódico	Reativação Tectônica	Relevo/ Regime Pluvial	Alto	Muito Estreita
Cenoman.	Relativam. Maturo	Episódico	Recuo de Escarpa	Variação do Nível do Mar	Moderado	Estreita
Albiano	Relativam. Maturo	Cíclico/ Tendência	Recuo de Escarpa	Variação do Nível do Mar	Baixo	Ampla

Tabela 1 – Maturidade, padrão petrográfico interno, processos geodinâmicos, controle estratigráfico e paleogeografia dos sistemas arenosos de águas profundas da fase de margem divergente da Bacia de Campos.

Referências

Antunes, R.L., Shimabukuro, S., Oliveira, L.C.V., Rosa, A.L.Z., Costa, S.O., Cunha, A.A.S. e Lima, F.H.O. 2004. Origem e evolução estrutural do Sistema de Riftes Cenozóicos do Sudeste do Brazil. Bol. Geoc. Petrobras, 12:421-427.

Azambuja Filho, N.C. 1990. The Oligo-Miocene turbidites and associated facies of Campos Basin, offshore Brazil. London. 456 p. Tese (PhD) Imperial College.

Bahorich, M. e Farmer, S. 1995. 3D Seismic discontinuity for faults and stratigraphic features: The coherence cube. The Leading Edge, 14:1053-1058.

Beaumont, C., Kooi, H. e Willett, S. 2000. Coupled tectonic-surface process models with applications to rifted margins and collisional orogens. In: M. Summerfield (ed.), Geomorphology and Global Tectonics. New York, John Wiley & Sons, p. 29-55.

Bruhn, C.H.L. e Walker, R.G. 1995. High-resolution stratigraphy and sedimentary evolution of coarse-grained canyon-filling turbidites from the Upper-Cretaceous transgressive megasequence, Campos Basin, offshore Brazil. J. Sed. Res., 65:426-442.

Bruhn, C.H.L. 1993. High-resolution stratigraphy, reservoir geometry, and facies characterization of Cretaceous and Tertiary turbidites from Brazilian passive margin basins. Hamilton, Canadá. 433 p. Tese (PhD) McMaster University.

Bruhn, C.H.L., Gomes, J.A.T., Del Luchese, C., e Johann, P.R.S. 2003. Campos Basin: reservoir characterization and management – historical overview and future challenges. In: OTC-Houston, paper OTC 15220, p. 1-14.

Caddah, L.F.G., Alves, D.B. e Mizusaki, A.M.P. 1998. Turbidites associated with bentonites in the Upper-Cretaceous of the Campos Basin, offshore Brazil. Sed. Geol., 115:175-184.

Cartwright, J. e Huuse, M. 2005. 3D seismic technology: the geological ‘Hubble’. Basin Res., 17:1-20.

Catuneanu, O. 2006. Principles of Sequence Stratigraphy. Amsterdam, Elsevier, 375 p.

Chamberlin, R.T. 1910. The Appalachian folds of Central Pennsylvania. J. Geol., 18:225-251.

Chopra, S. e Marfurt, K.J. 2006. Seismic Attribute Mapping of Structure and Stratigraphy. Tulsa, Soc. Explor. Geoph., 226 p. (SEG/EAGE Distinguished Instructor Series, 9).

Chopra, S. e Marfurt, K.J. 2007. Curvature attribute applications to 3D surface seismic data. The Leading Edge, 26:404-414.

Cibin, U., Spadafora, E., Zuffa, G.G. e Castellarin, A. 2001. Continental collision history from arenites of episutural basins in the Northern Apennines, Italy. GSA Bull., 113:04-19.

Cobbold, P.R., e Szatmari, P. 1991. Radial gravitational gliding on divergent margins. Tectonophys., 188:249-289.

Cobbold, P.R., Meisling, K.E. e Mount, S.V. 2001. Reactivation of an obliquely-rifted margin - Campos and Santos basins, SE Brazil. AAPG Bull., 85:1925-1944.

Critelli, S. 1993. Sandstone detrital modes in the Paleogen Liguride Complex, accretionary wedge of the Southern Apennines (Italy). J. Sed. Petrol., 63:464-476.

Dahlstrom, C.D.A. 1969. Balanced cross sections. Can. J. Earth Sci., 6:743-757.

Davis, G.H. e Reynolds S.J. 1996. Structural Geology of Rocks and Regions. New York, John Wiley & Sons, 776 p.

Demercian, S., Szatmari, P., e Cobbold, P.R. 1993. Style and pattern of salt diapirs due to thin-skinned gravitational gliding, Campos and Santos basins, offshore Brazil. Tectonophys., 228:393-433.

Dickinson, W.R. e Suczec, C.A. 1979. Plate tectonics and sandsdtone compositions. AAPG Bull., 63:2164-2182.

Dickinson, W.R. 1970. Interpreting detrital modes of greywacke and arkose. **J**. Sed. Petrol., 40:695-707.

Dickinson, W.R. 1985. Interpreting provenance relations from detrital modes of sandstones. In: G.G. Zuffa (ed.) Provenance of Arenites. Dordrecht, D. Reidel Publ. Co., p. 333-361. (NATO ASI Series, Math. Phys. Sci., 148).

Dickinson, W.R. 1988. Provenance and sediment dispersal in relation to paleotectonics and paleogeography of sedimentary basins. In: K.L. Kleinspehn e C. Paola (eds.) New Perspectives in Basin Analysis. New York, Springer-Verlag, p. 03-25.

Dickinson, W.R., Beard, L.S., Brakenridge, G.R., Erjavec, J.L., Ferguson, R.C., Inman, K.F., Kneep, R.A., Lindberg, F.A. e Ryberg, P.T. 1983. Provenance of North American Phanerozoic sandstones in relation to tectonic setting. GSA Bull., 94:222-235.

Fontana, D., Zuffa, G.G. e Garzanti, E. 1989. The interaction of eustacy and tectonism from provenance studies of the Eocene Hecho Group turbidite complex (South-Central Pyrenees, Spain). Basin Res**.**, 2:223-237.

Gallagher, K. e Brown, R. 1999. The Mesozoic denudation history of the Atlantic margins of southern Africa and southeast Brazil and the relationship to offshore sedimentation. In: N.R. Cameron, R.H. Bate, e V.S. Clure, (eds.) The Oil and Gas Habitats of the South Atlantic. London, The Geological Society, p. 41-53. (Geol. Soc. London, Spec. Publ., 153).

Gazzi, P. 1966. Le arenaire del flysch sopracretaceo de´ll Appennino modenese, correlazioni con il flysch di Monghidoro. Mineral. et Petrogr. Acta, 12:69-97.

Gradstein, F.M., Ogg, J.G., Smith, A.G., Bleeker, W. e Lourens, L.J. 2004. A new Geologic Time Scale with special reference to Precambrian and Neogene. Episodes, 27:83-100.

Gibbs, A.D. 1983. Balanced cross-section construction from seismic sections in areas of extensional tectonics. J. Struct. Geol., 5:153-160.

Gilchrist, A.R. e Summerfield, M.A. 1990. Differential denudation and flexural isostasy in the formation of rifted-margin upwarps. Nature, 346:739-742.

Hossack, J.R. 1979. The use of balaced cross-sections in the calculation of orogenic contraction: a review. J. Geol. Soc. London, 136:705-711.

Ingersoll, R.V., Bullard, T.F., Ford, R.L., Grimm, J.P., Pickle, J.D. e Sares, S.W. 1984. The effect of grain size on detrital modes: a test of the Gazzi-Dickinson point-counting method. J. Sed. Petrol., 54:103-116.

Lima, C.C. 1999. Expressions topographiques et structurales de l´etat de compression généralisée au sein de la plaque Sud-Américaine. Rennes, France. 353 p. Tese (PhD) Université Rennes 1.

Lima, C.C. 2003. Ongoing compression across South American plate: observations, numerical modelling and some implications for petroleum geology. In: M. Ameen (ed.) Fracture and In-Situ Stress Characterization of Hydrocarbon Reservoirs. London, The Geological Society, p. 87-100. (Geol. Soc. London, Spec. Publ., 209).

Marchesini, L., Amorosi, A., Cibin, U., Zuffa, G.G., Spadafora, E. e Preti, D. 2000. Sand composition and sedimentary evolution of a Late Quaternary depositional sequence, Northwestern Adriatic Coast, Italy. J. Sed. Res., 70:829-838.

Mutti, E., Tinterri, R., Benevelli, G., di Biase, Davide, e Cavanna, G. 2003. Deltaic, mixed and turbidite sedimentation of ancient foreland basins. Mar. Petrol. Geol., 20:733-755.

Nunns, A.G. 1991. Structural restoration of seismic and geologic sections in extensional regimes. AAPG Bul.., 75:278-297.

Ollier, C.D. 1985. Morphotectonics of continental margins with great escarpments. In: M. Morisawa e J.T. Hack (eds.) Tectonic Geomorphology. Boston, Allen & Unwin, p. 3-25.

Pereira, M.J. 1994. Seqüências deposicionais de 2ª. e 3ª. ordens (50 a 2 Ma) e tectono-estratigrafia no Cretáceo de cinco bacias marginais do Brasil - comparações com outras áreas do globo e implicações geodinâmicas. Porto Alegre. 430 p. Tese de Doutorado em Geociências, Instituto de Geociências, Curso de Pós-Graduação em Geociências, Universidade Federal do Rio Grande do Sul.

Peres, W.E. 1993. Shelf-fed turbidite system model and its application to the Oligocene deposits of the Campos Basin, Brazil. AAPG Bull., 77:81-101.

Rowan, M.G. 1993. A systematic technique for the sequential restoration of salt structures. Tectonophys., 228:331-348.

Saenz, C.A.T., Hackspacker, P.C., Hadler Neto, J.C., Iunes, P.J., Guedes, S., Ribeiro, L.F.B., e Paulo, S.R. 2003. Recognition of Cretaceous, Paleocene, and Neogene tectonic reactivation through apatite fission-track analysis in Precambriam areas of southeast Brazil - association with the opening of the south Atlantic ocean. J. South Am. Earth Sci., 15:765-774.

Scarton, J.C. 1993. Análise estratigráfica do Terciário Inferior da Bacia de Campos – Uma visão moderna (com ênfase na região dos campos petrolíferos de Corvina e Malhado). Porto Alegre. 403 p. Tese de Doutorado em Geociências, Instituto de Geociências, Curso de Pós-Graduação em Geociências, Universidade Federal do Rio Grande do Sul.

Schultz-Ela, D.D. 1991. Practical restoration of extensional cross-sections. Geobyte, 6:14-23.

Schultz-Ela, D.D. 1992. Restoration of cross-sections to constrain deformation processes of extensional terranes. Mar. Pet. Geol., 9:372-388.

Sibson, R.H. 1995. Selective fault reactivation during basin inversion - potential for fluid redistribution through fault-valve action. In: J.G. Buchanan e P.G. Buchanan (eds.) Basin Inversion. London, The Geological Society, p. 3-19. (Geol. Soc. London, Spec. Publ., 88).

Souza Cruz, C.E. 1995. Estratigrafia e sedimentação de águas profundas do Neogeno da Bacia de Campos, Estado do Rio de Janeiro, Brasil. Porto Alegre. 186 p. Tese de Doutorado em Geociências, Instituto de Geociências, Curso de Pós-Graduação em Geociências, Universidade Federal do Rio Grande do Sul.

Souza Jr., O.G. 1997. Stratigraphie séquentielle et modélisation probabiliste d´un cône sous-marine profond, champ de Namorado. Paris. 231 p. Tese (PhD) Université Paris VI.

Storti, F., Holdsworth, R.E., e Salvini F. 2003. Intraplate strike-slip deformation belts. In: F. Storti, R.E. Holdsworth, e F. Salvini (eds.) Intraplate Strike-slip Deformation Belts. London, The Geological Society, p. 3-19. (Geol. Soc. London, Spec. Publ., 210)

Thomaz Filho, A., de Cesaro, P., Mizusaki, A.M.P. e Leão, J.G. 2005. Hot spot volcanic tracks and their implications for South American plate motion, Campos Basin (Rio de Janeiro state), Brazil. J. South Am. Earth Sci., 18:383-389.

Vail, P.D., Mitchum Jr., R.M., and Thompson III, S. 1977. Seismic stratigraphy and global changes of sea level, Part 4: Global cycles of relative changes of sea level. In: C.E. Payton (ed.) Seismic Stratigraphy – Applications to hydrocarbon exploration. Tulsa, AAPG, p. 83-97. (AAPG Memoir, 26).

Valloni, R. e Zuffa, G.G. 1984. Provenance changes for arenaceous formations of the Northern Apennines, Italy. GSA Bull., 95:1035-1039.

Weissel, J.K. e Karner, G.D. 1989. Flexural uplift of rift flancs due to mechanical unloading of the lithosphere during extension. J. Geophys. Res., 94:13919-13950.

Zalán, P.V. e Oliveira, J.A.B. 2005. Origem e evolução estrutural do Sistema de Riftes Cenozóicos do Sudeste do Brazil. Bol. Geoc. Petrobras, 13:269-300.

Ziegler, P.A., Cloetingh, S., e van Wees, J.D. 1995. Dynamics of intra-plate compressional deformation: the Alpine foreland and other examples. Tectonophys., 252:7-59.

Zuffa, G.G. 1980. Hybrid arenites: their composition and classification. J. Sed. Petrol., 50:21-29.

Zuffa, G.G. 1991. On the use of turbidite arenites in provenance studies: critical remarks. In A.C. Morton, S.P. Todd e P.D.W. Haughton, (eds.) Developments in Sedimentary Provenance Studies. London, The Geological Society, p. 23-29. (Geol. Soc. London, Spec. Publ., 57).

Zuffa, G.G. 1985. Optical analysis of arenites: influence of methodology on composition. In: G.G. Zuffa (ed.) Provenance of Arenites. Dordrecht, D. Reidel Publ. Co., p. 165-189. (NATO ASI Series, Math. Phys. Sci., 148).

Zuffa, G.G. 1987. Unravelling hinterland and offshore paleogeography from deep-water arenites. In: J.K. Leggett e G.G. Zuffa, (eds.) Marine Clastic Sedimentology. London, Graham & Trotman, p. 39-61.

Zuffa, G.G., Cibin, U. e Di Giulio, A. 1995. Arenite petrography in sequence stratigraphy. The J. of Geol., 103:451-459.

Zuffa, G.G., Normark W.R., Serra, F., e Brunner, C.A. 2000. Turbidite megabeds in an ocean rift valley recording jökulhlaups of the Late Pleistocene lakes in the western United States. The J. of Geol., 108:253-274.

Artigos Publicados

Artigo I. An active divergent margin: petrographic and seismic evidence on the geodinamically-controlled deposition of Campos Basin giant turbidite reservoirs, southeastern Brazil (Submitted to Geology).

An active passive margin: petrographic and seismic evidence for the geodynamically-controlled deposition of giant sand-rich turbidite reservoirs in the Campos Basin, offshore Brazil

Marcos Fetter[a]*, Carlos H. L. Bruhn[a] and Luiz F. De Ros [b#]

[a]Petrobras E&P, Av. Chile, 65/1702, Rio de Janeiro, RJ, Brazil, 20035-900;
[b]UFRGS, Institute of Geosciences, Av. Bento Gonçalves, 9500, Porto Alegre, RS, Brazil, 21501-970;
e-mail: *fetter@petrobras.com.br; [#]lfderos@inf.ufrgs.br

Abstract

Thick turbidite reservoirs composed of feldspathic, coarse-grained and poorly-sorted sandstones were deposited during the Late Cretaceous in the Campos Basin, southeastern Brazilian margin. Conversely to what would be expected for the evolution of a passive divergent margin under transgression, the sandstones became more feldspathic and coarser-grained from the Albian-Cenomanian to the Santonian and the Campanian-Maastrichtian. Simultaneously tectonic reactivation of the basement fabric generated strike-slip systems bordering structural highs associated with steep rift phase fault zones, causing en-echelon folding of Albian to Turonian successions. Additionally, it was observed a significant increase in the contribution of volcanic rock fragments in the uppermost Cretaceous because of the magmatic activity associated with the passage of the Campos Basin border above the Trindade mantle plume. The abundance and distribution of such sandy turbidites and the structural features indicate that the evolution of Campos Basin deviated substantially from a typical passive margin, being affected by intense and increasing tectonism, magmatism and uplift along the coastal chain source terrains during the Late Cretaceous. The deposition of geodymamically-controlled, thick, sand-rich turbidites during a major transgression indicates that, even at passive margins, the classic eustatic lowstand model of deepwater fan deposition is too simplistic and restrictive to be used for the exploration for turbidite reservoirs in frontier deepwater areas. An integrated approach is proposed for the understanding of sand-rich deepwater systems in divergent margins, based on quantitative petrography, and on the analysis of the geodynamic evolution.

Keywords: Deepwater sediment supply, paleogeographic interpretation, passive margin geodynamics, sand-rich turbidites, basement uplift

Introduction

The association of deepwater fans with eustatic sea level lowstands is a classic paradigm of sequence stratigraphy (Shanmugan and Moiola, 1982). Nevertheless, some deepwater systems are in disagreement with this model (Piper and Normark, 1983; Kolla and Perlmutter, 1993; Mutti et al., 1996; Normark et al., 2006). Most of the objections to the classic eustatic lowstand model for deepwater fans were based on data from active margin systems. For passive margin basins, the association between eustatic sea level lowstands and deepwater fans remains accepted as a general rule (Shanmugan et al., 1985; Milliman and Syvitski, 1992; Covault et al., 2007). The development of deepwater fans is fundamentally related to sediment supply itself, which can be controlled by eustatic sea level, but also by the geodynamic evolution of source-terrains and basins, by coastal and shelf physiography, by deltaic progradation rates, and by

climatic cycles (Ricci-Luchi, 1985; Mutti, 1985; Weltje and De Boer, 1993; Burges and Hovius, 1998; Piper and Normark, 2001).

More recently, the critical role of sediment supply in the development of thick, sand-rich deepwater fans in both ancient and recent active margins has been discussed on the basis of high-resolution stratigraphy (Carvajal and Steel, 2006), and piston cores and high-resolution seismic data (Covault et al., 2007). In the present work we develop further that discussion, taking it both to a wider, geodynamic scale, and to a detailed, petrographic view. It is interesting to observe that we reach similar conclusions to that of Carvajal and Steel (2006) and Covault et al. (2007) in a very different geologic setting, as we have studied turbidite petrography, structural geology, tectonics and magmatism in a South Atlantic divergent margin basin, during the Upper Cretaceous second-order eustatic sea-level highstand (Haq et al., 1987).

Geological Setting

Thick, sand-rich turbidite systems were deposited from the Late Albian to the Maastrichtian in the Campos Basin (Fig. 1), the most prolific oil province in Brazil, which was originated during the Early-Cretaceous break-up of the Gondwana and opening of South Atlantic Ocean. The basin follows the classic rift-drift model for passive margin basins (Falvey, 1974; Le Pichon and Sibuet, 1981). The Early-Cretaceous was characterized by intense magmatic activity, contemporaneous with the massive extrusion of tholeiithic lavas in the Paraná Basin (Mizusaki et al., 1992). Taphrogenic successions thicker than 3.5 km were deposited on a basal volcanogenic sequence from the Valaginian to the Barremian (Fig. 1). During the Aptian, a transitional siliciclastic and evaporitic succession was deposited over the breakup unconformity, at thermal subsidence conditions. The divergent margin stage began during Albian, and is still going on (Chang et al., 1992). Thermal subsidence and sediment loading allowed the deposition of an up to 7 km thick transgressive-regressive marine succession. The basin is presently bordered by an up to 2 km high coastal ridge (Fig. 1).

During the Late Cretaceous, in agreement with eustatic sea level curves (e.g. Haq et al., 1987), a second-order transgressive succession was deposited in the Campos Basin, following the drowning of a shallow carbonate ramp formed during the Albian (Fig. 1). Upper Cretaceous continental and shallow marine deposits are poorly-preserved in Campos Basin. However, thick (up to 300 m) sand-rich systems were deposited

throughout the transgression, particularly during the Late Albian (Bruhn et al., 1998), the Late Cenomanian (Souza Jr., 1997), the Santonian (Bruhn and Walker, 1995), and the Campanian-Maastrichtian (Santos et al., 1999).

Turbidite petrography

Petrographic analysis was performed on 61 thin sections sampled along 456 m of cores from 5 wells, selected in order to represent the above cited turbidite systems: Upper Albian (17 samples), Upper Cenomanian (14 samples), Santonian (10 samples), and Campanian-Maastrichtian (20 samples). Three hundred points were counted per thin section, using the Gazzi-Dickinson point-counting method (Ingersoll et al., 1984; Zuffa, 1987; 1991).

All samples are of feldspathic sandstones, and most plot into the Basement Uplift field of the Dickinson QtFL diagram (Dickinson, 1985; Fig. 2). Campanian-Maastrichtian and Santonian samples are very immature, displaying poorer sorting, higher feldspar content, and coarser grain size than Cenomanian and Albian samples (Fig. 2). Such increase in compositional immaturity is expressed in the Dickinson QtFL plot by an Albian to Maastrichtian trend towards the feldspar pole (Fig. 2, dashed arrow).

Some Campanian-Maastrichtian samples show also a departure towards a litho-feldspathic trend (Fig. 2, dotted arrow) caused by an increase in the contribution of volcanic rock fragments (Fig. 3b). Cenomanian and Albian samples show significant contribution of intrabasinal carbonate grains from the contemporaneous shallow carbonate ramp (Figs. 3f, 3h).

The variation in the maturity of the analyzed sandstones is further indicated by plotting the ratio of detrital quartz to feldspar content (Q/F) against the modal grain size (Fig. 4). It is clearly perceived that Albian and Cenomanian turbidite systems were supplied by finer-grained and more quartzose sands than Santonian and Campanian-Maastrichtian systems (Fig. 4). This trend is opposite to that expected for a passive margin under transgression.

Structural evolution, tectonics, and magmatism

The detached structural style in the Campos Basin is characterized by basement horsts and grabbens limited by steep normal faults active during the extensional rift phase in the Early Cretaceous (Fig. 2; Chang et al., 1992), and by thin-skinned salt tectonics with extensional-proximal and compressional-distal domains active during

divergent margin phase since the Early Albian (Fig. 2; Cobbold and Szatmari, 1991). However it is possible to observe departures from this general style, caused by episodic reactivation of the basement fabric that occurred during the divergent margin phase (Cobbold et al., 2001; Fetter et al., 2002). The tectonic reactivation in the Campos Basin during the Late Cretaceous is represented by strike-slip fault systems that caused en-echelon folding of Albian to Turonian successions (Fig. 5). The deformation had been concentrated at basement highs associated with steep shear zone systems previously activated during the rift phase. The folds are symmetric with 1 km wavelength, 100 m amplitude, and up to 6 km long sinuous fold axes (Fig. 5).

During the Late Cretaceous Campos Basin was the site of alkaline magmatism with compositional affinity to ocean-island basalts (OIB), associated to its dislocation above the Trindade mantle plume (Misuzaki et al., 1992; Almeida et al., 1996; Thompson et al., 1998; Thomaz Filho et al., 2005). This coincides with the occurrence of volcanic ash layers intercalated with Santonian turbidites (Caddah et al., 1998), and with the significant contribution of volcanic rock fragments in the Campanian-Maastrichtian turbidites (Figs. 2 and 3).

Geodynamic and paleogeographic interpretation of the deepwater sand supply

The evolution of divergent margins is currently described by a few geodynamic processes: (i) continuous escarpment retreat of rift shoulders with flexural isostatic adjust to the unloading caused by denudation (Ollier, 1985; Gilchrist and Summerfield, 1990; Kooi and Beaumont, 1994), (ii) episodic intraplate tectonic reactivations related to plate border orogenies (Ziegler et al., 1995; Lima, 2003), and (iii) magmatic underplating related to episodic mantle plume activity (Brodie and White, 1995); (iv) reactivation of secondary (edge-driven) convection cells in the upper mantle (Praeg et al., 2005).

As previously discussed, there is compelling evidence of Late Cretaceous basement tectonic reactivation and magmatic activity in the Campos Basin. Besides, the compositional and textural immaturity of deepwater sandstones indicates that the geodynamic and paleogeographic evolution of the basin border cannot be explained by a continuous escarpment retreat during the Late Cretaceous, which would be better expressed by a petrographic trend of increasing maturity. The role of tectonism and magmatism as major controls on the evolution of the Campos Basin physiography during the Late Cretaceous was previously suggested (Pereira, 1994; Bruhn and Walker,

1995; Caddah et al., 1998). Nevertheless, the aspect that the deposition of the giant turbidite reservoirs cannot be related to the classic eustatic lowstand model for deepwater fans remains poorly explored and explained.

The increase in quartz to feldspar ratio and grain size of the turbidites from the Albian to the Maastrichtian agrees with the seismic evidence of Upper Cretaceous tectonic reactivation represented by strike-slip fault systems and by en-echelon folding. The petrographic and seismic evidence are also in agreement with the fission-track indication of uplift of the coastal source terrains (Lima, 2003), and with the distribution of magmatism in the basin, associated to its dislocation above the Trindade mantle plume (Thompson et al., 1998; Thomaz Filho et al., 2005). The whole set of evidence indicates that: (a) Campos Basin and adjacent sectors of the southeastern Brazilian margin behaved as a tectonically active, rather than as a passive margin during the Late Cretaceous; (b) the deposition of large turbidite reservoirs was controlled by the geodynamic evolution, and supplied by the recurrently uplifted basement terrains along the border of the Campos Basin, during a major transgressive period; and (c) the classic eustatic lowstand model of deepwater fan deposition is too simplistic and restrictive to be used for the prediction of turbidite reservoirs in deepwater frontier areas at divergent margin settings.

Conclusions

The deepwater sand-supply in divergent continental margins is not exclusively controlled by eustatic sea level changes and fluvial-deltaic progradation, as stated by the current paradigm of sequence-stratigraphy. It was shown that the sand budget in deepwater during the evolution of a typical passive margin basin can be constrained by episodic tectonism and magmatism, just as in active margin settings. Thick sandy turbidites can be deposited along divergent margins even during major eustatic transgressive periods, as emphatically illustrated by Campos Basin giant turbidite reservoirs.

The composition and texture of turbidite sandstones can be used to unravel the paleogeographic and geodynamic evolution of passive margin systems in the same way as they are used in active margins. The combination of petrographic and structural analyses allows the understanding of the tectonic versus eustatic controls on the turbidite deposition. The proposed approach can positively impact the prediction of reservoirs in deepwater frontier areas at divergent margins, as it envisages a broader

spectrum of physiographic possibilities for the development of thick sand-rich turbidite systems.

Acknowledgements

This work is part of a doctorate research developed by M. Fetter at Rio Grande do Sul Federal University (UFRGS – Porto Alegre, Brazil) sponsored by Petrobras. We acknowledge the discussions with Cláudio Lima and Luci Arienti from Petrobras Research Center, and Carlos Rodrigues from Petrobras E&P International. We wish to thank also Eliane de Freitas Ferreira from Petrobras Documentation Center.

References

Almeida, F.F.M., Carneiro, C.D.R., and Mizusaki, A.M.P., 1996. Correlação do magmatismo das bacias da margem continental brasileira com o das áreas emersas adjacentes. Rev. Bras. Geoc. 26, 125-138.

Brodie, J. and White, N., 1995. The link between sedimentary basin inversion and igneous underplating. In: J.G. Buchanan and P.G. Buchanan (Editors) Basin Inversion. Geol. Soc. London Spec. Publ. 88, 21-38.

Bruhn, C.H.L., and Walker, R.G., 1995. High-resolution stratigraphy and sedimentary evolution of coarse-grained canyon-filling turbidites from the Upper-Cretaceous transgressive megasequence, Campos Basin, offshore Brazil. J. Sed. Res. 65, 426-442.

Bruhn, C.H.L., Barroso, A.S., Fetter, M., Sarzenski, D.J., Abreu, C.J., and Silva, C.M.A., 1998. High-resolution stratigraphy and reservoir heterogeneities of Upper Albian turbidite reservoirs of Albacora field, Campos Basin, offshore Brazil. 1998 AAPG Annual Conv., Salt Lake City, Ext. Abstr., AAPG Bull. 82.

Caddah, L.F.G., Alves, D.B., and Mizusaki, A.M.P., 1998. Turbidites associated with bentonites in the Upper-Cretaceous of the Campos Basin, offshore Brazil. Sed. Geol. 115, 175-184.

Carvajal, C.R., and Steel, R.J., 2006. Thick turbidite succesions from supply-dominated shelves during sea level highstand. Geology 34, 665-668.

Chang, H.K., Kowsmann, R.O., Figueiredo, A.M.F., and Bender, A.A., 1992. Tectonics and stratigraphy of the East Brazil Rift system: an overview. Tectonophys. 213, 97-138.

Cobbold, P.R., and Szatmari, P., 1991. Radial gravitational gliding on passive margins. Tectonophys. 188, 249-289.

Cobbold, P.R., Meisling, K.E., and Mount, S.V., 2001, Reactivation of an obliquely-rifted margin - Campos and Santos basins, SE Brazil: AAPG Bull., v. 85, p. 1925-1944.

Covault, J.A., Normark, W.R., Romans, B.W., and Graham, S.A., 2007. Highstand fans. In the California borderland: The overlooked deep-water depositional systems. Geology 35, 783-786.

Falvey, D.A., 1974. The development of continental margins in plate tectonics theory. Australian Petr. Expl. Ass. Journal, 14, 95-106.

Fetter, M., Lima, C.C., Silva, A.T., Machado, D., Castro, D.D., and Adams, T., 2002. Interaction between salt related extension and basement strike-slip reactivation in northern Campos Basin, deepwater Brazil. SEG 72nd Ann. Meet., Salt Lake, Exp. Abstr., 2413-2416.

Gilchrist, A.R. and Summerfield, M.A., 1990. Differential denudation and flexural isostasy in the formation of rifted-margin upwarps. Nature, 346, 739-742.

Haq, B.U., Hardenbol, J., and Vail, P.R., 1987. Chronology of fluctuating sea levels since the Triassic. Science 235, 1156-1167.

Ingersoll R.V., Bullard T.F., Ford R.L., Grimm J.P., Pickle J.D., and Sares S.W., 1984. The effect of grain size on detrital modes: a test of the Gazzi-Dickinson point-counting method. J. Sedim. Petrol., 54, 103-116.

Kolla, V., and Pelmutter, M.A., 1993. Timing of turbidite sedimentation on the Mississipi Fan. AAPG Bull. 77, 1129-1141.

Kooi, H. and Beaumont, C., 1994. Escarpment retreat on high-elevation rifted continental margins: Insights derived from a surface-process model that combines diffusion, reaction and advection. J. Geophys. Res., 99, 12191-12209.

Le Pichon, X., and Sibuet, J.C., 1981. Passive margins: A model of formation. J. Geophys. Res. 86, 3708-3720.

Lima, C.C., 2003. Ongoing compression across South American plate: observations, numerical modelling and some implications for petroleum geology. In: M. Ameen (Editor) Fracture and In-Situ Stress Characterization of Hydrocarbon Reservoirs. Geol. Soc. London, Spec. Publ. 209, 87-100.

Milliman, J.D. and Syvitski, J.P.M., 1992. Geomorphic/tectonic control of sediment discharge to the ocean: the importance of small mountainous rivers. J. Geol. 100, 525-544.

Mizusaki, A.M.P., Petrini, R., Bellieni, G., Comin-Chiaramonti, P., Dias, J., De Min, A., and Piccirillo, E.M., 1992. Basalt magmatism along the passive continental margin of SE Brazil (Campos Basin). Contrib. Min. Petrol. 111, 143-160.

Mutti, E., 1985. Turbidite systems and their relations to depositional sequences. In G.G. Zuffa (Editor) Provenance of Arenites. D. Reidel Publ. Co., NATO ASI Series, Math. Phys. Sci. 148, 65-93.

Mutti, E., Davoli, G., Tinterri, R., and Zavala, C., 1996. The importance of fluvio-deltaic systems dominated by catastophic flooding in tectonically active basins. Mem. Sci. Geol. Padova, 48, 233-291.

Normark, W.R., 1978. Fan valleys, channels and depositional lobes on modern submarine fans: characters for recognition of sandy turbidite enviroments. AAPG Bull. 62, 912-931.

Normark, W.R., Piper, D.J.W., and Sliter, R., 2006. Sea level and tectonic control of middle to late Pleistocene turbidite systems in Santa Monica Basin, offshore California. Sedimentology 53, 867-897.

Ollier, C.D., 1985. Morphotectonics of continental margins with great escarpments. In: M. Morisawa and J.T. Hack (Editors) Tectonic Geomorphology. Allen & Unwin, 3-25.

Pereira, M.J., 1994. Seqüências deposicionais de 2ª. e 3ª. ordens (50 a 2 Ma) e tectono-estratigrafia no Cretáceo de cinco bacias marginais do Brasil: Comparações com outras áreas do globo e implicações geodinâmicas. PhD Thesis. UFRGS, Porto Alegre, Brazil.

Piper, D.J.W., and Normark, W.R., 1983. Turbidite depositional patterns and flow characteristics, Navy submarine fan, California borderland. Sedimentology 30, 681-691.

Piper, D.J.W. and Normark, W.R., 2001. Sandy fans – from Amazon to Hueneme and beyond. AAPG Bull. 85, 1407-1438.

Praeg, D., Stoker, M.S., Shannon, P.M., Ceramicola, S., Hjelstuen, B., Laberg, J.S., and Mathisen, A., 2005. Episodic Cenozoic tectonism and the development of the NW European ‘passive’ continental margin. Mar. Petr. Geol. 22, 1007-1030.

Ricci-Lucchi, F., 1985. Influence of transport processes and basin geometry on sand composition. In G.G. Zuffa (Editor) Provenance of Arenites. D. Reidel Publ. Co., NATO ASI Series, Math. Phys. Sci. 148, 19-45.

Santos, P. R. S., Rangel, H. D., Quintaes, C. M. S. P., and Caixeta, J. M., 1999. Turbidite reservoir distribution in Roncador field, Campos Basin, Brazil. 1999 AAPG International Conference and Exhibition, Birmingham, England. Extended Abstracts, 530–531.

Shanmugan, G., and Moiola, R.J., 1982. Eustatic control of turbidites and winnowed turbidites. Geology 10, 231-235.

Shanmugam, G., Moiola, R.J., and Damuth, J.E., 1985. Eustatic control of submarine fan development. In: A.H. Bouma et al. (Editors) Submarine fans and related turbidite systems. Springer-Verlag, 23-28.

Souza Jr., O.G., 1997. Stratigraphie séquentielle et modélisation probabiliste d´un cône sous-marine profond, champ de Namorado. PhD Thesis. Université Paris VI, Paris, France.

Thomaz Filho, A., de Cesero, P., Mizusaki, A.M., and Leão, J.G., 2005. Hot spot tracks and their implications for South American Plate motion, Campos Basin (Rio de Janeiro state), Brazil. J. South Am. Earth Sci. 18, 383-389.

Thompson, R.N., Gibson, S.A., Mitchell, J.G., Dickin, A.P., Leonardos, O.H., Brod, J.A., and Greenwood, J.C., 1998. Migrating Cretaceous-Eocene magmatism in the Serra do Mar alkaline province, SE Brazil: melts from the deflected Trindade mantle plume. J. Petrol. 39, 1493-1526.

Weltje, G., and de Boer, P.L., 1993. Astronomically induced paleoclimatic oscillations reflected in Pliocene turbidite deposits on Corfu (Greece): implications for the interpretation of higher order cyclicity in ancient turbidite systems. Geology 21, 307-310.

Ziegler, P.A., Cloetingh, S., and van Wees, J.D., 1995. Dynamics of intra-plate compressional deformation: the Alpine foreland and other examples. Tectonophys. 252, 7-59.

Zuffa, G.G., 1987. Unravelling hinterland and offshore paleogeography from deep-water arenites. In J.K. Leggett and G.G. Zuffa (Editors) Marine Clastic Sedimentology. Graham & Trotman, 39-61.

Zuffa, G.G., 1991. On the use of turbidite arenites in provenance studies: critical remarks. In A.C. Morton, et al. (Editors). Developments in Sedimentary Provenance Studies. Geol. Soc. Spec. Publ., 57, 23-29.

List of Figures

Figure 1 - Structural section through central Campos Basin, offshore Brazil. The inserts show basin location and the position of the section in the basin. The grayscale map indicates the basement structure with darker gray tones in deeper portions, and the digital topographic model of the coastal mountains in white and lighter gray tones.

Figure 2 - QtFL Dickinson ternary diagram for Campos Basin Cretaceous turbidites. Most samples plot along the continental block quartz-feldspathic trend. Dashed arrow shows an increase in feldspar content from Upper Albian to Maastrichtian turbidites. Dotted arrow indicates a departure from quartz-feldspathic trend caused by an increase in the contribution of volcanic rock fragments in the Campanian-Maastrichtian turbidites.

Figure 3 - Photomicrographs taken with crossed polarizers from thin sections of typical Campos Basin turbidites: (a) Very poorly-sorted arkose; coarse, angular microcline grains indicate very limited or no reworking by fluvial or shelf systems. (b) Medium-grained, lithic arkose with volcanic rock fragment. (c) Coarse-grained arkose. (d) Medium- to coarse-grained, poorly selected arkose. (e) Fine- to medium-grained, poorly-sorted arkose. (f) Fine- to medium-grained arkose with carbonate bioclast. (g) Fine-grained, well-sorted arkose. (h) Fine-grained hybrid arenite with carbonate ooids.

Figure 4 - Change in deepwater supply patterns in the Campos Basin from finer-grained and more quartzose sand during the Albian and Cenomanian to coarser and more feldspathic sand during the Santonian and Campanian-Maastrichtian.

Figure 5 – Basement tectonics during the Late Cretaceous in Campos Basin. (a) Dip map of Albian horizon. Observe sinuous pattern of en-echelon fold axes in Albian strata. The structure can be interpreted as a strike-slip reactivation of NNW-SSE basement fabric. (b) 3D perspective with seismic section and attribute map of Albian horizon. Observe that low dip defines very well the fold axes in Albian successions of the early divergent margin phase. (c) Depth-converted seismic section (see the regional position of section B in the insert). Observe thrust-faulted and folded strata ranging in age from Barremian to Turonian.

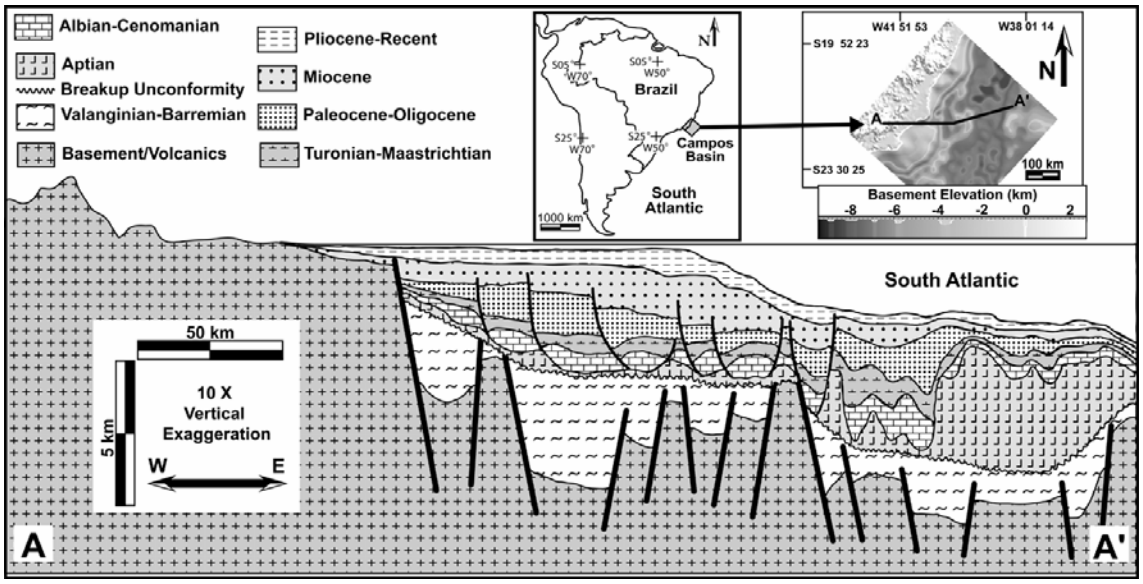
Albian-Cenomanian
Aptian
Breakup Unconformity
Valanginian-Barremian
Basement/Volcanics
Pliocene-Recent
Miocene
Paleocene-Oligocene
Turonian-Maastrichtian
Brazil
South Atlantic
Campos Basin
1000 km
W41 51 53
W38 01 14
S19 52 23
S23 30 25
100 km
Basement Elevation (km)
-8 -6 -4 -2 0 2
South Atlantic
50 km
10 X
Vertical
Exaggeration
5 km
W
E
A
A'

Figure 1

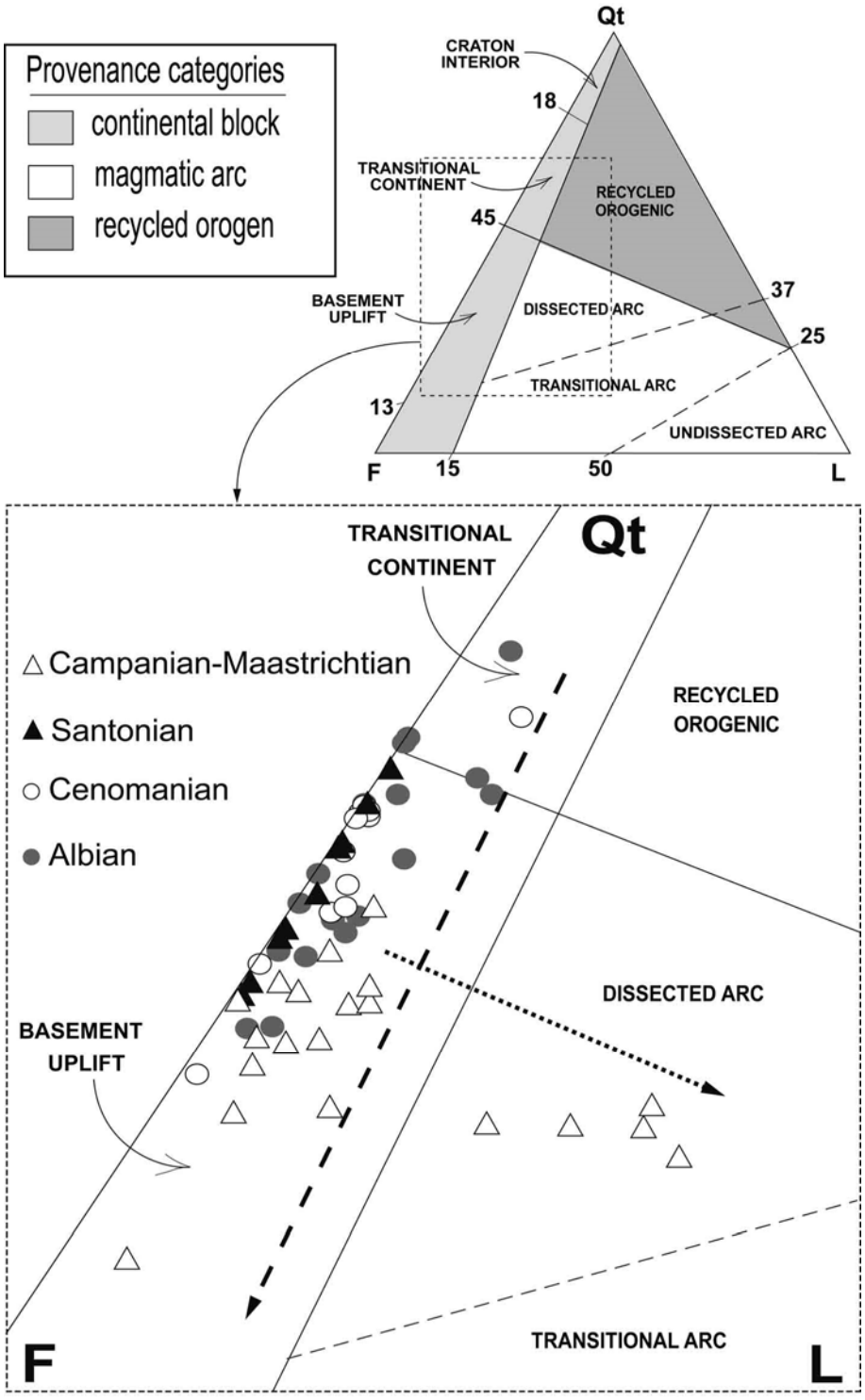
Provenance categories
continental block
magmatic arc
recycled orogen
Qt
CRATON INTERIOR
18
TRANSITIONAL CONTINENT
RECYCLED OROGENIC
45
37
BASEMENT UPLIFT
DISSECTED ARC
25
TRANSITIONAL ARC
13
UNDISSECTED ARC
F
15
50
L
TRANSITIONAL CONTINENT
Qt
△ Campanian-Maastrichtian
▲ Santonian
○ Cenomanian
● Albian
RECYCLED OROGENIC
DISSECTED ARC
BASEMENT UPLIFT
TRANSITIONAL ARC
F
L

Figure 2

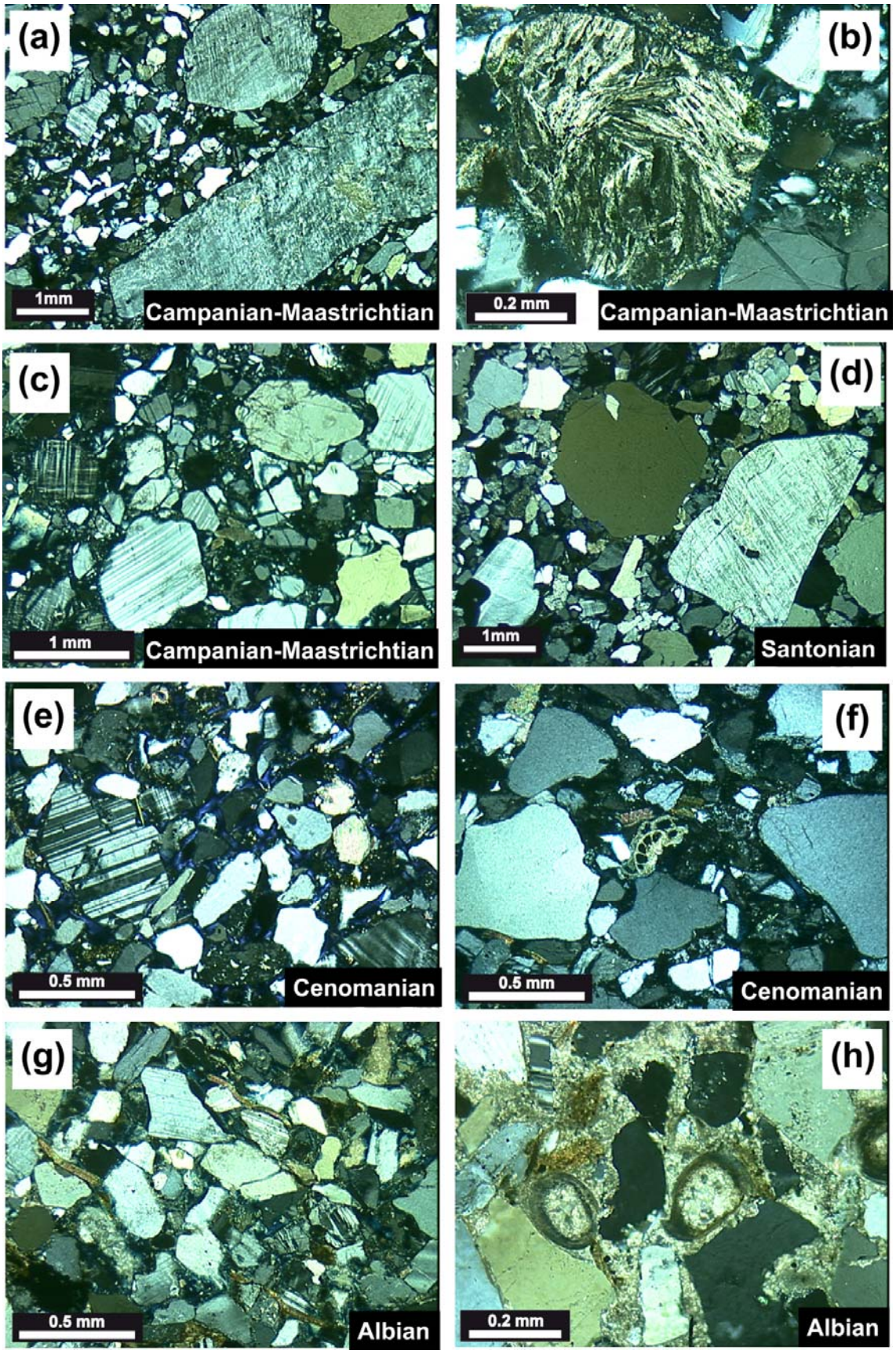
(a)
1mm
Campanian-Maastrichtian
(b)
0.2 mm
Campanian-Maastrichtian
(c)
1 mm
Campanian-Maastrichtian
(d)
1mm
Santonian
(e)
0.5 mm
Cenomanian
(f)
0.5 mm
Cenomanian
(g)
0.5 mm
Albian
(h)
0.2 mm
Albian

Figure 3

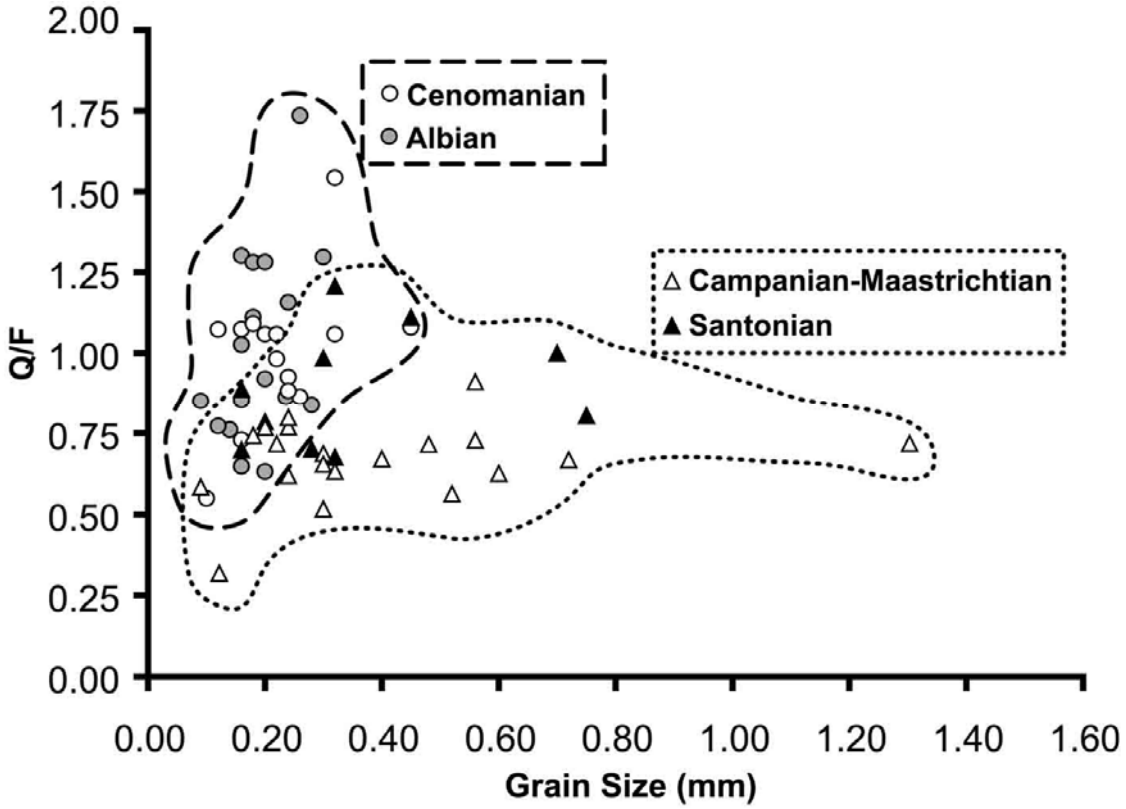
Cenomanian
Albian
Campanian-Maastrichtian
Santonian
Q/F
Grain Size (mm)
2.00
1.75
1.50
1.25
1.00
0.75
0.50
0.25
0.00
0.00
0.20
0.40
0.60
0.80
1.00
1.20
1.40
1.60

Figure 4

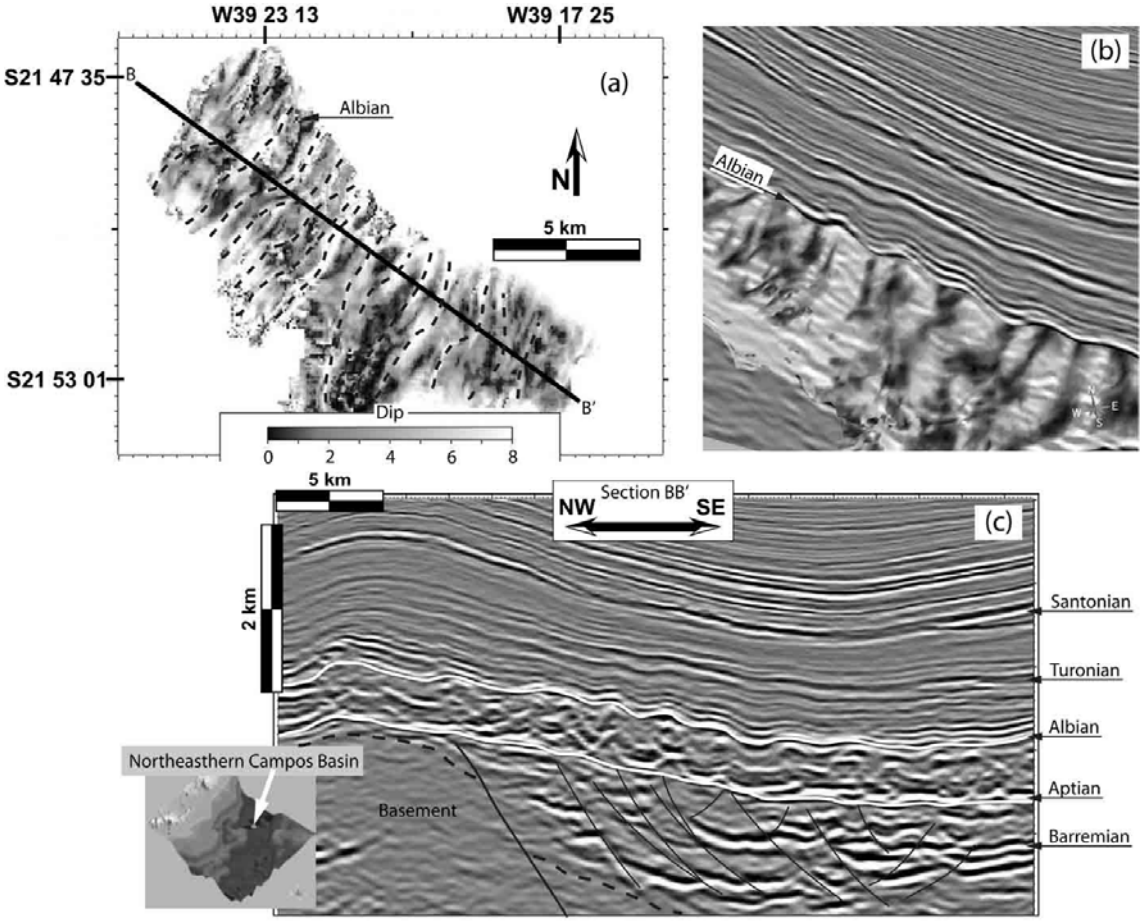
W39 23 13
W39 17 25
S21 47 35
S21 53 01
B
B'
(a)
Albian
N
5 km
Dip
0
2
4
6
8
(b)
Albian
5 km
NW
Section BB'
SE
(c)
2 km
Santonian
Turonian
Albian
Aptian
Barremian
Northeasthern Campos Basin
Basement

Figure 5

Artigo II. The role of basement tectonic reactivation on the structural evolution of Campos Basin, offshore Brazil: evidence from 3D seismic analysis and section restoration (Submitted to Marine and Petroleum Geology).

The role of basement tectonic reactivation on the structural evolution of Campos Basin, offshore Brazil: evidence from 3D seismic analysis and section restoration

Marcos Fetter[a]*

[a]Petrobras E&P, Av. Chile, 65/1702, Rio de Janeiro, RJ, Brazil, ZIP 20035-900
*e-mail address: fetter@petrobras.com.br

Abstract

The structural analysis of regional 3D seismic data based on geometric seismic attributes, associated with restored balanced cross-sections show evidence of important basement tectonic reactivations during the divergent margin phase of Campos Basin, offshore Brazil. Such tectonic activity is episodic and controls salt tectonic pulses. Additionally, major basin features like the Neogene progradation front and the salt tectonic domains are constrained by the main basement trends. As the basement involved structures observed in Campos Basin can be attributed to general geodynamic processes, it is suggested that basement tectonic reactivations can be as relevant as isostatic adjustments and detached tectonics on the evolution of divergent margin settings.

Keywords: Divergent margin tectonics; salt tectonics; section restoration; geometric seismic attributes; structural analysis; seismic interpretation.

Introduction

The structural analysis of divergent margin basins has been improved during the past decades as a function of seismic coverage acquired by oil industry. The extensional structural style of the rift-drift divergent margin model was initially observed in 2D seismic surveys (Falvey, 1974), and was soon after associated with the geodynamic model of mechanical-thermal subsidence caused by lithospheric stretching (McKenzie, 1978; Le Pichon and Sibuet, 1981). The improvement in the quality of 2D seismic data allowed important advances in the field of detachment tectonics related to shale and salt (Doust and Omatsola, 1989; Jackson, 1995), and in the technology of section restoration of extensional structures (Gibbs, 1983; Rowan and Kligfield, 1989; Nunns, 1991). Subsequently there was a continuous progress in detailed structural analysis with local 3D surveys (Hesthammer and Fossen, 1997; Cartwright and Huuse, 2005), particularly with the use of geometric seismic attributes (Chopra and Marfurt, 2006).

With recent increasing oil prices and lowering acquisition and processing costs many divergent margin basins are now also covered with extensive 3D seismic surveys. The interpretation of this kind of detailed and extensive dataset has rendered possible a substantial advance in the structural analysis of divergent margin basins. In the Campos Basin, the most prolific oil province of Brazil, one of the main improvements obtained with the structural analysis of recent regional 3D seismic surveys was the definition of the structural style produced by the interaction between dominant detachment salt tectonics and strike-slip reactivations of the basement fabric (Fetter et al., 2002). In the

present work it is shown that this interaction can be well defined by the analysis of geometric seismic attributes, with the aid of balanced cross-sections based on seismic horizons tied to biostratigraphic markers. A remarkable observation is that even being apparently subdued, basement tectonics appears to control salt tectonics pulses. If this reactive model of salt tectonics triggered by basement tectonic pulses is accepted, as it is indicated by evidence from Campos Basin, the current model, purely epeirogenic and related to escarpment retreat and mantle plume activity, assumed for the geodynamic evolution of the southeastern continental margin of Brazil should be revised.

Geological Setting

Campos Basin is located at the South Atlantic continental margin along the southeastern coast of Brazil (Fig. 1). The basin formation was initiated during the Late Jurassic/Early Cretaceous break-up of the Gondwana supercontinent. Early mechanical subsidence was accomplished by episodic events that reactivated main Proterozoic basement fabric along regional E-W extension (Ponte and Asmus, 1976; Rabinowitz and LaBrecque, 1979; Mohriak and Dewey, 1987; Dias et al., 1990; Chang et al., 1992). The lowermost Cretaceous was characterized by intense magmatic activity, contemporaneous to the Paraná Basin continental basalt floods (Hawkesworth et al., 1992; Mizusaki et al., 1992; Wilson, 1992). Up to 3.5 km thick fault-controlled taphrogenic successions were deposited from uppermost Valaginian to Barremian with volcanogenic contribution at the base. During the Aptian a widespread transitional siliciclastic and evaporitic succession was deposited over the break-up unconformity at already thermal subsidence conditions. From this, it has been suggested that the extensional tectonic phase in the Campos Basin ended by Aptian times (Chang et al., 1992). The divergent margin stage began at Albian and is still going on. Thermal subsidence and sediment loading allowed the deposition of up to 7 km-thick, transgressive-regressive marine successions (Fig. 2).

The overall structural style in Campos Basin is detached (Fig. 1). The main structural features in the basement are horsts and grabbens limited by steep normal faults active during the rift phase in the Early Cretaceous (Dias et al., 1990; Chang et al., 1992). The thin-skinned salt tectonics with extensional-proximal and compressional-distal domains have been active during divergent margin phase since the Albian, and is characterized by listric fault-rollover systems, turtle-back structures, raft tectonics, downbuilding diapirs, salt walls, and compressional salt tongues (Cobbold and Szatmari, 1991;

Demercian et al., 1993). The salt tectonic domains are controlled by the basement structure, with extensional structures to the West, and diapirs, salt walls, and compressional structures to the East of the main trend of internal basement highs (Fig. 1).

A regional basement map of Campos Basin (Fig. 2) was obtained by the integration of regional 3D seismic datasets, with complementary 2D seismic surveys to fill 3D acquisition gaps, and with the digital topographic model of the continental margin. This map was converted from time to depth with a single basin scale velocity model, which is another product of regional seismic data integration. The integrated basement map suggests that the Proterozoic fabric, defined in the basin by NE-SW and NNW-SSE basement highs, controls the main depocenters of rift phase, as it is commonly observed in many rift systems (Michon and Sokoutis, 2005). It is important to observe that the basement trends have been controlling also the progradation of the divergent margin phase, as it is suggested by the perfect fitting between the internal basement highs and the limits of present continental rise (Figs. 1 and 2).

Structural Analysis of Seismic Data

Most of the previous work published about the structural geology of Campos Basin was based on 2D seismic data, and on magnetic and gravimetric data (Mohriak and Dewey, 1987; Dias et al., 1990; Cobbold and Szatmari, 1991; Chang et al., 1992; Demercian et al., 1993). With the available data it was indicated the general detached structure of the basin. It was also possible to define the main basement highs and depocenters of the rift phase, and to get a good picture of the dominant salt tectonic structural style of the divergent margin phase. More recently, with mapping of 3D seismic surveys, it was suggested that the Campos Basin structure is not completely detached (Fetter et al., 2002). It was observed that basement fabric appears to have been subjected to episodic strike-slip reactivations during the divergent margin phase, and that the coupling between basement reactivations and salt tectonics can be observed at structural highs.

In the following examples it is shown that further evidence of basement strike-slip reactivation can be obtained from regional 3D seismic surveys, with the analysis of geometric seismic attributes. Geometric attributes are robust images computed from 3D seismic data that define the morphology and lateral variability of seismic reflectors, so that they are very useful for structural analysis (Chopra and Marfurt, 2006). In the

present work were used three types of geometric attributes: (i) dip - first derivative of structure; (ii) curvature - second derivative of structure, and (iii) semblance - inverse of amplitude variance.

Lower Cretaceous Transpression

The basement reactivation in the Early Creataceous was observed at the southern portion of Campos Basin in a 500 km^2 area of folding with rhombohedral shape (Fig. 3). The structural trend NE-SW is sub-parallel to the Proterozoic basement fabric. Up to 1800 m thick taphrogenic and transitional strata, ranging in age from Barremian to Aptian were folded by flexural slip under NNW-SSE shortening. The fold pattern, well defined by the maximum curvature map, is quite regular and sinuous (Figs 3a and 3b), with 1 km wavelength and 100 m amplitude (Fig. 3c). Fold axes are slightly rotated counter-clockwise in relation to the main NE-SW structural trend (Fig. 3a). The rhombohedral folded area is interpreted as a transpressive structure related to left-lateral strike-slip reactivation of steep basement shear zones trending NE-SW (insert of Fig. 3a). As post-Aptian strata are not deformed, it is possible to place deformation in the Early Cretaceous, still under the regional stress field of the rift phase with N-S maximum horizontal stress (SHmax). This deformation phase is related to the end of extension, but there was not yet a rotation of the regional stress field. It is also interesting to observe the alkaline magmatic activity during the Paleogene in southern Campos Basin, represented by the volcanic structure in Figures 3b and 3c.

Lower Cretaceous and Upper Cretaceous Transpression

The second example of tectonic reactivation during the Cretaceous was observed in a 90 km^2 area faulted and folded in northeastern Campos Basin (Fig. 4). The deformation of pre-Aptian successions (up to 1200 m thick) is given by quite complex thrust-faulting and folding (Fig. 4c). The strata ranging in age from Albian to Turonian (up to 1000 m thick) were subjected to more regular folding with 1km wavelength and 100 m amplitude. Fold axes trending NE-SW show interference between Z and S sinuous patterns disposed *en-echelon* (Fig. 4a). The observed geometry is interpreted as a result of transpression caused by strike-slip reactivation of NNW-SSE basement fabric with right-lateral followed by left-lateral kinematics. The right-lateral Lower Cretaceous transpression represents the end of regional E-W extension still related to a regional loading with N-S SHmax, as in the example in Figure 3. The left-lateral Upper Cretaceous kinematics is related to the rotation of the regional SHmax to E-W caused by the ridge-push stress associated with the development of the South Atlantic mid-

oceanic spreading center. The structure was probably amplified by salt movement across the section and by a buttress effect of the basement high (Fig. 4c).

Paleogene Transpression

Next example is contiguous to the previous one in northeastern Campos Basin, and is characterized by a huge fold with 3 km half-wavelength and 300 m amplitude affecting up to 2700 m of Upper-Cretaceous to Paleogene strata (Fig. 5). The structure is interpreted as a fault-propagation fold (Suppe, 1985), and is clearly episodic with well constrained pre-kinematics, sin-kinematics and post-kinematics phases (Fig. 5c). The main deformation phase in the Eocene is indicated by onlap pattern and section growth (Fig. 5c). The fold was probably related to transpression associated with left-lateral reactivation of the NNW-SSE basement fabric during the Paleogene still under E-W maximum horizontal stress. It appears that transpression caused the inversion of Lower Albian normal faults (Fig. 5c).

Paleogene Transtension and Salt Tectonics

In central Campos Basin, 100 km to the south of previous example of transpression, the Paleogene reactivation event is characterized by normal faulting and section growth (Fig. 6). Most of the faults are restricted to Paleogene and older strata, and are concentrated above a basement high (Fig. 6b). The faults are planar and discontinuous, and the fault system is characterized by a dispersed distribution of orientations around NNE-SSW (Fig. 6a and 6c). The structure is interpreted as a negative flower caused by transtension (Woodcock and Schubert, 1994). The observed dispersion of fault orientation distribution was probably caused by the strong coupling between stress fields related to both basement reactivation and detached gravitational gliding above the basement high.

In a contiguous area just to the west of the flower structure is observed a detached listric fault-rollover system related to extensional salt tectonics (Fig.7). There is no strong coupling with basement reactivation because the area is sufficiently far from the influence of the basement high to the East (Fig. 7c). The fault orientation distribution is concentrated around NNW-SSE (Fig. 7d). The fault system was active from Albian to Recent time, but the imprint of Paleogene basement reactivation is indicated by extra section growth at the antithetic fault of the rollover system (Fig. 7b). Farther south, Paleogene magmatism was indicated by the volcanic structure showed above (Fig. 3c). Tectonic and magmatic reactivation along the Paleogene southeastern continental margin of Brazil was already well documented (Mizusaki and Mohriak, 1992; Chang et

al., 1992; Scarton, 1993; Almeida et al., 1996; Thompson et al., 1998; Thomaz Filho et al., 2005).

Neogene Transpression

Just to the west of the rollover system, still in central Campos Basin, the Neogene deformation is characterized by folding (Fig. 8). Observe that the anticline trending NE-SW is positioned exactly above the basement high (Fig. 8b). The structure is interpreted as an inversion fold that can be properly defined according to both the clay models of Eisenstad and Withjack (1995), and the conceptual model of Sibson (1995). The inversion of listric normal faults related to gravitational gliding extension active from Cretaceous to Paleogene was probably caused by transpression at the basement high during Neogene (Figs. 8c and 8d). The Neogene folding is quite synchronous with the extra displacement of Lower Miocene horizon at the main fault of the rollover system just to the West (Fig. 7b). As the fold plane lie at high angle to the main rollover fault, the folding and the extra extension can be associated with the same reactivation event.

Overview of structural analysis

The structural analysis of regional 3D seismic data indicates four periods of basement reactivation during the divergent margin phase in Campos Basin (Table 1). The timing of the Neogene and Paleogene deformation events is very well constrained. The kinematical interpretation and the involved strata indicate two phases of deformation during the Cretaceous, but the timing of the basement reactivation has a certain degree of uncertainty. The deformation is subtle and sparse, with open folds and moderate fault inversion observed mainly at regional and local basement highs. The reactivation has an overall strike-slip kinematical pattern.

Section Restoration

Section restoration is another relevant improvement of structural analysis in divergent margin basins because balanced cross-sections can generate quantitative chronological information about the kinematics of structural models (Nunns, 1991). In present work five sections of the extensional salt tectonic domain in Campos Basin were restored (sections HH', II', JJ', KK' and LL' in Fig. 2). The objective was to get a quantitative approach to the kinematical pattern of salt tectonics during the divergent margin phase in order to investigate if the synchronicity between basement and salt tectonic pulses suggested in central Campos Basin (Figs. 6, 7 and 8) is a general rule.

A very uniform restoration methodology was adopted because the objective was to get a general pattern. The five sections, defined in 3D seismic datasets, cut perpendicular to major detached extensional fault systems, and range from 18 km to 23 km in length (Figs. 9 to 13). It was assumed that the basement and the rift phase successions were not involved in the extensional deformation, and that the Aptian salt layer is a regional detachment surface. Eleven horizons were interpreted in each section ranging in age from Aptian to Recent (Table 2). The horizons were interpreted within a sequence-stratigraphy framework, and were tied to biostratigraphic markers that correspond to time intervals between 9 Ma and 19 Ma, except for the 1 Ma interval between the Sea Bottom and the Pleistocene at the top of the sections. The sections were restored in 9 steps, from Sea Bottom (0 Ma) to Albian (99 Ma). This time span corresponds to the divergent margin phase in Campos Basin. So that, the rift phase deformation was not restored in present work.

Restoration was performed with the RECON package (PETROBRAS/TECGRAF-PUCRJ - Brazil). It was used a standard sequential restoration procedure recommended for detached extensional sections, with isostatic adjustment and decompaction (Schultz-Ela, 1991; Schultz-Ela, 1992; Rowan, 1993). Isostatic adjustment was local, with a fine discrete mesh. Decompaction was computed by a power-law porosity function:

$$\phi = \phi_0 e^{-cz},$$

where ϕ is the compacted porosity, ϕ_0 is the initial decompacted porosity, c is the porosity decay parameter, and z is depth. The appropriated parameters for decompaction of shale, sandstone and carbonate in Campos Basin were defined by fitting the power-law function to a typical sonic porosity log (Table 3). For all sections, fault restoration was computed by an algorithm of movement along fault trace with antithetic shear strain in the moving block.

With the uniform procedure described above it was possible to restore quite well all the five sections with the assumption of detached deformation (Figs. 9 to 13). During the divergent margin phase in the restored sections from Campos Basin, since the Albian (99 Ma), total extension ranges from 2.78 km to 5.07 km, with rates between 28 m/Ma and 51 m/Ma (Table 4). Section JJ', positioned far from the basement highs has the lower extension rate (Table 4).

Taking a closer look to the extension measured in the sections since the Pleistocene (Table 5), it is possible to interpret the average total extension rate around 40 m/Ma (Table 4) as a background because the extensional process can reach up to 570 m/Ma

episodic peak rates (Section KK', Fig. 12). If this episodic behavior is extended for the divergent margin phase as a whole, and assuming that the deformation has been concentrated in time intervals around 1 Ma, it is possible to infer even higher peaks of extension rates (Fig. 14). The choice of the 1 Ma interval was based on the rates measured for the restored Pleistocene horizon, but is important to observe that the episodic nature of extension measured in the restored sections is independent of the time interval used to compute the extension rates. It also is important to observe that the deformation peaks are quite synchronous in the five restored sections, particularly the Paleogene and Neogene peaks. The same episodic and synchronous pattern is indicated by the conventional engineering strain curves of the five restored sections (Fig. 15). So that, section restoration indicates that the detached extension related to gravitational gliding above the Aptian salt in Campos Basin is characterized by an episodic and synchronous pattern. Four deformation peaks were observed during the divergent margin phase: Neogene, Paleogene, Upper Cretaceous, and Lower Cretaceous (Figs. 14 and 15). The detached extensional peaks can be well correlated with the basement reactivation events interpreted in 3D seismic surveys (Table 1).

Discussion

Campos Basin has been interpreted with the classic rift-drift detached model, characterized by shallow gravitational gliding above a quiet passive basement (Cobbold and Szatmari, 1991; Chang et al., 1992). The high elevations at the basin margin (Figs. 1 and 2) have been attributed to isostatic models related to rift shoulder rebound, escarpment retreat, mantle plume activity, and magmatic underplating (Weissel and Karner, 1989; Gallagher et al., 1995; Thompson et al., 1998; Thomaz Filho et al., 2005; Zalán and Oliveira, 2005). Conversely, there are already some reported suggestions of basement reactivations in the southeastern continental margin of Brazil (Assumpção, 1998; Gallagher and Brrown, 1999; Lima, 1999; Cobbold et al., 2001; Fetter et al., 2002; Saenz et al., 2003), as well as in other divergent margins (Stein et al., 1989; Withjack et al., 1995; Bezerra and Vita-Finzi, 2000; Cramez and Jackson, 2000; Hudec and Jackson, 2004). No matter the proposed model, previous work was all based in regional information, magnetic and gravimetric data, apatite fission-track analysis, sparse 2D seismic lines and local 3D seismic data. In present work, even considering the relevance of salt tectonics and isostatic processes, it is sustained, with three lines of evidence depicted from regional 3D seismic surveys and section restoration, that the

structural style of the divergent margin phase in Campos Basin may fit better a geodynamic model that encompass episodic tectonic reactivations.

The first line of evidence indicating basement reactivation came from Campos Basin regional sections and maps (Figs. 1 and 2). Regional data show that the present progradation front is controlled by the main structural highs of the basin. If the basement has been completely passive it hardly could control the present major sedimentation trend, which would be controlled by salt tectonic structures. In fact, the salt tectonics major domains are also controlled by the basement structure. Besides, there are depocenters beyond the structural highs during the Cretaceous and the Paleogene (Fig. 1), suggesting that the stronger sedimentation constraint was established in the Neogene.

The second group of evidence of basement tectonic activity came from the structural analysis of 3D seismic surveys. In section AA' it is observed that up to 1800 m of sediments were folded in a 500 km^2 area, probably during the Lower Cretaceous, at the beginning of the divergent margin phase (Fig. 3c). The kinematical interpretation can be questioned, but the folding of Lower Cretaceous taphrogenic and transitional successions can not be attributed to salt tectonics. Therefore, it is a concrete evidence of basement reactivation.

In section BB' it is possible to observe the regular folding of up to 1000 m of early divergent margin phase sediments (Fig. 4). The proposed kinematical model can be questioned, but the structure can hardly be attributed to salt tectonics, instead it can be better interpreted as a result of transpression caused by basement reactivation because the fold axes are sinuous and disposed *en echelon* (Woodcock and Schubert, 1994). The section CC', in the same area, shows a huge fault-propagation fold active during the Paleogene (Fig. 5). The episodic character and the timing of the structure are quite evident. As section CC' is contiguous to section BB' (Figs. 2, 4 and 5), it is reasonable to interpret both folding events as results of successive reactivations of the same basement structure. It seems unlikely that both structures (sections BB' and CC') had been generated by one single Paleogene event because affected strata and structural style are very different.

Sections DD', FF' and GG' show a transition from extension during the Paleogene to compression during the Neogene above a basement high (Figs. 2, 6 and 8). Both structures can hardly be attributed to salt tectonics. They can be better interpreted as a result of stress field rotation, with basement transtension followed by transpression. In

the same area, but sufficiently far from the basement high it is possible to observe a listric fault-rollover system in section EE' (Figs. 2 and 7). The rollover is a typical salt tectonic structure that was active since the Albian. Nevertheless it shows the effects of both Paleogene and Neogene basement reactivations (Fig. 7).

The third group of evidence about the relevance of basement tectonics came from balanced cross-sections. Section restoration of five major detached structures indicates that the extensional process have been episodic and synchronous during the divergent margin phase in Campos Basin. Four main extension events were defined: Neogene, Paleogene, Upper Cretaceous, and Lower Cretaceous. These events can be well correlated with the basement reactivation events interpreted in regional 3D seismic datasets (Table 1). This correlation suggests that salt tectonics have been controlled by basement tectonics during the divergent margin phase in Campos Basin. Additionally, the general correlation pattern is reinforced by a few local details:

(i) The less deformed detached system (Section JJ') is positioned relatively far from the main basement highs (Figs. 2, 11, and 14; Tables 4 and 5).

(ii) In southern Campos Basin, Section HH' show no extension during Lower Cretaceous, at the same time of the folding event observed in section AA' (Figs. 2, 3, 9, and 14). As both structures trend NE-SW (Figs. 3 and 9), the detached extension was inhibited by the compressive event.

(iii) In central Campos Basin, the Neogene extension rate is relatively low in section II', during the inversion event interpreted in sections FF' and GG' (Figs. 2, 8, 10, and 14). Again, as both structures trend NE-SW (Figs. 8 and 10), the detached extension was subdued by the compressive inversion.

Considering the presented field evidence of basement reactivation in Campos Basin, it is important to discuss about an adequate geodynamic model for the evolution of divergent margins. According to the Wilson Cycle model, continental rift systems eventually evolve to mid-ocean spreading centers at a new plate border, leaving behind passive continental margins at intraplate position. The evolution of the basement in divergent margin basins is characterized by cooling (Sleep, 1971; Mckenzie, 1978), and by a transition from extension to compression (Le Pichon and Sibuet, 1981; Withjack et al., 1998). Possible sources of compression are related to ridge push (Bott, 1992), to spreading stresses (Stein et al., 1989), to flexural compressive stresses associated with sediment loading (Stein et al., 1989), and to the remote effect of active margin processes (Ziegler et al., 1995). Additionally, the crust is thin, weak and prone of basement shear

zones bellow divergent margin basins (Mckenzie, 1978; Le Pichon and Barbier, 1987; Lister et al., 1991). So that, the tectonic reactivation in divergent margin basins is not only possible, actually it seems to be expected, as it has been suggested in other intraplate settings (Storti et al., 2003).

Conclusions

Campos Basin was subjected to episodic tectonic reactivations during the divergent margin phase, from Albian to Recent time. The structural style indicates a strike-slip kinematical pattern for the reactivations. Deformation has been concentrated above main structural highs and probably reflects the coupling between divergent margin sediments and active basement shear zones.

The interference between basement tectonics and detached gravitational gliding inferred from the interpretation of 3D seismic data was confirmed by quantitative information obtained from section restoration of detached extensional structures. The detached extension, previously attributed exclusively to salt tectonics, is also episodic and synchronous in Campos Basin, and the extensional events can be well correlated with basement tectonic pulses interpreted in regional 3D seismic datasets: Neogene, Paleogene, Upper Cretaceous, and Lower Cretaceous.

The basement highs control also major basin features like the present front of Neogene progradation and the salt tectonic domains. So that it is possible to conclude that basement tectonics has been exerting an important control on the structural and stratigraphic evolution of the divergent margin phase in Campos Basin. Additionally, it is suggested that basement tectonic reactivations can be as relevant as isostatic adjustments and detached tectonics on the evolution of divergent margin settings, because the basement involved structures observed in Campos Basin can be attributed to general geodynamic processes.

Acknowledgements

Present work was developed as part of a doctorate research project at Geosciences Graduate Program of Rio Grande do Sul Federal University (UFRGS – Porto Alegre, Brazil) sponsored by Petrobras. I acknowledge the supervision by Luiz Fernando De Ros, Carlos Bruhn, and Cláudio Lima. I wish to thank also Anderson Moraes, Maria José Oliveira, and Mario Neto de Araujo from Petrobras Research Center, Eliane de Freitas Ferreira from Petrobras Documentation Center, Marcio Santi and André Derraik from Tecgraf/PUCRJ, and François Lafferriére and Mathieu Moriss from Paradigm-Gocad. A very special thank to my kids Pedro and Isabel, and to my wife Marcella, with love.

References

Almeida, F.F.M., Carneiro, C.D.R., and Mizusaki, A.M.P., 1996. Correlação do magmatismo das bacias da margem continental brasileira com o das áreas emersas adjacentes. Rev. Bras. Geoc., 26, 125-138.

Assumpção, M., 1998. Seismicity and stresses in the Brazilian divergent margin. Bull. Seismol. Soc. Am., 88, 160-169.

Bezerra, F.H.R. and Vita-Finzi, C., 2000. How active is a divergent margin? Paleoseismicity in northeastern Brazil. Geology, 28, 591-594.

Bott, M.H., 1992. The stress state regime associated with continental break-up, in: B.C. Storey, T. Alabaster, and R.J. Pankhurst (Eds.), Magmatism and the Causes of Continental Break-up. Geol. Soc. London Spec. Publ., 68, pp. 125-136.

Bruhn, C.H.L., and Walker, R.G., 1995. High-resolution stratigraphy and sedimentary evolution of coarse-grained canyon-filling turbidites from the Upper-Cretaceous transgressive megasequence, Campos Basin, offshore Brazil. J. Sed. Res., 65, 426-442.

Caddah, L.F.G., Alves, D.B., and Mizusaki, A.M.P., 1998. Turbidites associated with bentonites in the Upper-Cretaceous of the Campos Basin, offshore Brazil. Sed. Geol., 115, 175-184.

Cartwright, J. and Huuse, M., 2005. 3D seismic technology: the geological 'Hubble'. Basin Res., 17, 1-20.

Chang, H.K., Kowsmann, R.O., Figueiredo, A.M.F., and Bender, A.A., 1992. Tectonics and stratigraphy of the East Brazil Rift system: an overview. Tectonophys., 213, 97-138.

Chopra, S., and Marfurt, K.J., 2006. Seismic Attribute Mapping of Structure and Stratigraphy. SEG/EAGE Distinguished Instructor Series, 9.

Cobbold, P.R., Meisling, K.E., and Mount, S.V., 2001. Reactivation of an obliquely-rifted margin: Campos and Santos basins, SE Brazil. AAPG Bull., 85, 1925-1944.

Cobbold, P.R., and Szatmari, P., 1991. Radial gravitational gliding on divergent margins. Tectonophys., 188, 249-289.

Cramez, C., and Jackson, M.P.A., 2000. Supperposed deformation straddling the continental-oceanic transition in deep-water Angola. Mar. Petr. Geol., 17, 1095-1109.

Demercian, S., Szatmari, P., and Cobbold, P.R., 1993. Style and pattern of salt diapirs due to thin-skinned gravitational gliding, Campos and Santos basins, offshore Brazil. Tectonophys., 228, 393-433.

Dias, J.L., Scarton, J.C., Guardado, L.R., Esteves, F.R., and Carminatti, M., 1990. Aspectos da evolução tectono-sedimentar e da ocorrência de hidrocarbonetos na Bacia de Campos, in: G.P. Raja-Gabaglia and E.J. Milani (Eds.), Origem e Evolução de Bacias Sedimentares. Petrobras, Rio de Janeiro, pp. 333-360.

Doust, H., and Omatsola, E., 1989. Niger Delta, in: J.D. Edwards and P.A. Santogrossi (Eds.), Divergent Margin Basins. AAPG Memoir, 48, pp. 201-238.

Eisenstad, G., and Withjack, M.O., 1995. Estimating inversion: results from clay models, in: J.G. Buchanan and P.G. Buchanan (Eds.), Basin Inversion. Geol. Soc. London Spec. Publ., 88, pp. 119-136.

Falvey, D.A., 1974. The development of continental margins in plate tectonics theory. Australian Petr. Expl. Ass. Journal, 14, 95-106.

Fetter, M., Lima, C.C., Silva, A.T., Machado, D., Castro, D.D., and Adams, T., 2002. Interaction between salt related extension and basement strike-slip reactivation in northern Campos Basin, deepwater Brazil. SEG 72nd Ann. Meet., Salt Lake City, Exp. Abstr., pp. 2413-2416.

Gallagher, K., and Brown, R., 1999. The Mesozoic denudation history of the Atlantic margins of southern Africa and southeast Brazil and the relationship to offshore sedimentation, in: N.R. Cameron, R.H. Bate, and V.S. Clure (Eds.), The Oil and Gas Habitats of the South Atlantic. Geol. Soc. London Spec. Publ., 153, pp. 41-53.

Gallagher, K., Hawkesworth, C.J., and Mantovani, M.S.M., 1995. Denudation, fission track analysis and the long-term evolution of divergent margin topography: application to southeast Brazilian margin. J. South. Am. Earth Sci., 8, 65-77.

Gibbs, A.D., 1983. Balanced cross-section construction from seismic sections in areas of extensional tectonics. J. Struct. Geol., 5, 153-160.

Hawkesworth, C.J., Gallagher, K., Kelley, S., Mantovani, M., Peate, D.W., Regelous, M., and Rogers, N.W., 1992. Paraná magmatism and the opening of the South Atlantic, in: B.C. Storey, T. Alabaster, and R.J. Pankhurst (Eds.), Magmatism and the Causes of Continental Break-up. Geol. Soc. London Spec. Publ., 68, pp. 221-240.

Hesthammer, J. and Fossen, H., 1997. Seismic attribute analysis in structural interpretation of the Gulfalks Field, northern North Sea. Petrol. Geosc., 3, 13-26.

Hudec, M.R. and Jackson, M.P.A., 2004. Regional restoration across the Kwanza Basin, Angola: Salt tectonics triggered by repeated uplift of a metastable divergent margin. AAPG Bull., 88, 971-990.

Jackson, M.P.A., 1995. Retrospective salt tectonics, in: M.P.A. Jackson, D. G. Roberts and S. Snelson (Eds.), Salt Tectonics: A Global Perspective. AAPG Memoir, 65, pp. 201-238.

Le Pichon, X., and Barbier, F., 1987. Divergent margin formation by low-angle faulting within the uuper crust. Tectonics, 6, 133-150.

Le Pichon, X., and Sibuet, J.C., 1981. Divergent margins: A model of formation. J. Geophys. Res., 86, 3708-3720.

Lister, G.S., Etheridge, M.A., and Symonds, P.A., 1991. Detachment models for the formation of passive continental margins. Tectonics, 10, 1038-1064.

Lima, C.C., 1999. Expressions topographiques et structurales de l´etat de compression généralisée au sein de la plaque Sud-Américaine. PhD Thesis. Univ. Rennes 1, France.

McKenzie, D., 1978. Some remarks on the development of sedimentary basins. Earth Planet. Sci. Lett., 40, 25-32.

Michon, L., and Sokoutis, D., 2005. Interaction between structural inheritance and extension direction during graben and depocenter formation: an experimental approach. Tectonophys., 409, 125-146.

Mizusaki, A.M.P., and Mohriak, W.W., 1992. Sequências vulcano-sedimentares na região da plataforma continental de Cabo Frio (RJ). Anais 37^{o}. Congr. Soc. Bras. Geol., pp. 52-56.

Mizusaki, A.M.P., Petrini, R., Bellieni, G., Comin-Chiaramonti, P., Dias, J., De Min, A., and Piccirillo, E.M., 1992. Basalt magmatism along the passive continental margin of SE Brazil (Campos Basin). Contrib. Min. Petrol., 111, 143-160.

Mohriak, W.U., and Dewey, J.F., 1987. Deep seismic reflectors in the Campos Basin, offshore Brazil. Geophys. J. R. Astron. Soc., 89, 133-140.

Nunns, A.G., 1991. Structural restoration of seismic and geologic sections in extensional regimes. AAPG Bull., 75, 278-297.

Ponte, F.C., and Asmus, H.E., 1976. Brazilian marginal basins: Current state of knowledge. Anais Acad. Bras. Ciências, 48, 215-239.

Rabinowitz, P.D., and LaBrecque, J., 1979. The Mesozoic South Atlantic Ocean and evolution of its continental margins. J. Geophys. Res., 84, 5973-6002.

Rowan, M.G., and Kligfield, R., 1989. Cross section restoration and balancing as an aid to seismic interpretation in extensional terranes. AAPG Bull., 73, 955-966.

Rowan, M.G., 1993. A systematic technique for the sequential restoration of salt structures. Tectonophys., 228, 331-348.

Saenz, C.A.T., Hackspacker, P.C., Hadler Neto, J.C., Iunes, P.J., Guedes, S., Ribeiro, L.F.B., and Paulo, S.R., 2003. Recognition of Cretaceous, Paleocene, and Neogene tectonic reactivation through apatite fission-track analysis in Precambriam areas of southeast Brazil: association with the opening of the south Atlantic ocean. J. South. Am. Earth Sci., 15, 765-774.

Scarton, J.C., 1993. Análise estratigráfica do Terciário Inferior da Bacia de Campos – Uma visão moderna (com ênfase na região dos campos petrolíferos de Corvina e Malhado). PhD Thesis. UFRGS, Porto Alegre, Brazil.

Schultz-Ela, D.D., 1991. Pratical restoration of extensional cross-sections. Geobyte, 6, 14-23.

Schultz-Ela, D.D., 1992. Restoration of cross-sections to constrain deformation processes of extensional terranes. Mar. Petrol. Geol., 9, 372-388.

Sibson, R.H., 1995. Selective fault reactivation during basin inversion: potential for fluid redistribution through fault-valve action, in: J.G. Buchanan and P.G. Buchanan (Eds.), Basin Inversion. Geol. Soc. London Spec. Publ., 88, pp. 3-19.

Sleep, N.H., 1971. Thermal effects of the formation of Atlantic continental margins by continental break up. Geophys. J. R. Astron. Soc., 24, 325-350.

Stein, S., Cloetingh, S., Sleep, N.H., and Wortel, R., 1989. Divergent margin earthquakes, stresses, and rheology, in: S. Gregersen and PW Basham (Eds.), Earthquakes at North-Atlantic Divergent margins: Neotectonics and Post Glacial Rebound. Kluwer Academic, pp. 231-259.

Storti, F., Holdsworth, R.E., and Salvini F., 2003. Intraplate strike-slip deformation belts, in: F. Storti, R.E. Holdsworth, and F. Salvini (Eds.), Intraplate Strike-slip Deformation Belts. Geol. Soc. London Spec. Publ., 210, pp. 1-14.

Thomaz Filho, A., de Cesaro, P., Mizusaki, A.M.P., and Leão, J.G., 2005. Hot spot volcanic tracks and their implications for South American plate motion, Campos Basin (Rio de Janeiro state), Brazil. J. South Am. Earth Sci., 18, 383-389.

Thompson, R.N., Gibson, S.A., Mitchell, J.G., Dickin, A.P., Leonardos, O.H., Brod, J.A., and Greenwood, J.C., 1998. Migrating Cretaceous-Eocene magmatism in the Serra do Mar alkaline province, SE Brazil: melts from the deflected Trindade mantle plume. J. Petrol., 39, 1493-1526.

Weissel, J.K., and Karner, G.D., 1989. Flexural uplift of rift flancs due to mechanical unloading of the lithosphere during extension. J. Geophys. Res., 94, 13919-13950.

White, R. and McKenzie, D., 1989. Magmatism at rift zones: The generation of volcanic continental margins and flood basalts. J. Geophys. Res., 94, 7685-7729.

Withjack, M.O., and Olsen, P.E., Schlische, R.W., 1995. Tectonic evolution of the Fundy rift basin, Canada: Evidence of extension and shortening during divergent margin development. Tectonics, 14, 390-405.

Withjack, M.O., Schlische, R.W., and Olsen, P.E.,1998. Diachronous rifting, drifting, and inversion on the divergent margin of central eastern North America: An analogue for other divergent margins. AAPG Bull., 82, 817-835.

Woodcock, N.H., and Schubert, C., 1994. Continental strike-slip tectonics, in: P. Hancock (Ed.), Continental Deformation. Oxford Pergamon Press, pp. 251-263.

Zalán, P.V., and Oliveira, J.A.B., 2005. Origem e evolução estrutural do Sistema de Riftes Cenozóicos do Sudeste do Brazil. Bol. Geoc. Petrobras, 13, 269-300.

Ziegler, P.A., Cloetingh, S., and van Wees, J.D., 1995. Dynamics of intra-plate compressional deformation: the Alpine foreland and other examples. Tectonophys., 252, 7-59.

List of Tables

List of Figures

Figure 5 – (a) Structural map of Santonian horizon showing an anticline trending NE-SW and plunging to NE. (b) 3D perspective of the anticline. (c) Depth-converted seismic section showing a huge fold (3 km half-wavelength; around 300 m amplitude); insert show section position (see the regional position of section CC' in Fig. 2). Up to 2700 m of Upper Cretaceous and Paleogene strata where folded during the Eocene. The main deformation phase is indicated by onlap and section growth in the Eocene. The structure is interpreted as a fault propagation fold associated with inversion of Albian listric normal faults. Inversion was probably caused by transpression along NW-SE basement fabric at northeastern Campos Basin. The structure is contiguous to the folding area of Figure 4.

Figure 6 – (a) Semblance map of Maastrichtian horizon showing a NNE-SSW fault system. (b) Depth-converted seismic section of the fault system and insert with section position (see the regional position of section DD' in Fig. 2). Observe fault activity and section growth during the Paleogene indicated by black bars. (c) Stereonet contour plot of the faults mapped in the area showing a quite dispersed distribution (188 fault poles). Faulting is interpreted as a negative flower structure associated with transtension caused by reactivation of NNE-SSW basement fabric.

Figure 7 – (a) Semblance map of Lower Miocene horizon showing a NNW-SSE fault system. (b) Depth-converted seismic section showing the listric fault-rollover system and insert with section position (see the regional position of section EE' in Fig. 2). Observe that the system have been active from Albian to Recent time, but there are extra section growth during Paleogene (black bar along antithetic fault), and Neogene (black bar along main rollover fault). (c) 3D perspective showing the fault system above a basement low. (d) Stereonet contour plot of the faults mapped in the area showing a concentrated distribution (106 fault poles). The structure can be interpreted as a listric fault-rollover system related to extensional salt tectonics.

Figure 8 – (a) Structural map of Lower Miocene horizon showing an anticline trending NE-SW. (b) 3D perspective of the structure and insert with position of the area in central Campos Basin (see the regional position of sections FF' and GG' in Fig. 2). (c) Depth-converted seismic sections showing an inversion fold. Observe that Paleogene depocenters (indicated by black bars) were inverted during Neogene. Fold axial plane is vertical and oriented at N40E. Folding was probably caused by transpression related to reactivation of basement fabric at structural highs.

Figure 9 – Restoration steps of Section HH'. Local position of the section is indicated in the semblance map. Regional position of the section is indicated in Figure 2.

Figure 10 - Restoration steps of Section II'. Local position of the section is indicated in the semblance map. Regional position of the section is indicated in Figure 2.

Figure 11 - Restoration steps of Section JJ'. Local position of the section is indicated in the semblance map. Regional position of the section is indicated in Figure 2.

Figure 12 - Restoration steps of Section KK'. Local position of the section is indicated in the semblance map. Regional position of the section is indicated in Figure 2.

Figure 13 - Restoration steps of Section LL'. Local position of the section is indicated in the semblance map. Regional position of the section is indicated in Figure 2.

Figure 14 – Curves of extension rate vs time for the five sections restored in Campos Basin. Extension rates were computed for a constant 1 Ma deformation interval. Observe the episodic character of the extensional process defined by the synchronous peaks of extension rates. The extension peaks can be well correlated with the basement reactivation events interpreted in 3D seismic surveys. Observe also that the choice of a larger deformation interval can change the extension rate values, but not the episodic nature of the curves.

Figure 15 - Curves of conventional engineering strain vs time for the five sections restored in Campos Basin.

Age	Structural Style	Kinematics	Position in the basin
Neogene	Inversion fold	Transpression or compression	Center
Paleogene	Fault-propagation fold; negative flower	Transpression; transtension	Northeastern; Center
Upper Cretaceous	Regular folds with sinuous axes	Transpression	Northeastern
Lower Cretaceous	Regular folds with sinuous axes	Transpression	South; Northeastern

Table 1

Horizon	Age (Ma)
Sea Bottom	0
Pleistocene	1
Middle Miocene	12
Lower Miocene	21
Lower Oligocene	30
Eocene	47
Maastrichtian	65
Santonian	84
Albian	99
Salt Top	112
Salt Base	120

Table 2

Lithology	ϕ_0	c
shale	0.60	0.38
sandstone	0.56	0.27
carbonate	0.46	0.33

Table 3

Section	Original Length (km)	Total Extension (km)	Extension Rate (m/Ma)
HH’	18.93	5.07	51
II’	14.62	3.38	34
JJ’	19.22	2.78	28
KK’	18.93	4.07	41
LL’	13.87	4.13	42
Average	17.11	**3.89**	**39**
StdDev	-	**0.77**	**7.8**

Table 4

Section	Pleistocene Extension Rate (m/Ma)
HH’	230
II’	270
JJ’	50
KK’	570
LL’	170
Average	**258**
StdDev	**172.8**

Table 5

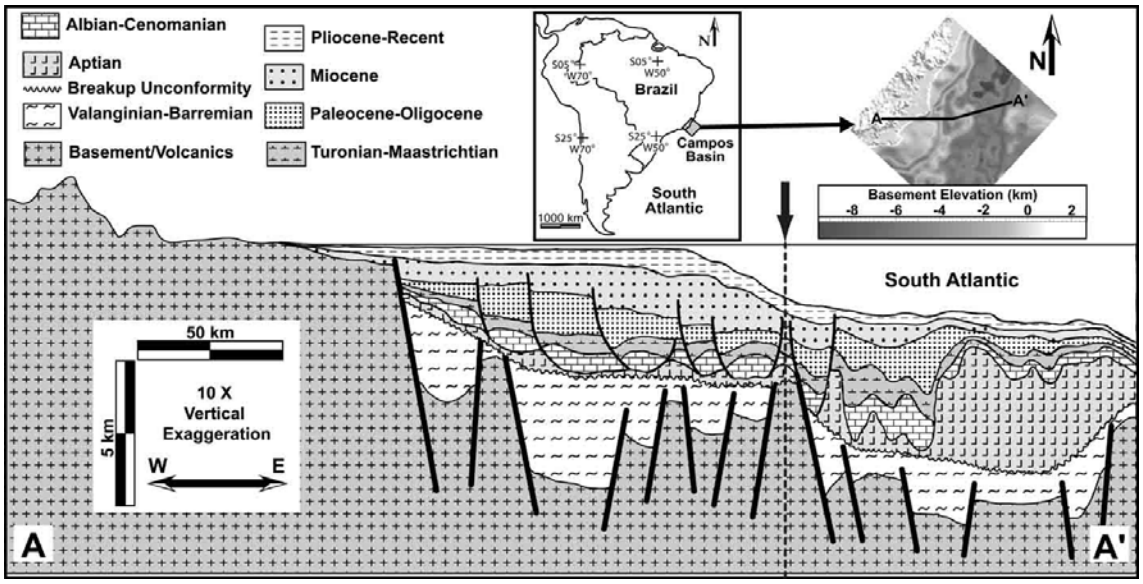

Figure 1

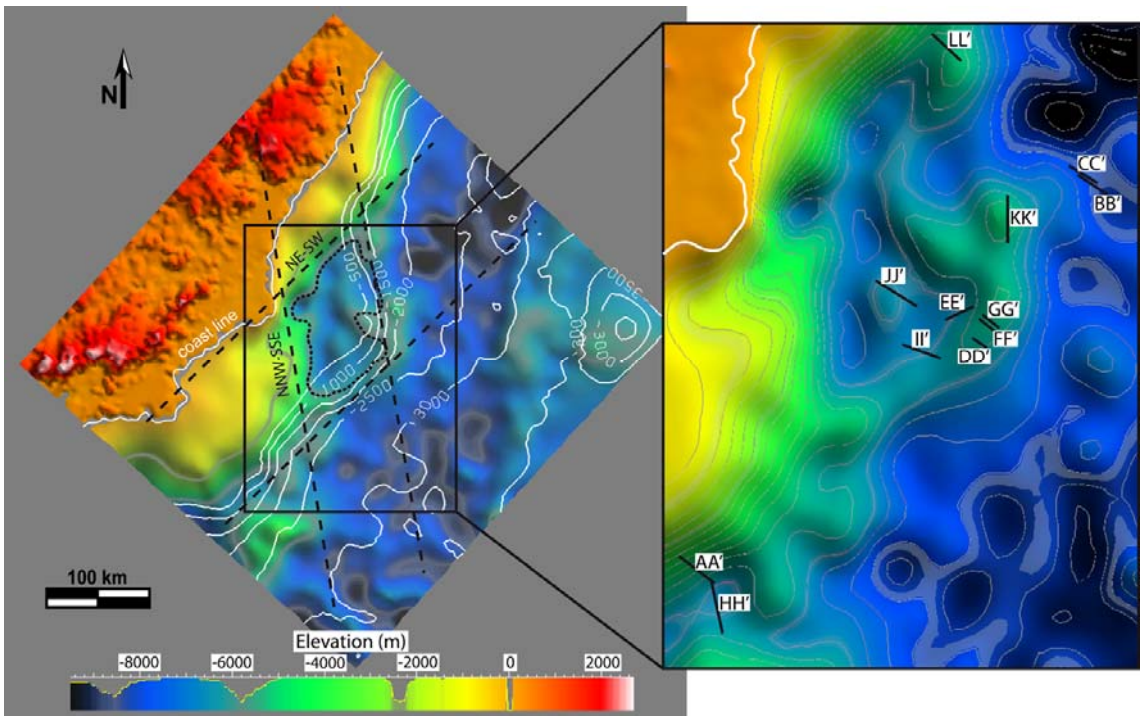

Figure 2

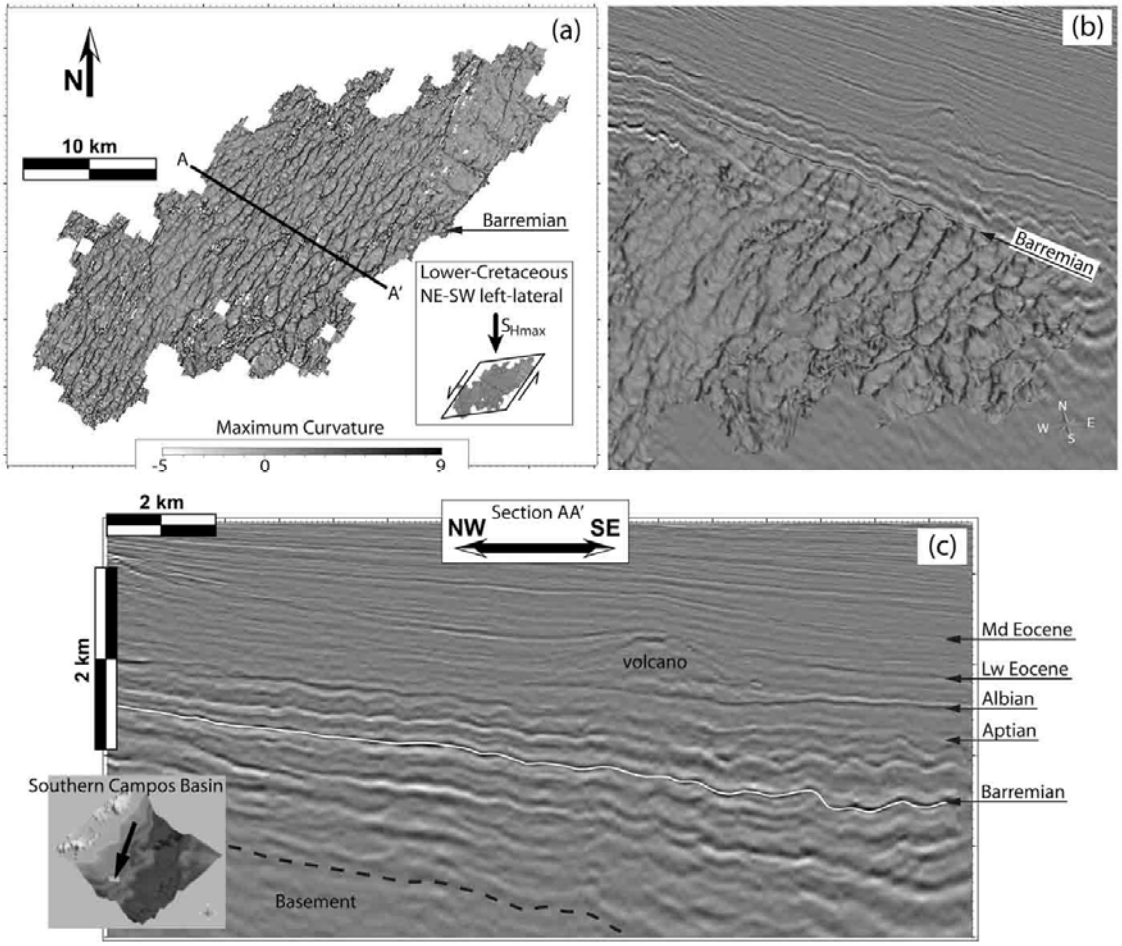
(a)
N
10 km
A
A'
Barremian
Lower-Cretaceous
NE-SW left-lateral
S_{Hmax}
Maximum Curvature
-5
0
9
(b)
Barremian
N
W
E
S
2 km
NW
Section AA'
SE
(c)
2 km
volcano
Md Eocene
Lw Eocene
Albian
Aptian
Barremian
Southern Campos Basin
Basement

Figure 3

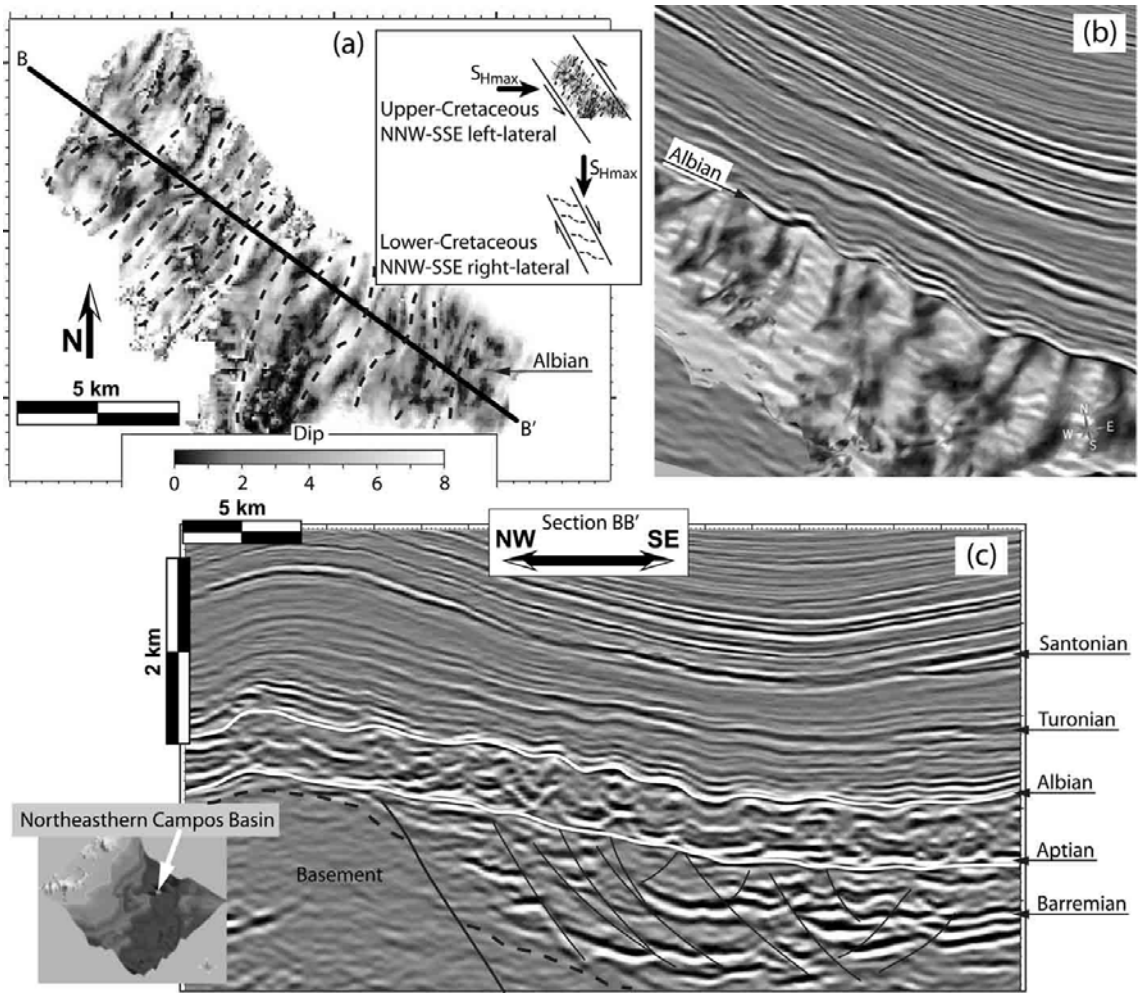
(a)
B
B′
N
5 km
Albian
Dip
0
2
4
6
8
S_{Hmax}
Upper-Cretaceous
NNW-SSE left-lateral
S_{Hmax}
Lower-Cretaceous
NNW-SSE right-lateral
(b)
Albian
5 km
2 km
NW
Section BB′
SE
(c)
Santonian
Turonian
Albian
Aptian
Barremian
Basement
Northeasthern Campos Basin

Figure 4

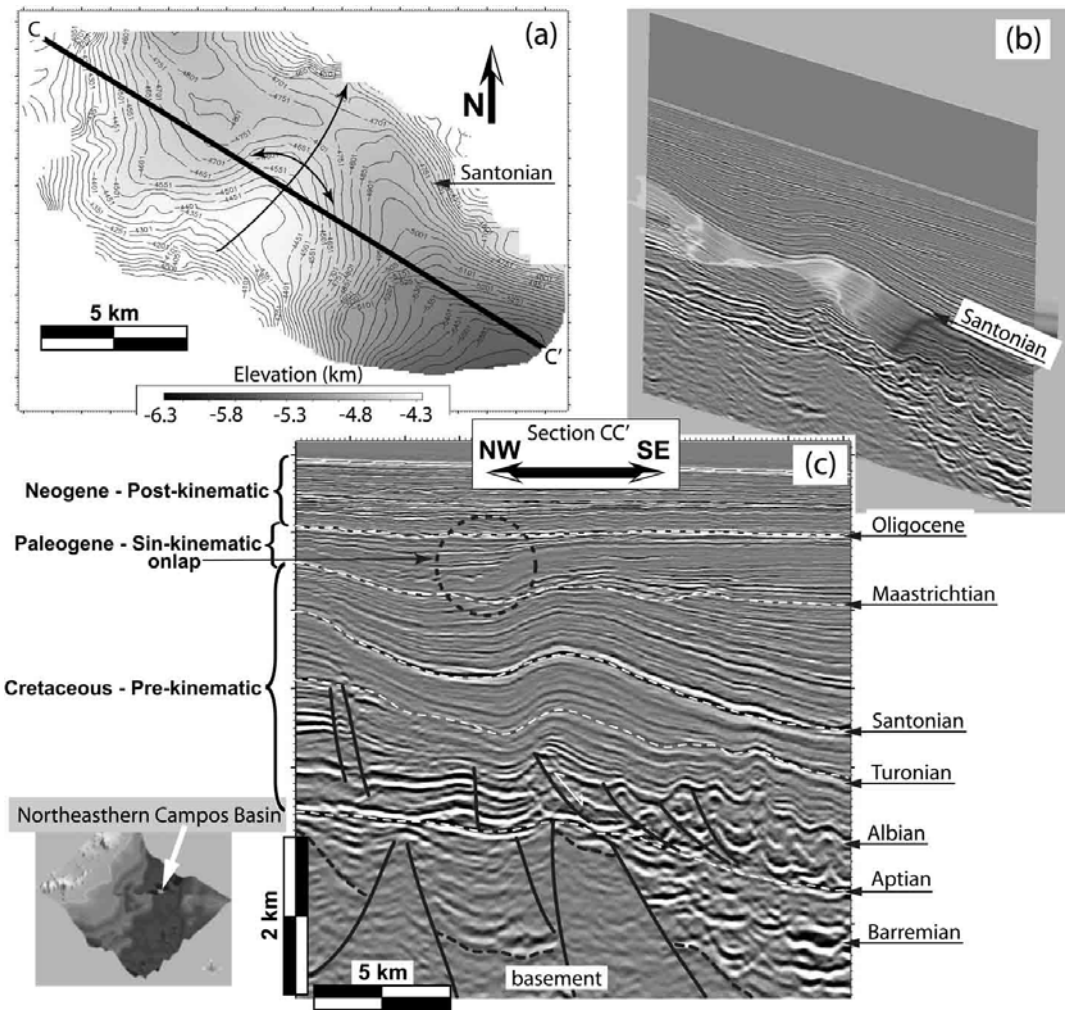
C
(a)
N
Santonian
5 km
C'
Elevation (km)
-6.3 -5.8 -5.3 -4.8 -4.3
(b)
Santonian
Section CC'
NW
SE
(c)
Neogene - Post-kinematic
Paleogene - Sin-kinematic onlap
Cretaceous - Pre-kinematic
Oligocene
Maastrichtian
Santonian
Turonian
Albian
Aptian
Barremian
Northeasthern Campos Basin
2 km
5 km
basement

Figure 5

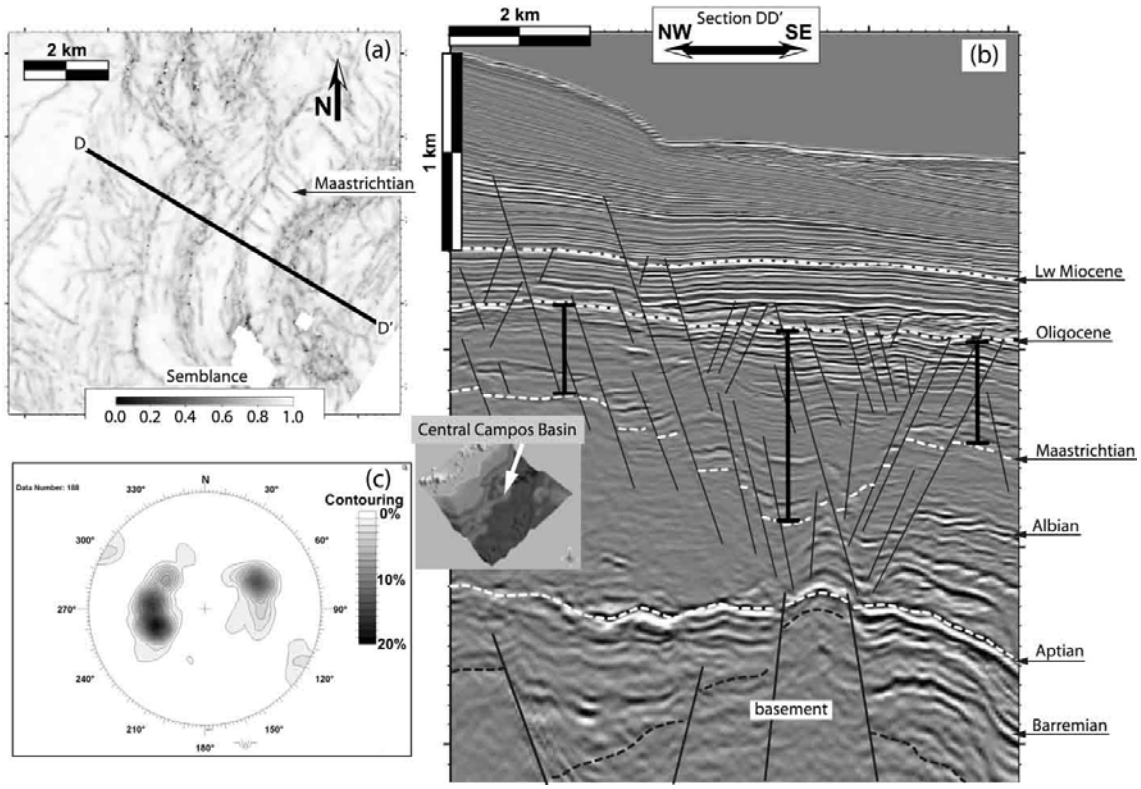

Figure 6

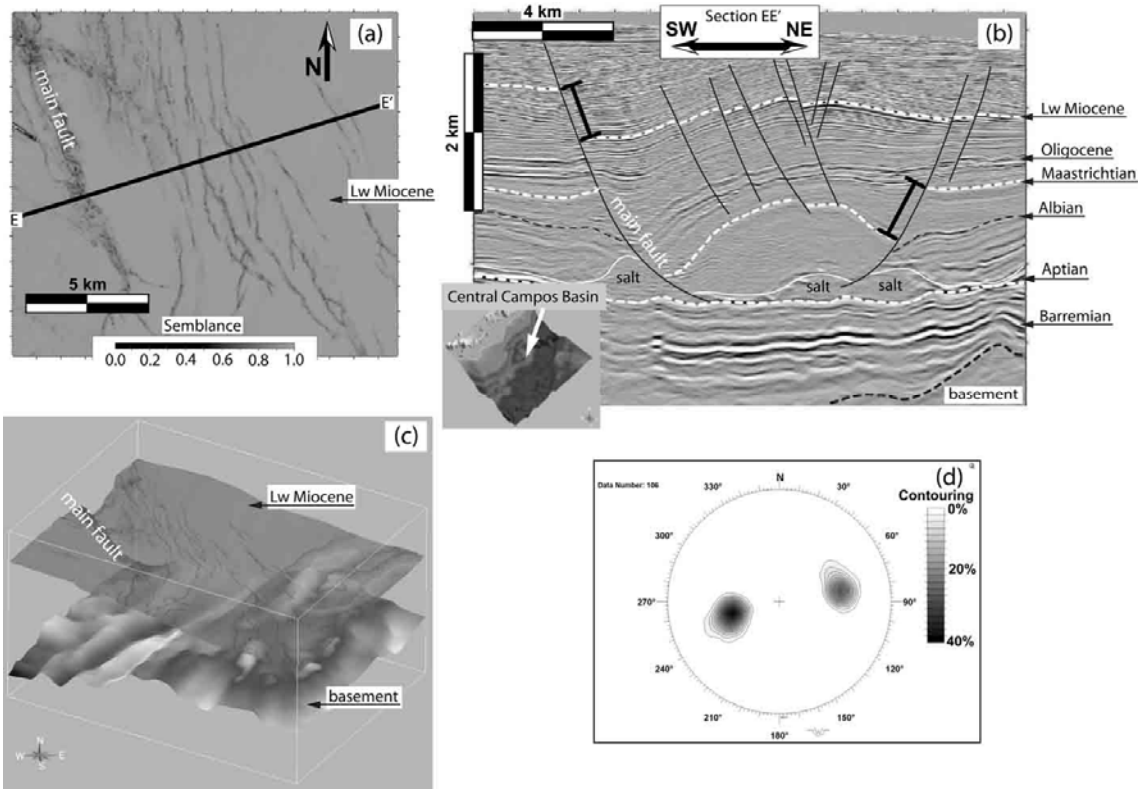

Figure 7

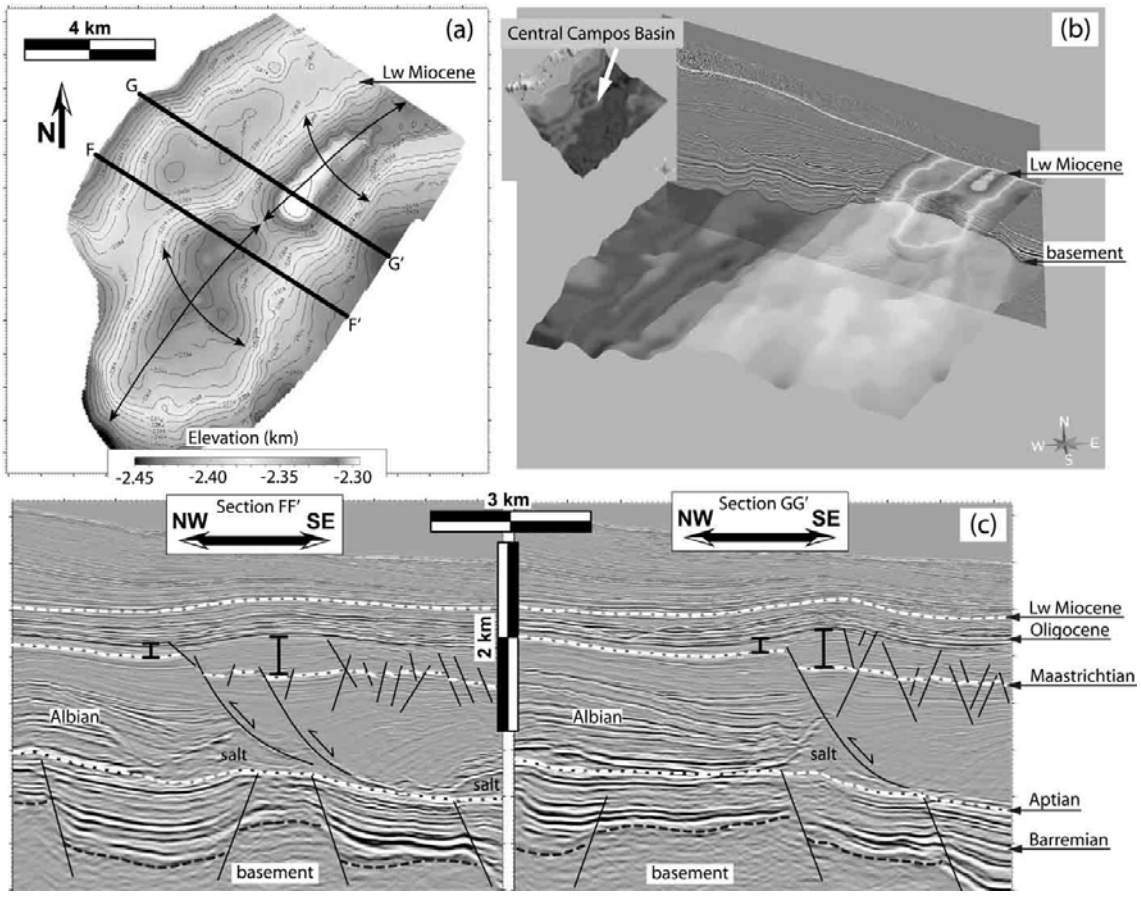

Figure 8

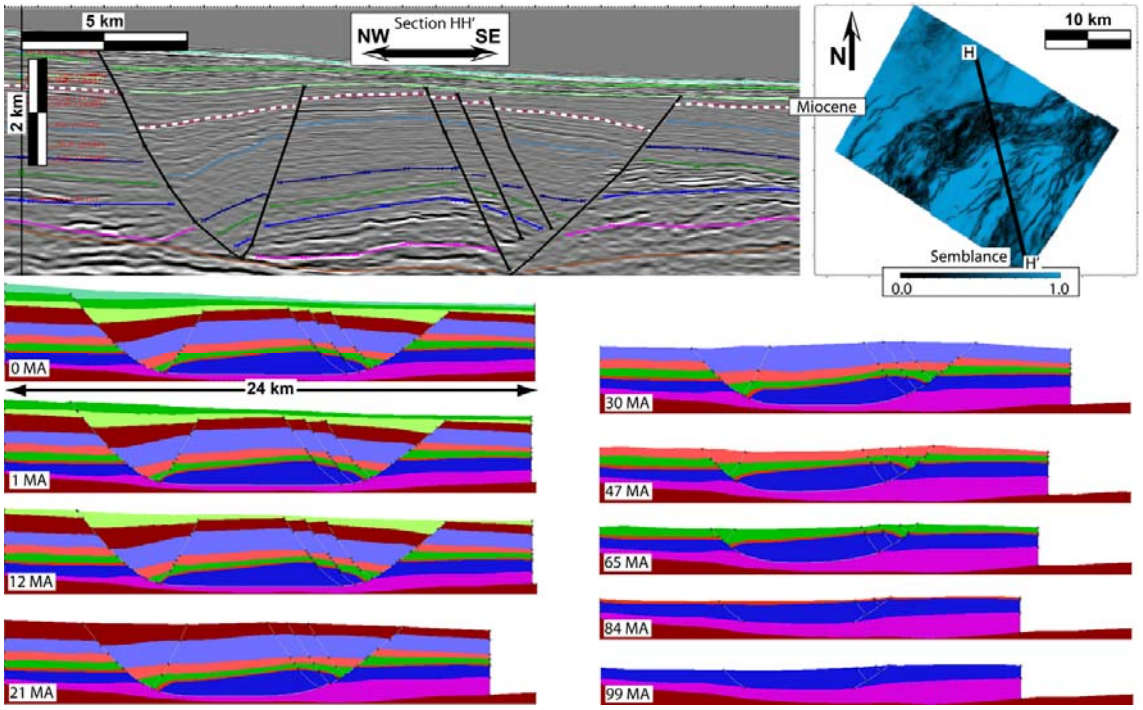

Figure 9

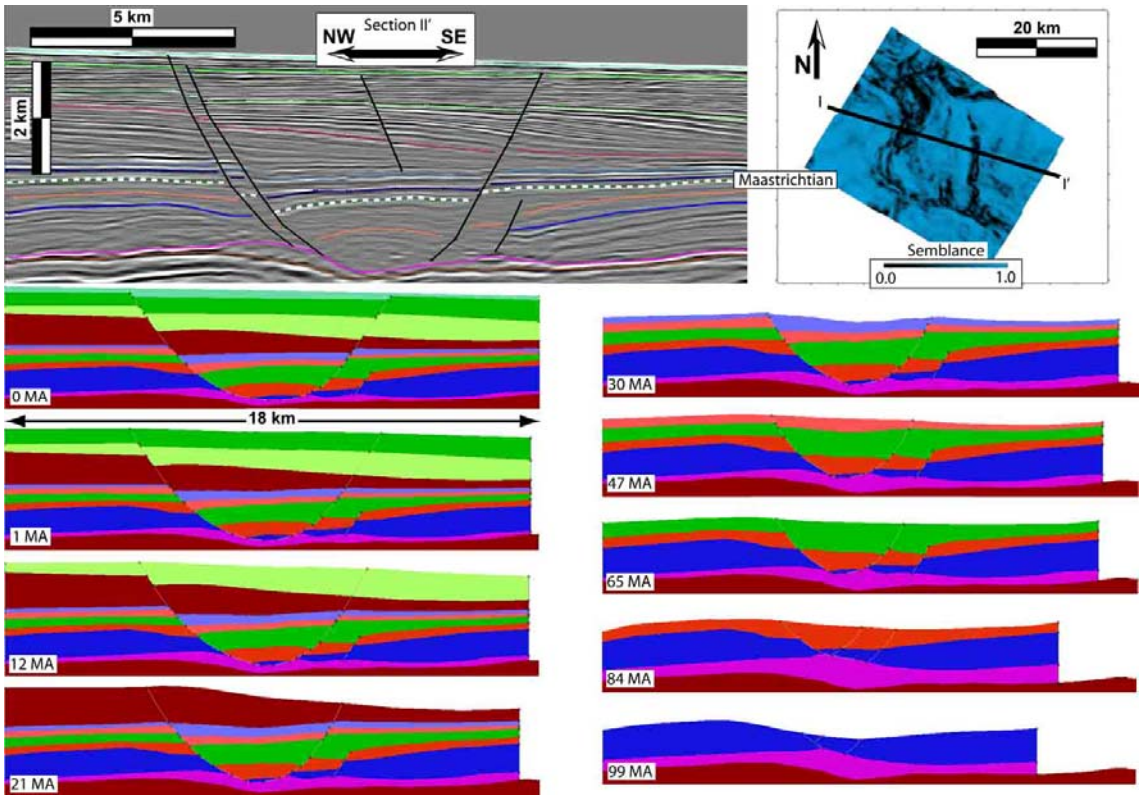

Figure 10

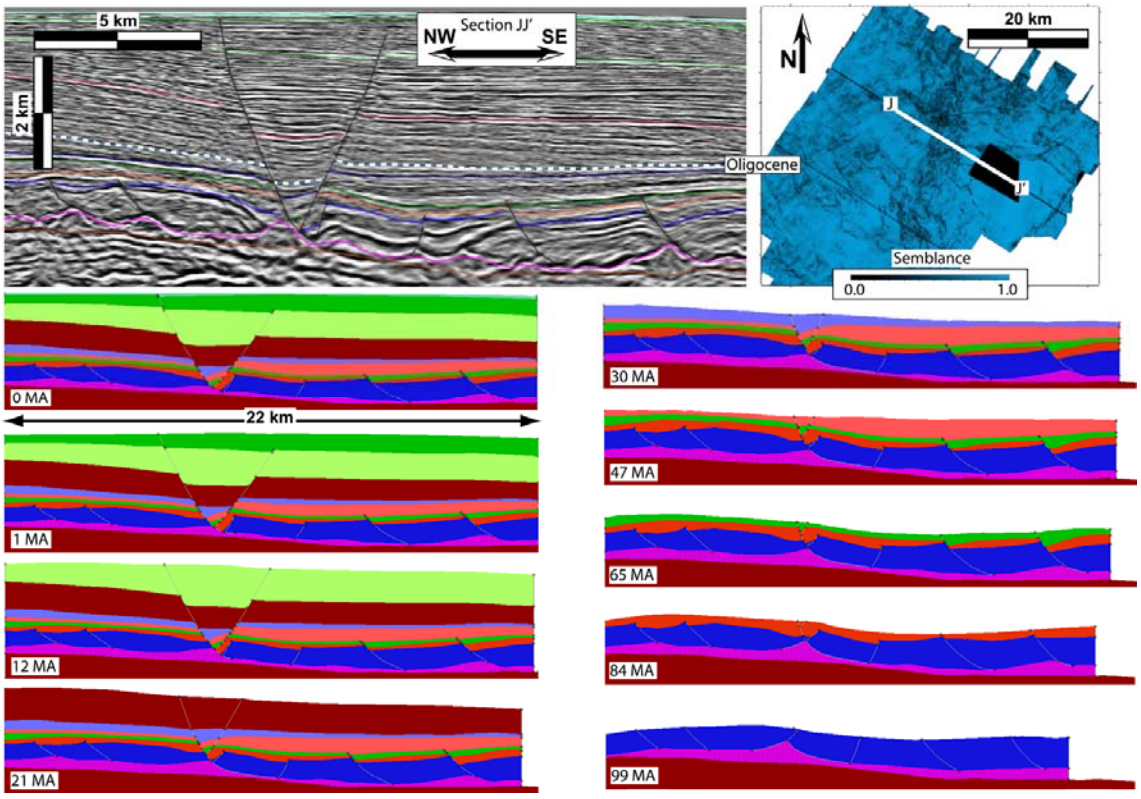

Figure 11

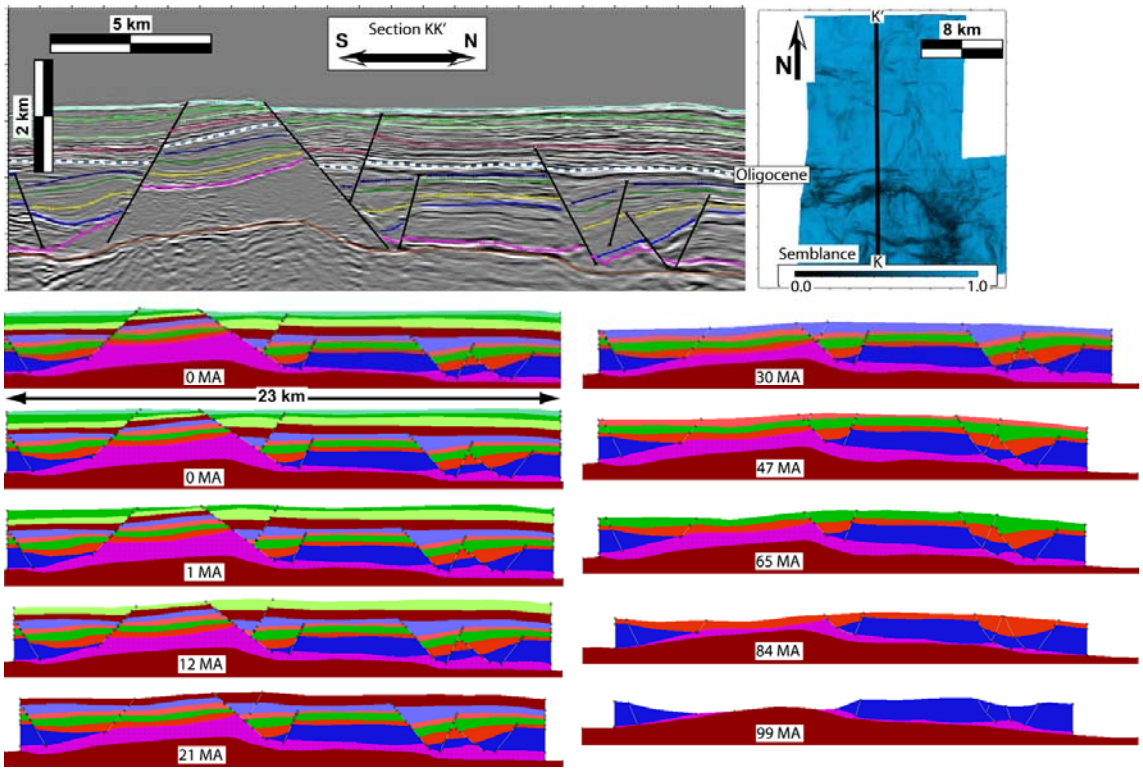

Figure 12

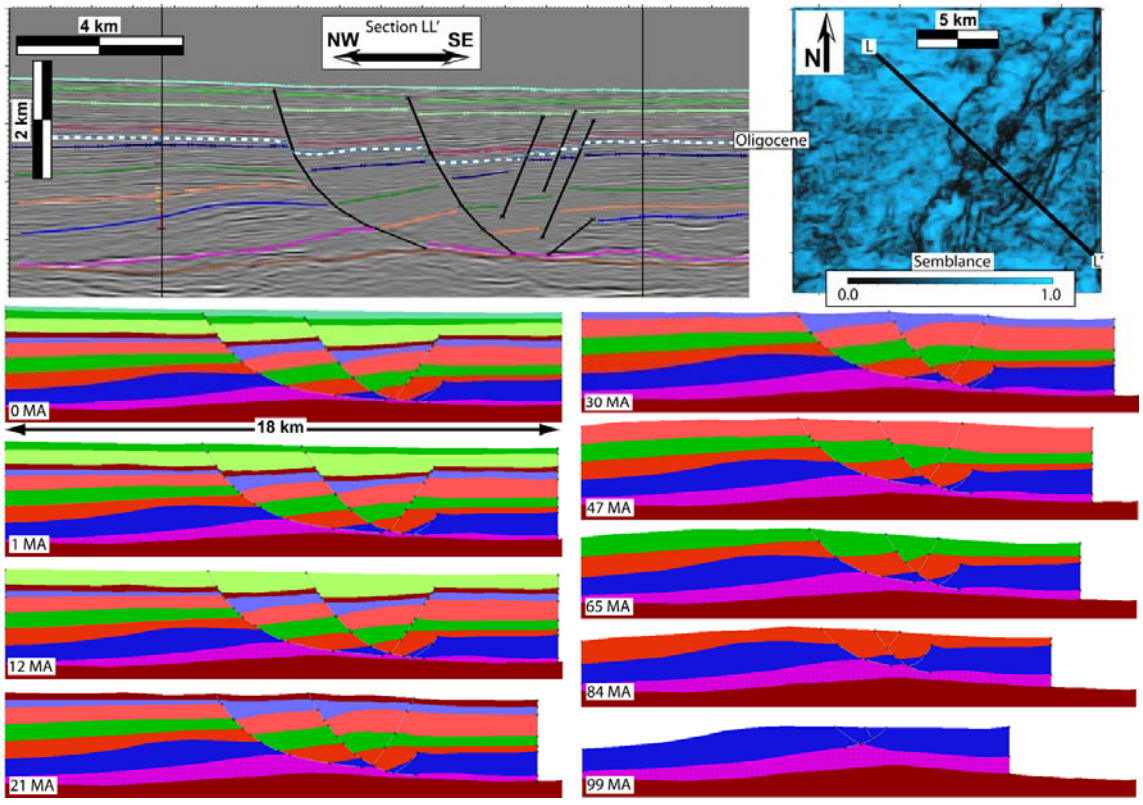

Figure 13

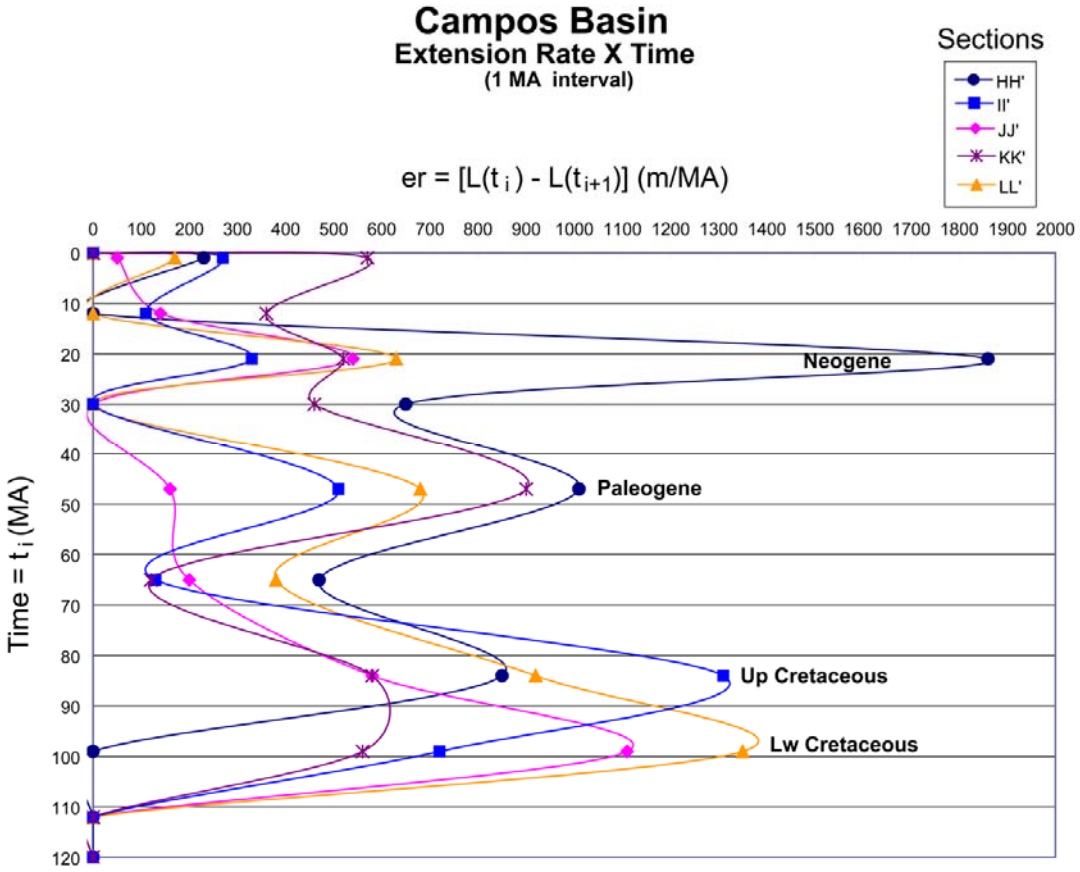
Campos Basin
Extension Rate X Time
(1 MA interval)
er = [L(t i) - L(t i+1)] (m/MA)
Sections
HH'
II'
JJ'
KK'
LL'
Time = t i (MA)
Neogene
Paleogene
Up Cretaceous
Lw Cretaceous

Figure 14

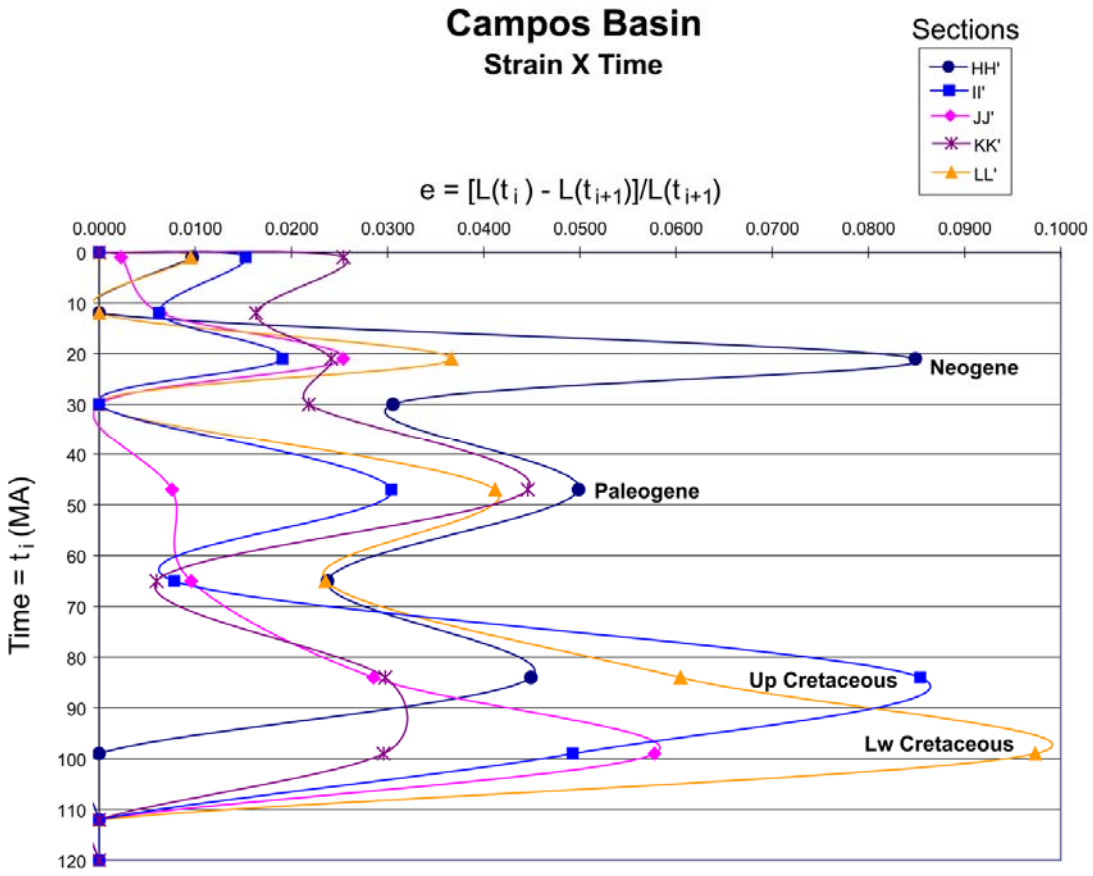
Campos Basin
Strain X Time
Sections
HH'
II'
JJ'
KK'
LL'
e = [L(t i) - L(t i+1)]/L(t i+1)
0.0000
0.0100
0.0200
0.0300
0.0400
0.0500
0.0600
0.0700
0.0800
0.0900
0.1000
0
10
20
30
40
50
60
70
80
90
100
110
120
Time = t i (MA)
Neogene
Paleogene
Up Cretaceous
Lw Cretaceous

Figure 15

Artigo III. Petrographic and seismic evidence for the depositional setting of giant turbidite reservoirs and the paleogeographic evolution of Campos Basin, offshore Brazil (Submitted to Earth and Science Reviews).

Petrographic and seismic evidence for the depositional setting of giant turbidite reservoirs and the paleogeographic evolution of Campos Basin, offshore Brazil

Marcos Fetter[a]*, Luiz F. De Ros [b#], and Carlos H. L. Bruhn[a]

[a]Petrobras E&P, Av. Chile, 65/1702, Rio de Janeiro, RJ, Brazil, 20035-900;
[b]Federal University of Rio Grande do Sul, Institute of Geosciences, Av. Bento Gonçalves, 9500, Porto Alegre, RS, Brazil, 21501-970l;
e-mail adress: *fetter@petrobras.com.br; [#]lfderos@inf.ufrgs.br

Abstract

The paleogeographic evolution of Campos Basin, major oil-province of Brazil, during the deposition of its giant turbidite reservoirs was reinterpreted based on the integration of quantitative sandstone petrography and structural analysis of regional 3D seismics. The major detrital compositional trends indicate that the geodynamic evolution of the continental margin, rather than global eustatic sea level fluctuations, has exerted the main control on sand supply to the deepwater systems. This control was imposed by the interaction of three geodynamic processes: (i) escarpment retreat of the coastal mountain chains, (ii) mantle plume-related dynamic uplift and magmatic activity, and (iii) tectonic reactivation of major basement fault-zones. The pattern of distribution of compositional and textural parameters within the turbidite sequences indicated that the sand supply to deepwater was also constrained by high-frequency stratigraphic processes of the climate Milankovitch band. This new approach to the controls on the formation of the sand-rich deepwater systems in Campos Basin will be of key importance to generate realistic models for the exploration of new turbidite reservoirs and for the optimized development of producing turbidite oilfields in such a world-class hydrocarbon province. As it is very simple, the proposed integrated methodology can help to unravel the controls on the deposition of deepwater sand-rich reservoirs in other divergent margin settings.

Keywords: Turbidite reservoirs, quantitative petrography, structural analysis, divergent margins, mantle plumes, intraplate tectonics, paleogeography, sequence stratigraphy.

1. Introduction

Campos Basin (Fig. 1) is by far the most prolific oil province in Brazil. Up to 93% of the 8.5 billion bbl proven hydrocarbon reserves in Campos Basin are contained in sand-rich turbidite reservoirs deposited in deepwater settings during the divergent margin phase from the Albian to the Miocene (Bruhn et al., 2003). As many other divergent margin settings, the structural and stratigraphic evolution of Campos Basin and the adjacent basins along eastern Brazilian continental margin have been studied with classic approaches such as lithospheric stretching, escarpment retreat, sequence stratigraphy, and detached salt tectonics (Dias et al., 1990; Cobbold and Szatmari, 1991; Chang et al., 1992; Peres, 1993; Gallagher et al., 1995; Souza Cruz, 1995). However, this conventional conceptual background was not able to define the controls for the development of the large deepwater hydrocarbon reservoirs of Campos Basin. This question remains open probably because the methods and data used for the analysis of

Campos Basin are inadequate for unraveling the conditions for the deposition of deepwater sand-rich systems in such a complex tectonic-stratigraphic setting.

Campos Basin turbidites show strong compositional and textural immaturity, conversely to the pattern typical of passive divergent margins (Scarton, 1993; Bruhn and Walker, 1995; Caddah et al., 1998). Large volumes of gravel and sand were deposited in deepwater during the Upper Cretaceous transgression, when the sea-level was, in average, 200 m higher than the present (Bruhn and Walker, 1995; Caddah et al., 1998; Santos et al., 1999). Additionally, the Upper Cretaceous and Paleogene stratigraphic record of Campos Basin cannot be correlated with the global 3rd order sea-level cycles defined according to the conventional sequence stratigraphic concepts (Scarton, 1993; Pereira, 1994; Bruhn and Walker, 1995).

In the present work, an integrated approach combining quantitative petrography and structural analysis is proposed to improve the understanding of the deepwater sand-rich systems in Campos Basin. Quantitative petrography of deepwater sandstones is a powerful source of information on the paleogeographic evolution of source-basin systems (Zuffa, 1987; 1991; Zuffa et al., 1995; 2000). The structural analysis of regional 3D seismic datasets was focused on the evidence of basement tectonic reactivations observed during the divergent margin phase in Campos Basin (Cobbold et al., 2001; Fetter et al., 2002).

2. Geological Setting

The development of Campos Basin was initiated during the Late-Jurassic/Early-Cretaceous break-up of Gondwana supercontinent, followed by the opening of the South Atlantic Ocean. Early mechanical subsidence was accomplished by episodic events that reactivated the Proterozoic basement fabric under regional E-W extension (Ponte and Asmus, 1976; Rabinowitz and LaBrecque, 1979; Mohriak and Dewey, 1987; Dias et al., 1990; Chang et al., 1992; Karner, 2000). Thermal subsidence started during the Aptian, which was characterized by evaporitic-rich sedimentation, and has proceeded during the oceanic phase from the Albian to the Recent.

Most of the Campos Basin border corresponds to the Neo-Proterozoic Ribeira Belt (Figs. 2 and 3), which is the northernmost expression of a NE-SW trending orogenic system mostly controlled by steep strike-slip shear belts (Campos Neto, 2000). From Neo-Proterozoic to Middle Cambrian NE-SW oriented shearing accommodated the amalgamation of several terrains and crustal shortening along the Ribeira Belt. The

northern limit of the Ribeira Belt is defined by the Vitória-Colatina shear zone (Chang et al., 1992), a major long-lived Proterozoic structure trending NNW-SSE (Fig. 3).

2.1. Mantle plumes and magmatism

Intense magmatic activity took place in Campos Basin during the lowermost Cretaceous, which may have been associated with the Tristão da Cunha mantle plume. This magmatism resulted in the extrusion of basalts, geochemically similar to the continental flood basalts of the Paraná Basin magmatic province (Fig. 1) – CFB affinity (Hawkesworth et al., 1992; Mizusaki et al., 1992; Wilson, 1992).

A new pulse of magmatic activity, associated with the Trindade mantle plume (Fig. 1), is observed in the Upper Cretaceous and the Paleogene. The basic-alkaline rocks generated by this magmatism show a compositional correlation with ocean island basalts – OIB affinity (Thompson et al., 1998).

2.2. Stratigraphy

The stratigraphic record of Campos Basin can be subdivided in two major 2nd-order sequences. During the extensional phase (Valaginian to Barremian), an up to 3.5 km thick, 2nd-order sequence formed by fault-controlled taphrogenic successions was deposited, with volcanogenic contribution at the base (Fig. 2). The second, up to 7 km-thick, 2nd-order sequence started to accumulate during the Aptian, with a transitional siliciclastic, carbonatic, and evaporitic succession, which was followed by an early Albian shallow carbonate platform, and a late Albian to Recent marine transgressive to regressive succession (Fig. 2).

Thermal subsidence and sediment loading allowed the deposition of the transgressive-regressive marine succession, which contains several turbidite systems ranging in age from late Albian to Miocene. The thermal subsidence and the global sea-level rise allowed a transgressive setting for entire Upper Cretaceous, with the maximum transgression achieved in the early Paleocene.

During the Paleogene, there was intense sea-level variation, with the development of many 3rd-order sequences, but the overall stratigraphic pattern is slightly progradational (Fig. 2). The mainly regressive sedimentation started in the Neogene, and is presently going on; it has been characterized by an expressive progradation that has been building a wide continental shelf in the Campos Basin (Figs. 2 and 3).

2.3. Structural geology and tectonics

The overall structural style in Campos Basin is detached (Fig. 2). The main structural features in the basement are horsts and grabbens limited by steep normal faults active during the Early Cretaceous rift phase (Dias et al., 1990; Chang et al., 1992). The basement structural fabric is dominated by two main directions: (i) NE-SW, associated with the Ribeira Orogenic Belt, and (ii) NNW-SSE, associated with the Vitória-Colatina shear zone (Fig. 3).

The thin-skinned salt tectonics with extensional-proximal and compressional-distal domains have been active during divergent margin phase since the Early Albian, and is characterized by listric fault-rollover systems, turtle-back structures, raft tectonics, downbuilding diapirs, salt walls, and compressional salt tongues (Cobbold and Szatmari, 1991; Demercian et al., 1993). More recently it was observed that the overall detached structural style has been disturbed by episodic strike-slip reactivations of the basement structures during the divergent margin phase in Campos Basin (Cobbold et al., 2001; Fetter et al., 2002).

From a geodynamic point of view it is important to mention the presence of tall mountains of the *Serra do Mar* (Sea Ridge), constituted of uplifted terrains of the Ribeira Orogenic Belt, along the basin border (Figs 2 and 3). The persistence of up to 2700 m high elevations at around 75 km from the rift border 130 Ma after the main extensional rift phase suggests that the continental margin adjacent to Campos Basin has not been exactly a tectonically passive setting.

3. Petrography

In the present work we performed quantitative petrographic analysis of the main turbidite systems deposited in Campos Basin during the divergent margin phase. The petrographic analysis was developed on 121 thin sections sampled along 990 m of cores from 10 wells representative of 11 turbidite systems ranging in age from the Albian to the Miocene (Fig. 4; Table 1). The Gazzi-Dickinson point-counting method (Gazzi, 1966; Dickinson, 1970; Dickinson and Suczec, 1979; Ingersoll et al., 1984; Zuffa, 1985) was used, with 300 points counted per thin section.

Most of the analyzed samples correspond to arkoses (*sensu* Folk, 1968), and just a few samples of the Maastrichtian samples are classified as lithic arkoses (Fig. 5). According to the high-hierarchy grain origin classification of Zuffa (1980), most of the samples show a siliciclastic, non-carbonate extrabasinal composition (NCE), with

departures towards a carbonate intrabasinal (CI) contribution during the Albian and the Late Eocene, and towards a non-carbonate intrabasinal (NCI) contribution during the Santonian and the Paleocene (Fig. 6). The Cenomanian and the Miocene reservoirs show a mixed contribution from CI and NCI, and a departure towards the field of hybrid arenites (*sensu* Zuffa, 1980; Fig. 6).

The extrabasinal composition of most Campos Basin deepwater sand-rich systems corresponds to the uplifted basement block field in the tectonic provenance diagram of Dickinson and Suczec (1979) and Dickinson (1985), which is typical of rift basins and immature divergent margins (Fig. 7). The Upper Oligocene samples show a consistent departure towards the field of transitional continent field, typical of mature divergent margins (Fig. 7). The Maastrichtian reservoir shows a not expected compositional trend towards the volcanic arc field (Fig. 7).

The overall results of turbidite petrography, and the integrated analysis of the classification diagrams (Figs. 5, 6 and 7), indicate the most significant petrographic parameters for the study of the paleogeographic evolution of Campos Basin divergent margin phase (Table 2). The main parameters are the quartz to feldspar ratio (Q/F) and the grain size. The content of volcanic rock fragments (VRF), the carbonate intrabasinal contribution (CI), and the content of non-carbonate intrabasinal grains (NCI, mainly mud intraclasts and glaucony) also seem to be very diagnostic of the type of connection between the sediment source areas and the deepwater depositional sites. The content of micaceous grains is related to the long term evolution of the continental margin.

3.1. Albian

The petrographic analysis of the Albian turbidite reservoir (Well 01; Fig. 4; Tables 1 and 2) indicates, in average, an arkose composition with quartz to feldspar ratio Q/F = 1.02, and fine sand grain size. The sand grains are sub-angular to sub-rounded, with moderate to good sorting (Fig. 8).

There is a well-defined pattern for the internal variation of composition and texture (Fig. 9). Although the fine sand grain size is quite constant along the core, the Q/F ratio shows high-frequency cyclicity, with a growing upwards trend.

The contribution of carbonate intrabasinal grains (CI) is very high (Figs. 8b, 8e, 8f, and 9), and their distribution follows that of Q/F ratio, with a high-frequency cyclicity superimposed to a growing upwards trend (Fig. 9). Calcite cementation is widespread (Fig. 8), probably due to the source and nuclei provided by carbonate intraclasts, bioclasts and ooids, as well as by the proximity to Albian carbonate successions. The

content of mica grains is also high (Fig. 8c), and a few foliated, low-grade metamorphic rock fragments where observed (Fig. 8a). The contents of volcanic rock fragments, mud intraclasts, and glaucony are low.

3.2. Cenomanian

The petrography of the Cenomanian turbidite reservoir (Well 02; Fig. 4; Tables 1 and 2) indicates, in average, an arkose composition with quartz to feldspar ratio Q/F = 1.00, and fine sand grain size. The sand grains are sub-angular to sub-rounded, with moderate sorting (Fig. 10). Plutonic rock fragments up to cobble-size where observed in poorly-sorted conglomeratic sandstone samples (Fig. 10e). There is no recognizable cyclic pattern of compositional and textural internal variation as for the Albian deepwater system.

The carbonate intrabasinal contribution (Fig. 10a) is smaller than in the Albian reservoir, but is still fairly high. Calcite cementation is widespread (Fig. 10), probably for the same reasons invoked for the Albian. On the other hand, there is a significant increment in the intraclast content (Fig. 10f). The content of micaceous grains is quite significant (Fig. 10d). The volcanic contribution and the glaucony content are low.

3.3. Santonian

The petrographic analysis of the Santonian deepwater sand-rich system (Well 03; Fig. 4; Tables 1 and 2) indicates, in average, an arkose composition with low quartz to feldspar ratio (Q/F = 0.88), and medium sand grain size. The sand grains are sub-angular to sub-rounded, with poor to moderate sorting (Fig. 11). Up to cobble-size feldspar grains where observed in very poorly-sorted conglomeratic sandstone samples (Fig. 11e). The internal compositional and textural variation shows a direct correlation between the grain size and the quartz to feldspar ratio (Fig. 12).

The content of mud intraclasts is very high. The intraclasts are compacted into pseudo-matrix, and commonly replaced by opaline silica or by calcite (Figs. 11a, 11b, and 11c). There is a significant drop in the contents of carbonate intrabasinal grains and of micaceous grains relative to the Albian and Cenomanian. The glaucony content and the volcanic contribution are still low.

3.4. Campanian

The Campanian turbidite reservoir (Well 04; Fig. 4; Tables 1 and 2) corresponds in average, to an arkose composition with very low quartz to feldspar ratio (Q/F = 0.69),

and medium sand grain size. The sand grains are sub-angular to sub-rounded, with poor to moderate sorting (Fig. 13). The internal variation pattern of composition and texture is not well-defined.

The content of mud intraclasts is high (Fig. 13b), as well as the contribution of volcanic rock fragments (Figs. 13d and 13e). The content of micaceous grains is very significant. The contents of intrabasinal carbonate and glaucony grains are very low.

3.5. Maastrichtian

The Maastrichtian turbidite reservoir (Well 05; Fig. 4; Tables 1 and 2) represents to a major deepwater sand-rich system in Campos Basin with huge sand volumes in northeastern, northern and southern portions of the basin. The petrographic analysis indicates, in average, a lithic arkose composition with very low quartz to feldspar ratio (Q/F = 0.65), and medium sand grain size. The sand grains are sub-angular to sub-rounded, with poor sorting (Fig. 14). There is no recognizable trend of internal variation of composition and texture.

The contribution of volcanic rock fragments is very high (Figs. 14a and 14f). The intraclast content is lower than in the Santonian and Campanian reservoirs, but is still significant, as well as the content of micaceous grains (Figs. 14d and 14e). There is also a significant contribution of carbonaceous fragments with features indicative of charcoal (burned wood; Figs. 14d and 14e). The carbonate intrabasinal (CI) and the glaucony contents remain very low.

3.6. Paleocene

The petrographic analysis of the Paleocene deepwater sand-rich system (Well 06; Fig. 4; Tables 1 and 2) indicates, in average, an arkose composition with low quartz to feldspar ratio (Q/F = 0.75), and medium sand grain size. The sand grains are sub-angular to sub-rounded, with moderate to poor sorting (Fig. 15).There is a good correlation between grain size and quartz to feldspar ratio (Fig. 12).

The amounts of volcanic rock fragments (Figs. 15b, 15c, and 15e) and of intraclasts (Figs. 15d and 15f) are very high. The contribution of carbonate intrabasinal grains is also important (Figs. 15d and 15e). There is a significant contribution of glaucony peloids and intraclasts (Figs. 15d and 15f), and a significant drop in the content of micaceous grains.

3.7. Middle Eocene

The Middle Eocene turbidite reservoir (Well 06; Fig. 4; Tables 1 and 2) corresponds to thick deepwater sand-rich systems that fill fault controlled troughs in Campos Basin. The petrographic analysis indicates, in average, an arkose composition with low quartz to feldspar ratio (Q/F = 0.77), and medium sand grain size. The sand grains are sub-angular to sub-rounded, with moderate to poor sorting (Fig. 16). The internal variation of composition and texture shows a fairly good correlation between the grain size and the quartz to feldspar ratio (Fig. 12).

The content of mud intraclasts is very high (Fig. 16f). The glaucony content is lower than in the Paleocene, but still significant (Fig. 16a). There is a drop in the contribution of volcanic rock fragments, carbonate intrabasinal grains (CI), and micaceous grains. It is important to mention the presence of large mud fragments with internal textures typical of soils (Fig. 16d) and of laminated microbialite fragments (Fig. 16e) in the conglomeratic turbidites.

3.8. Upper Eocene

The petrography of the Upper Eocene turbidite reservoir (Well 06; Fig. 4; Tables 1 and 2) indicates, in average, an arkose composition with very low quartz to feldspar ratio (Q/F = 0.71), and medium sand grain size. The sand grains are sub-angular to sub-rounded, with moderate to poor sorting (Fig. 17). As in other analyzed deepwater systems, there is a direct correlation between grain size and quartz to feldspar ratio (Fig. 12).

The contents of intrabasinal carbonate and glaucony grains are very high (Figs. 17a, 17c, 17e, and 17f). as the contribution of mud intraclasts. The content of micaceous grains is quite significant (Fig. 17b). The contribution of volcanic rock fragments is even lower than in the Middle Eocene turbidite system.

3.9. Lower Oligocene

The Lower Oligocene turbidite reservoir (Well 07; Fig. 4; Tables 1 and 2) corresponds in average, to an arkose composition with low quartz to feldspar ratio (Q/F = 0.82), and fine sand grain size. The sand grains are sub-angular to sub-rounded, with moderate sorting (Fig. 18). There is no recognizable pattern of internal variation of composition and texture.

The content of mud intraclasts is very high (Fig. 18c). The contribution of carbonate intrabasinal grains is also significant (Figs. 18a and 18e). The contents of volcanic rock

fragments and glaucony grains are very low. There is also a significant drop in the content of micaceous grains.

3.10. Upper Oligocene

The Upper Oligocene reservoir (Wells 08 and 09; Fig. 4; Tables 1 and 2) corresponds to another major deepwater system with huge sand volumes in central, northeastern, and northern Campos Basin. The petrography of this reservoir indicates, in average, an arkose composition with high quartz to feldspar ratio (Q/F = 1.40), and fine sand grain size. The sand grains are sub-angular to sub-rounded, with poor to moderate sorting (Fig. 19).

As in the Abian reservoir, the internal variation of composition and texture is well organized (Fig. 20). The fine sand grain size is dominant, with levels of medium size. The quartz to feldspar ratio (Q/F) shows a growing-upwards trend superimposed by a high-frequency cyclicity. There is also a well-defined step with higher quartz content in the upper-half of the cored section.

The content of carbonate intrabasinal grains (Figs. 19b and 19d), of mud intraclasts (Fig. 19e), and of volcanic rock fragments are significant, but lower than in the previously-described turbidite systems. The contents of glaucony and micaceous grains are very low.

3.11. Miocene

The petrographic analysis of the Miocene turbidite reservoir (Well 10; Fig. 4; Tables 1 and 2) indicates, in average, an arkose composition with low quartz to feldspar ratio (Q/F = 0.91), and fine sand grain size. The sand grains are sub-angular to sub-rounded, with moderate to good sorting (Fig. 21). Up to very coarse sand feldspar grains where observed in poorly-sorted sandstone samples (Fig. 21f). There is a fining-upwards trend from medium sand to very fine sand grain size, as well as a growing-upwards trend of the quartz to feldspar ratio (Fig. 22).

The contents of glaucony (Figs. 21d and 21e) and carbonate intrabasinal grains (Figs. 21a, 21b, 21c and 21f) are significant. The content of mud intraclasts is low. The contribution of volcanic rock fragments and micaceous grains are very low.

4. Average petrographic trends

It was observed in the previous section that the Albian, Upper Oligocene, and Miocene turbidite systems show well-defined variation of the compositional and textural parameters, with internal trends and cyclicity (Figs. 9, 20, and 22). Another

internal petrographic trend was observed in the Santonian and Paleogene deepwater sandstones, which show a fairly good correlation between grain size and quartz to feldspar ratio (Fig. 12). Below we compare the average petrographic parameters of the analyzed deepwater sand-rich systems, which also show defined trends during the divergent margin phase of Campos Basin (Table 2).

4.1. Quartz to feldspar ratio (Q/F) and grain size

The average quartz to feldspar ratio - Q/F (Fig. 23) starts with a value around 1.00 in the Albian and the Cenomanian, and drops almost linearly to 0.65 in the Maastrichtian. Then the ratio grows a little to 0.75 in the Paleocene and Middle Eocene, and drops again to 0.70 during the Upper Eocene. There is an exponential increase in Q/F from the average 0.75 during the Paleogene to 1.4 in the Upper Oligocene, and an equally strong drop to 0.90 in the Miocene.

The trend of average grain size (Fig. 24) starts with fine sand during the Albian and the Cenomanian and changes to medium sand from Santonian to Upper Eocene. There are shifts towards coarse sand limit during the Maastrichtian and during the Upper Eocene. The average grain size returns to fine sand from Lower Eocene to Miocene.

The cross-plot of the parameters grain size and quartz to feldspar ratio allows the definition of two types of deepwater sand-rich systems (Fig. 25). The first type is represented by the Albian, Cenomanian, Lower Oligocene, Upper Oligocene, and Miocene turbidite systems. This group has a relatively higher compositional and textural maturity, as it is characterized by a close to 1:1 quartz to feldspar proportion (Q/F = 1.00) and by fine sand grain size. The Upper Oligocene reservoir has the highest quartz to feldspar ratio of this group (Q/F = 1.40).

The second type is formed by the Santonian, the Campanian, the Maastrichtian, the Paleocene, the Middle Eocene, and the Upper Eocene reservoir systems (Fig. 25). This group is more immature compositional and texturally, as characterized by an around to 3:4 quartz to feldspar proportion (Q/F=0.75) and average medium grain size. In this group, the Maastrichtian reservoir has the lowest quartz to feldspar ratio (Q/F = 0.65).

4.2. Volcanic rock fragments

The background amount of volcanic rock fragments in Campos Basin turbidite reservoirs is around 1% (Fig. 26). There is an episodic pulse of volcanic contribution that reaches almost 9.00% during the Maastrichtian (Fig 26), up to 3.10% during the Campanian, and up to 4.50% during the Paleocene.

4.3. Intrabasinal carbonate grains

The contribution of carbonate intrabasinal grains (CI) to turbidite systems encompass mainly bioclasts and ooids generated at shallow-water settings in carbonate platforms and ramps. It may also comprise planktonic bioclasts and intraclasts from slope settings. Average CI content was initially high in Campos Basin deepwater sand-rich systems in the Albian (up to 13%), and later dropped progressively to zero in the Maastrichtian (Fig. 27). There was a strong oscillation of CI content during the Lower Paleogene that culminated with a peak around 18% in the Upper Eocene (Fig. 27). Then the average CI drops again to around 5% during the Oligocene, and grows again to 7.5% in the Miocene (Fig. 27).

4.4. Mud intraclasts

The contribution of mud intraclasts to the Campos Basin deepwater sand-rich systems was very low in the Albian (around 1%), and reaches a step above 10% from the Cenomanian to the Lower Oligocene (Fig. 28). During this period of high intraclast content there were a drop to around 8% in the Maastrichtian, and two peaks above 12% in the Santonian, and in the Lower Paleogene. The average content of mud intraclasts drops to around 5% during the Upper Oligocene and the Miocene (Fig. 28).

4.5. Glaucony

The background of glaucony content in Campos Basin turbidite reservoirs is less than 0.5% (Fig. 29). There are two peaks of glaucony content around 2% in the Paleocene and Miocene, and another peak of almost 5% in the Upper Eocene (Fig. 29).

4.6. Micaceous grains

The content of micaceous grains in Campos Basin deepwater sand-rich systems shows a pattern of oscillation between 1% and 3% (Fig. 30). This pattern is superimposed to a trend of decreasing micaceous content from 3.5% in the Albian to 0.5% in the Miocene (dashed arrow in Fig. 30).

5. Structural analysis of basin deformation through basement faults reactivation

In convergent margin basins, the quantitative petrographic analysis of deepwater sand-rich systems has shown that the physiographic evolution of source-basin systems and the compositional-textural character of turbidites are essentially controlled by the

tectonic activity (Fontana et al., 1989; Cibin et al., 2001). It is also already known that divergent margins are subjected to intraplate tectonic activity (Stein et al., 1989; Withjack et al., 1995; Bezerra and Vita-Finzi, 2000). Although the geodynamic energy involved in the tectonic processes in divergent margins is lower than in convergent margins, the amount of tectonic energy needed to change the physiography of the source-basin system and consequently the petrography of deepwater sediments is largely unknown. In order to investigate the possible effects of tectonic activity on the petrography of Campos Basin deepwater sand-rich reservoirs, it was performed a detailed analysis of basement structures involved with already documented strike-slip reactivations of the Proterozoic fabric (Cobbold et al., 2001; Fetter et al., 2002).

The structural analysis was developed with seismic attribute maps and sections selected from regional 3D seismic datasets recently acquired in Campos Basin (Fig. 31). All the seismic data was subjected to pre-stack time migration in order to improve the structural imaging. The depth-conversion was done with a basin-scale velocity model sufficiently smooth to avoid artifacts caused by local velocity bias. The velocity model was calibrated with an evenly distributed set of time-depth tables computed from check-shot data.

5.1. Albian-Cenomanian Transpression

The first example of basement reactivation was observed at the southern portion of Campos Basin in a 500 km^2 area of folding with rhombohedral shape (Fig. 32). The structural trend NE-SW is sub-parallel to Proterozoic basement fabric. Up to 1800 m thick taphrogenic and transitional strata, ranging in age from Barremian to Aptian were folded by flexural slip under NNW-SSE shortening. The fold pattern well-defined by the maximum curvature map is quite regular and sinuous (Figs 32a and 32b), with 1 km wavelength and 100 m amplitude (Fig. 32c). Fold axes are slightly rotated counter-clockwise in relation to the main NE-SW structural trend (Fig. 32a). The rhombohedral folded area is interpreted as a transpressive structure related to left-lateral strike-slip reactivation of steep basement shear zones trending NE-SW (insert of Fig. 32a). As post-Aptian strata are not deformed, it is possible to place deformation at the Albian-Cenomanian transition, still under the regional stress field of the rift phase with N-S maximum horizontal stress (SHmax). This deformation phase is related to the end of extension, but there was not yet a rotation of the regional stress field.

5.2. Albian-Cenomanian and Santonian Transpression

The second example of basement reactivation was observed in a 90 km^2 area faulted and folded in northeastern Campos Basin (Fig. 33). Deformation of pre-Aptian successions (up to 1200 m thick) is given by quite complex thrust-faulting and folding (Fig. 33c). Strata ranging in age from Albian to Turonian (up to 1000 m thick) were subjected to more regular folding with 1km wavelength and 100 m amplitude. Fold axes trending NE-SW show interference between Z and S sinuous patterns disposed *en-echelon* (Fig. 33a). Such geometry is interpreted as a result of transpression caused by strike-slip reactivation of NNW-SSE basement fabric with right-lateral followed by left-lateral kinematics. The right-lateral Albian-Cenomanian transpression represents the end of regional E-W extension still related to a regional loading with N-S SHmax, as in the example in Figure 31. The left-lateral Santonian kinematics is related to the rotation of the regional SHmax to E-W caused by the development of the South Atlantic mid-oceanic spreading center. The structure was probably amplified by salt movement across the section and by a buttress effect of the basement high (Fig. 33c).

Another example of transpression was observed in northwestern Campos Basin (Fig. 34). In this case, strata ranging in age from Albian to Santonian were subjected to *en-echelon* folding. The folds with axes oriented N-S can be interpreted as a result of right-lateral strike-slip reactivation of the NE-SW basement fabric related to the already mentioned rotation of the regional SHmax to E-W. As the Maastrichtian strata are not folded is possible to place this deformation phase at the Santonian.

5.3. Paleogene Transpression and Transtension

The Paleogene example of basement reactivation (section D, Fig. 35) is contiguous to the folding area in section B at northeastern Campos Basin (Fig. 31). A large fold with 3 km half-wavelength and 300 m amplitude affects up to 2700 m of Upper-Cretaceous to Paleogene strata (Fig. 35). The structure is interpreted as a fault propagation fold (Suppe, 1985). The deformation is clearly episodic with well-constrained pre-kinematic, sin-kinematic and post-kinematic phases (Fig. 35c). The main deformation phase in the Eocene is indicated by onlap pattern and section growth (Fig. 35c). The fold was related to transpression associated with left-lateral reactivation of NW-SE basement fabric during the Paleogene under E-W maximum horizontal stress. The shortening associated with transpression caused the inversion of Lower Albian listric normal faults (Fig. 35c).

In central Campos Basin, 80 km to the south of previous example of transpression, the Paleogene reactivation event is characterized by normal faulting and section growth (Fig. 36). Most of the faults are restricted to Paleogene and older strata, and are concentrated above a basement high (Fig. 36b). The faults are planar and discontinuous. The fault system is characterized by a dispersed distribution of orientations around NNE-SSW (Fig. 36a and 36c). The structure is interpreted as a negative flower caused by transtension (Woodcock and Schubert, 1994). The observed dispersion of fault orientations was probably caused by the coupling between stress fields related to both basement reactivation and gravitational gliding above the Aptian salt detachment.

The tectonic and magmatic reactivation along the southeastern continental margin of Brazil during the Paleogene was already well documented (Chang et al., 1992; Scarton, 1993; Almeida et al., 1996; Thompson et al., 1998; Cobbold et al., 2001; Thomaz Filho et al., 2005; Zalán and Oliveira, 2005). The Paleogene magmatic activity was particularly intense in southern Campos Basin, where many volcanic structures have been described (Mizusaki and Mohriak, 1992; Figs. 32b and 32c).

5.4. Neogene Transpression

Just to the north of the previous Paleogene negative flower structure, still in central Campos Basin, the Neogene deformation is characterized by folding (Fig. 37). Observe that the anticline trending NE-SW is positioned exactly above the basement high (Fig. 37b). The structure is interpreted as an inversion fold that can be properly defined according to both the clay models of Eisenstad and Withjack (1995), and the conceptual model of Sibson (1995). The inversion of listric normal faults related to gravitational gliding extension active from Cretaceous to Paleogene was caused by transpression at the basement high during Neogene (Figs. 37c and 37d).

Another structure that indicates Neogene transpression was observed in northeastern Campos Basin, 50 km to the north of the previous inversion fold (section H, Fig. 31). The structure is interpreted as an inverted grabben (Fig. 38). The grabben was formed by normal faulting during the Upper Cretaceous. The Cretaceous depocenter was inverted in the Neogene with the shortening caused by transpression related to the reactivation of the basement fabric (Fig. 38c).

5.5. Overview of the structural analysis

The structural analysis of regional 3D seismic data indicates four periods of basement reactivation during the divergent margin phase in Campos Basin (Table 3). The timing of the Neogene and Paleogene deformation events is very well-constrained.

The kinematic interpretation and the involved strata indicate two phases of deformation during the Cretaceous, but the timing of the basement reactivation has a certain degree of uncertainty.

Except by the Paleogene tectonic event, which has a more widespread manifestation in Campos Basin, and along the southeastern coast of Brazil (Chang et al., 1992; Zalán and Oliveira, 2005), the tectonic reactivation is selective and sparse, with open folds and moderate fault inversion observed mainly above basement structural highs. The structural style of the tectonic reactivation indicates an overall strike-slip kinematic pattern. This overall picture of the reactivation of basement structures in Campos Basin interpreted in the present work agrees with previously published observations (Scarton, 1993; Pereira, 1994; Bruhn and Walker, 1995; Lima, 1999; Cobbold et al., 2001; Fetter et al., 2002; Zalán and Oliveira, 2005), as well as with the events indicated by apatite fission track analysis along the southeastern continental margin of Brazil (Gallagher and Brown, 1999; Saenz et al., 2003). Nevertheless, the structural analysis developed in the present study allowed the definition of an accurate timetable for the tectonic events involving basement faults reactivation, with the indication of two deformation phases during the Cretaceous, and of a further tectonic event in the Neogene (Table 3).

6. Major controls on deepwater sedimentation within Campos Basin

The quantitative petrographic analysis indicates that the sandstones deposited in Campos Basin deepwater during the divergent margin phase do not follow the increasing maturity trend expected for tectonically passive margin basins. Actually, most of the petrographic parameters of Campos Basin turbidites show a quite complex evolution pattern (Figs. 23 to 30). Particularly, the variation of the parameters grain size and quartz to feldspar ratio (Q/F) indicates an alternated deposition of two main types of deepwater sandstones in Campos Basin (Fig. 25): (i) relatively mature turbidites with fine sand grain size and Q/F = 1.00, deposited in the Albian, Cenomanian, Oligocene and Miocene, internally characterized by well developed trend patterns (Figs. 9, 20, and 22); (ii) immature turbidites with medium sand grain size and Q/F = 0.75, deposited in the Santonian, Campanian, Maastrichtian, Paleocene and Eocene.

Therefore it is clear that the evolution of the physiography of source terrains and basin, and the formation of the deepwater sand-rich systems during the thermal subsidence phase in Campos Basin was not exclusively controlled by the processes conventionally postulated for the evolution of divergent continental margins, namely the

eustatic sea-level changes (Posamentier et al., 1988; Galloway, 1989), and the passive escarpment retreat associated with the flexural unloading caused by the erosion of the rift-shoulder relief (Ollier, 1985; Gilchrist and Summerfield, 1990). This indicates that an integrated model of geodynamic and stratigraphic evolution must be developed in order to understand the controls on the deepwater sedimentation in Campos Basin. This model must encompass all the petrographic trends previously described.

6.1. The exhumation of the Ribeira Orogenic Belt

The long-term evolution of the source-areas of Campos Basin can be envisaged by the trend of decrease, of about one order of magnitude, in the contribution of micaceous grains to the deepwater sandstones (dashed arrow in Fig. 30). This trend represents the increasing exhumation of the Ribeira Belt. The average mica content has progressively dropped as the mica-bearing medium grade metamorphic rocks of the orogenic belt were removed by uplift and erosion, exposing the mica-poor rocks of high metamorphic grade.

This long-term signal is related to the escarpment retreat geodynamic model, defined by progressive erosion, unloading and flexural uplift along the basin margin. It is important to observe that most of the other petrographic parameters would have followed the same simple long-term trend if other geodynamic processes have not been active during Campos Basin divergent margin phase.

6.2. The mantle plume control

The Campos Basin was positioned along the trajectory of the rotational drift of the South-American plate above the Trindade mantle plume (Fig. 39). The influence of the passage of the basin above the plume on the texture and composition of the deepwater systems is indicated by the nearly symmetric distribution of average grain size, Q/F and volcanic rock fragments of the turbidites around the Maastrichtian, when the plume was below the Campos Basin border (Figs. 25 and 39).

The major control of the dynamic uplift caused by the thermal anomaly of the plume on the compositional and textural character of the deepwater sandstones is indicated by the dominant medium average grain size and low quartz to feldspar ratio from the Santonian to the Eocene (Figs. 23, 24 and 39). However it is important to observe that the high content of volcanic rock fragments (VRF), which represents the magmatic activity of the plume at the Campos Basin border, is manifested in a shorter time period, from the Campanian to the Paleocene (Figs. 26 and 39).

6.3. The episodic tectonic control

Detailed structural analysis of regional seismic 3D datasets indicated four major deformation events of tectonic reactivation of Campos Basin basement fabric. Quantitative petrographic analysis of major sand-rich turbidite systems from Albian to Miocene confirmed that these tectonic events have indeed changed the physiographic character of the source-basin system during the divergent margin phase in Campos Basin (Table 3; Fig. 40).

The beginning of the divergent margin phase in Campos Basin during the Albian was characterized by the construction of a wide carbonate ramp, associated with tectonic stability and escarpment retreat of the rift-shoulder relief. Therefore, the Albian turbidite system is relatively mature with higher quartz to feldspar ratio (Q/F), and fine sand grain size (Figs. 23, 24, 25, and 40). With poorly developed slopes of essentially carbonatic composition, the contribution of glaucony and mud intraclasts to the deepwater systems were low (Figs. 28, 29, and 40).

The first evidence of paleogeographic reorganization, related to the tectonic reactivation at the Albian-Cenomanian transition (Fig. 40), can be recognized by slightly lower Q/F ratio and larger average grain size (close to the limit of medium sand) of the Cenomanian deepwater sandstones (Figs. 23, 24, 25, and 40). Additionally, a significant increase in mud intraclasts content is observed (Figs.28 and 40). These petrographic differences are well illustrated by the photomicrographs of the two deepwater systems (Figs. 8 and 10). This increasing immaturity is interpreted in terms of a rejuvenation of the coastal relief, associated with partial degradation of the shelf, and with changes in the sedimentary pathways from the coast to deepwater.

A more expressive paleogeographic change was caused by the Santonian tectonic event. Comparing with the previous systems, the Santonian deepwater sandstones are characterized by a significant decrease in the Q/F ratio, and a considerable increase in the grain size and in the content of mud intraclasts (Figs. 23, 24, 25, 28, and 40). The photomicrographs in Figure 11 illustrate the textural and compositional immaturity of the Santonian turbidites. Again the increasing immaturity is interpreted as consequence of the tectonic rejuvenation of the source-basin system. The glaucony contribution remained very low because of the further degradation of the shelf (Figs. 29 and 40).

Despite the relative tectonic quiescence from the Campanian to the Maastrichtian, the Trindade mantle plume was sufficiently close to Campos Basin to cause volcanic activity and dynamic uplift along the coast. Consequently, the deepwater systems

deposited during this period were also very immature, and particularly rich in volcanic rock fragments (Figs. 13, 14, 23, 24, 25, 26, and 40). There is a progressive decrease in the average content of mud intraclasts from Santonian to Maastrichtian (Figs. 28 and 40). This drop in the average content of intraclasts may be interpreted as a result of stable sedimentary supply routes to deep water through canyons deeply incised by recurrent currents in the slope that were kept constant because of the tectonic quiescence during this period. Due to the absence of a stable shelf, there is virtually no glaucony contribution to deepwater (Figs. 29 and 40). The increase in the contribution of volcanic fragments and the decrease in the content of mud intraclasts in Campos Basin turbidites during Upper Cretaceous illustrate well two different types of geodynamic impact along the continental margin (Fig. 40): (i) **tectonic reactivation** - coastal elevation plus reorganization of the source-basin system in the Santonian, and (ii) **effects of the mantle plume** - coastal elevation by dynamic uplift and volcanism without major physiographic reorganization in the Maastrichtian.

Campos Basin paleogeography was substantially changed again during the Paleocene owing to the beginning of the Paleogene basement reactivation. Additionally, with the end of the 2nd order transgression, a new shelf was built. The tectonic activity caused a rejuvenation of the coastal relief and a further reorganization of the source-basin system, still under the influence of the Trindade mantle plume. Consequently, the Paleocene deepwater sandstones remained very immature, with a significant contribution of volcanic rock fragments (Figs. 15, 23, 24, 25, 26, and 40). A significant increase in the mud intraclasts content was observed (Figs. 28 and 40), probably due to the redefinition of the bottom current pathways caused by the physiographic reorganization. This interpretation is further supported by the increase in the glaucony content (Figs. 29 and 40).

During Eocene the tectonic activity strengthened, and Campos Basin depocenters moved above Trindade mantle plume. Therefore, Eocene turbidite systems are very immature, with high mud intraclasts and glaucony contents (Fig. 40), as a consequence of coastal relief rejuvenation, and of the ongoing physiographic changes into the basin. On the other hand, a considerable drop in the contribution of volcanic rock fragments is observed, because the volcanic activity ceased along the coastal areas, being transferred to within the basin (Figs. 32b, 32c, and 40).

During Lower Oligocene, with the end of the Paleogene tectonic reactivation and without the effects of Trindade plume, then already relatively far from Campos Basin, a

significant increase in the maturity of the deepwater sandstones is observed (Figs. 25 and 40). The higher Q/F ratio and the fine sand grain size indicate a lowering of the relief and a widening of the shelf. The small contribution of glaucony (Fig. 40) indicates that the physiography and the sediment pathways along the shelf had been keeping stable. On the other hand, the relatively high content of mud intraclasts (Fig. 40) suggests a situation of active physiographic changes on the slope, which were probably related to the ongoing progradation and to salt tectonic activity.

As the mantle plume was very far, the Upper Oligocene tectonic quiescence allowed erosion and escarpment retreat along Campos Basin coast. In turn, the progradation related to the high sediment supply built a very wide shelf. This set of conditions caused a further increase in the maturity of the deepwater sandstones (Figs. 25 and 40). The grain size remained fine, and there was an expressive growth in the Q/F ratio (Fig. 40). The physiographic stability of the source-basin system is confirmed by the low contribution of glaucony and mud intraclasts (Fig. 40). As a consequence of the constant sediments pathways through the shelf and the slope to the deepwater settings, only minor contents of glaucony and intraclasts were taken by bottom currents to the Upper Oligocene deepwater sand-rich systems.

With the onset of the Neogene basement reactivation in the Miocene, the associated physiographic reorganization caused a relative decrease in the maturity of the Miocene turbidites. The average grain size remained fine, but there was a significant drop in Q/F ratio (Figs. 23, 24, and 40). There was an increase in the content of glaucony (Figs. 29 and 40), indicating shifting bottom currents trajectories along the shelf as a consequence of physiographic rejuvenation. On the other hand the content of mud intraclasts was relatively low (Figs. 28 and 40), suggesting that the sediment pathways in the shelf-edge and the slope were almost the same of the Upper Oligocene.

6.4. The downstream and the upstream control on the stratigraphic record

Sequence stratigraphy is undoubtedly the most powerful concept for the study of the patterns of sedimentary basins filling, particularly aiming at the prediction of reservoirs distribution. Nevertheless, the approach of sequence stratigraphy is strictly valid only for a well-defined set of boundary conditions.

The ideal set of conditions for the application of the classic sequence stratigraphy model, recently defined as the **downstream control** on the stratigraphic record by Catuneanu (2006), is related to wide shelves in stable tectonic settings, without significant changes in the topographic gradients and in the sediment supply. Under these

boundary conditions, relative sea-level changes will fully control the stratigraphic record, and systems tracts delimited by key stratigraphic surfaces will function as a predictive model for the pattern of basin filling.

Conversely, the boundary conditions may involve narrow shelves in active tectonic settings with pronounced changes in topographic gradients and sediment supply caused by tectonic pulses, ice melting, anomalous rainfall cycles, and mantle plume effects. Under these conditions, an **upstream control** on the stratigraphic record is established, and relative sea-level changes will not work so well as a predictive tool for basin filling pattern (Catuneanu, 2006).

Following this conceptual reasoning, it can be stated that the development of significant deepwater sand-rich systems is constrained by the type of stratigraphic control. Under downstream control, sand supply to deepwater is enhanced in the late stage of relative sea-level fall, and large turbidite systems may be deposited in the distal domain of the late forced-regression systems tract (Catuneanu, 2006). On the other hand, under upstream stratigraphic control, sand supply to deepwater can be enhanced by tectonic uplift or by river flooding caused by either ice melting, or episodic rainfall peaks. In this case important deepwater sand-rich systems may develop in any stage of relative sea-level, depending on the paleogeography of the source-basin system (Kolla and Perlmutter, 1993; Burgess and Hovious, 1998; Zuffa et al., 2000; Carvajal and Steel, 2006). Therefore, the definition of the balance between downstream and upstream stratigraphic control is a fundamental requisite for reservoir prediction in basin analysis.

The evidence supplied by the petrographic analysis of the turbidite reservoirs and the structural analysis of seismic data indicate that the deposition of sand-rich deep-water systems occurred in Campos Basin under alternating downstream control and upstream control, associated with tectonic reactivations of basement structures and with the effects of the Trindade mantle plume. The dominant type of control can be directly related to the two petrographic categories of deepwater sandstones defined in present work (Fig. 25): the relatively **mature systems** (Albian, Cenomanian, Oligocene and Miocene) were deposited under prevailing **downstream control**, while the **immature systems** (Santonian, Campanian, Maastrichtian, Paleocene, and Eocene) were formed under prevailing **upstream control**.

6.5. The high-order stratigraphic control

The biostratigraphic data in Campos Basin indicates that most of the deepwater systems were deposited within short time spans of one single biozone that corresponds

to intervals between 1 and 2 Ma (Antunes et al., 2004). Detailed cyclostratigraphic studies indicate that the Upper Oligocene turbidite system was deposited during an even shorter time interval into the respective biozone (Perlmutter and Azambuja, 2005). Additionally, it was previously observed that these deepwater sandstone successions were formed by amalgamation of multiple events (Bruhn and Walker, 1995; Bruhn et al., 1998; Barroso et al., 2000; Perlmutter and Azambuja, 2005). The evidence of multiple depositional events during time intervals around 1 Ma suggests that the sand supply to deepwater settings in Campos Basin has been also controlled by high-order stratigraphic processes, possibly of climate nature.

The internal organization of petrographic parameters observed in some Campos Basin deepwater systems confirms their amalgamated architecture. The Q/F ratio shows an internal high-frequency oscillation with constant grain size in the relatively mature Albian and Upper Oligocene turbidite systems (Figs. 9 and 20). In the Albian system the content of intrabasinal carbonate grains (CI) shows internal cyclicity parallel to the Q/F ratio (Fig. 9). These internal compositional oscillations are interpreted as a result of supply alternation between predominant reworked shelf sediments (higher Q/F and CI), during periods of normal rainfall, and first-cycle sediments from the upstream alluvial systems (lower Q/F and CI), during episodic torrential rainfall events.

7. Paleogeographic reconstruction

Campos Basin was not subjected to major climate changes related to plate drift during the divergent margin phase. The latitudes in Campos Basin have been restricted to a range between S20^{o} and 30^{o}, around the temperate-tropical climate boundary, from the Albian to the present time (Ford and Golonka, 2003).

During the Albian, at the onset of the divergent margin phase, a wide and shallow carbonate ramp was developed in Campos Basin (Spadini et al., 1988). The relatively mature Upper Albian deepwater sand-rich system, characterized by high carbonate intrabasinal content (CI), was deposited beyond this ramp under stratigraphic downstream control, probably during relative a 3rd order lowstand subjected to high-frequency climate oscillations.

The Albian ramp was destructed in the Upper Cretaceous by drowning and by gravitational gliding above the salt detachment triggered by the ongoing basement tectonic reactivation. The Upper Cenomanian turbidites were deposited still under downstream control, but are slightly more immature than the Albian turbidites, probably

because of the initial degradation of the Albian ramp, and of some coastal uplift associated with the tectonic reactivation phase at the Albian-Cenomanian transition. The deepwater system was probably formed during a punctuated 3rd order lowstand during the ongoing 2nd order transgression. With the proceeding transgression, and without further tectonic uplift of the source-areas, the formation of deepwater sand-rich systems was subdued during Turonian and Coniacian.

The immature Santonian deepwater sand-rich system was formed under fully upstream stratigraphic control. At this time, Campos Basin was bordered by a very narrow shelf. The coastal relief was actively uplifted by the Santonian tectonic reactivation phase, and the deepwater systems were fed by fan deltas or by short mountain rivers, similar to the equivalent environments already described in convergent margin basins (Mutti et al., 1996). The Santonian turbidites can be defined as sin-tectonic, as the deformation was in course during their deposition (Bruhn and Walker, 1995). The deposition of volcanic ash layers and the presence of significant amounts of burned palynomorfs in the Santonian fine-grained turbidites are related to the proximity of the Trindade mantle plume to Campos Basin (Caddah et al., 1998; Arai et al., 2005).

The formation of a new shelf was inhibited during Upper Cretaceous because of the overall transgression. Therefore, the Campanian and the Maastrichtian immature deepwater sand-rich systems were deposited also under upstream stratigraphic control, with a narrow shelf and high coastal relief. The significant contribution of volcanic rock fragments and the presence of burned wood fragments in the Maastrichtian coarse-grained turbidites indicate the arrival of the Trindade mantle plume to basin margin (Figs. 14 and 39). The coastal relief was probably very high, uplifted both by the tectonic Santonian reactivation phase and by the dynamic uplift of the mantle plume. Consequently, the deepwater systems were fed by short mountain-rivers and fan deltas.

After the end of the 2nd order transgression in the Lower Paleocene, a new shelf begins to form in Campos Basin, but still sufficiently narrow to allow an overall upstream control on the deposition of the immature Paleocene and the Eocene deepwater sand-rich systems. The coastal relief was kept high by the Paleogene tectonic reactivation, and the deepwater systems were still fed by mountain-rivers and fan deltas.

As the shelf was still narrow, the limited contribution of intrabasinal grains in the very immature Middle Eocene turbidites, including soil and microbialite fragments (Figs. 16, 27, and 40), can be interpreted as the contribution from offshore highs located very close to the deepwater depocenters, because these fragments would not resist long

transportation distances. These offshore islands were formed along the elevated footwall blocks of major fault systems activated during the Paleogene tectonic phase, under the influence of the dynamic uplift caused by the Trindade mantle plume that was then beneath Campos Basin depocenter (Fig. 39). The Paleogene uplift of the Campos Basin depocenter was previously documented by Scarton (1993). With the widening of the shelf during Upper Eocene, the intrabasinal contribution to deepwater systems was increased significantly (Figs. 17 and 27).

As the regression proceeded with the progradation driven by high sediment supply from the mountains formed during the Paleogene tectonic phase, a relatively wide shelf was built in Campos Basin by the Lower Oligocene. The Lower Oligocene deepwater sand-rich system was deposited during a 3rd order lowstand, beyond a renewed shelf, and under downstream stratigraphic control (Souza Cruz, 1995). It is characterized by increasing compositional and textural maturity, as compared with the Upper Cretaceous and Paleogene turbidites, owing to the feeding of deepwater systems by longer fluvial systems and by sediment reworked on the widening shelf.

With further progradation during the Oligocene, Campos Basin shelf continued to widen. The large Upper Oligocene deepwater system, which is the most mature turbidite system within Campos Basin, was also deposited during a 3rd order lowstand, under downstream stratigraphic control (Souza Cruz, 1995). As for the Lower Oligocene, the maturity of Upper Oligocene deepwater sandstones was probably related to both long transportation along an extensive fluvial system and sediment reworking on the shelf.

The costal physiography was rebuilt by the new tectonic pulse occurred during the Neogene. The high sediment supply associated with the renewed relief produced a rapid progradation front and a very wide shelf in Campos Basin (Figs. 2 and 3). The Lower Miocene turbidite system was also deposited during a 3rd order lowstand, under fully downstream stratigraphic control (Souza Cruz, 1995), but with significantly higher feldspar and glaucony content than the Upper Oligocene deepwater system, what is attributed to the rejuvenation of the relief caused by the Neogene tectonic reactivation. However the low content in mud intraclasts suggests that the sand supply to deepwater during the Miocene used the same pathways incised into shelf edge and slope that were previously used during Upper Oligocene.

8. Discussion

The energy necessary to promote the process of turbiditic mass transportation may be derived from two types of systems (Normark and Piper, 1991; Mutti et al., 2003): (i) potential energy of coastal relief or shelf gradient plus kinetic energy of river flooding; and (ii) potential energy of delta-front gradient plus kinetic energy of delta-front failure.

The potential energy supplied by coastal relief is a product of geodynamic processes, while the potential energy of shelf and delta-front gradients is fundamentally related to stratigraphic processes. In turn, the kinetic energy of river flooding is a product of climatic processes, either ice melt or rainfall flooding, while the kinetic energy of delta-front failure can be released by tectonic activity and/or by slope instability. Therefore, the recently proposed concept of downstream versus upstream control on the stratigraphic record (Catuneanu, 2006) can be applied to turbidite systems. Following this concept, geodynamic driven relief, climate flooding events and tectonic activity are upstream controls, while shelf gradients, delta progradation rates, and delta-front instabilities are downstream controls.

A process-response relation was observed between the type of energy system and the compositional and textural parameters of Campos Basin deepwater sand-rich systems (Table 4). The trends of average petrographic parameters and the overall paleogeographic evolution are well constrained by the major geodynamic and stratigraphic controls that were operating during the divergent margin phase of Campos Basin (Fig. 40; Table 4).

The geodynamic control is interpreted as a consequence of the interplay of three processes: (i) the passive escarpment retreat of the coastal relief, (ii) the dynamic uplift and the magmatic activity promoted by the Trindade mantle plume, and (iii) the episodic tectonic reactivations of major basement structures (Fig. 40; Table 4). None of these specific geodynamic controls alone can explain all the observed petrographic trends. A purely tectonic drive fails to explain the formation of the large Maastrichtian turbidite system with massive contribution of volcanic rock fragments, which was undoubtedly related to the passage of the southeastern continental margin of Brazil above the Trindade mantle plume (Fig. 39). However, it is important to observe that only large plumes, generated at the core-mantle boundary with CFB magmatic affinity, reach the base of the crust generating dynamic uplift in areas around 2000 km^2, with up to 1000 m elevations (Griffiths and Campbell, 1990). Small plumes with OIB magmatic affinity, as in the case of the Trindade plume, are generated into the mantle and tend to

arrive fast to the base of the crust, producing dynamic uplift in smaller areas, around 300 km^2, with lesser elevations (Griffiths and Campbell, 1990). In any case, the time span of the dynamic uplift caused by the passage above a mantle plume is even shorter than the exponential isostatic adjustment of the oceanic crust generated at mid-ocean ridges (Condie, 2001). Therefore, it is not reasonable to credit all the evolution of the coastal relief along Campos Basin border, indicated by turbidite petrography and structural analysis, to the Trindade plume. Actually, the observed relief rejuvenations and paleogeographic reorganizations are episodic, and have been occurring during at least 80 Ma (Figs. 39 and 40). It is suggested that episodic and repeated uplift of the coastal mountain chain along southeastern Brazilian margin (*Serra do Mar*) can be better explained by episodic tectonic reactivations of the major basement fabrics, probably enhanced by the thermal anomaly related to the plume during the Cretaceous-Paleogene transition (Cobbold et al., 2001). During the periods of tectonic quiescence, and without the plume effects, escarpment retreat has been the dominant geodynamic process acting along the Campos Basin border (Fig. 40, Table 4).

The above discussed geodynamic processes have been exerting a strong control on the stratigraphic record during the divergent margin phase in Campos Basin. The periods of passive escarpment retreat of the continental margin have been characterized by downstream stratigraphic control, largely constrained by base level changes. Therefore it is supposed that the respective relatively mature deepwater systems have been formed during 3rd order lowstands. As it was formed beyond a carbonate ramp, even the Albian turbidite system fits this interpretation, because the stratigraphic response to base level changes of carbonate ramps and siliciclastic platforms is similar (Catuneanu, 2006) . On the other hand, during the periods of tectonic reactivation and/or mantle plume activity, the upstream stratigraphic control has been dominant. In this case the immature deepwater systems could have been formed in any stage of the eustatic sea level.

The internal organization of the petrographic parameters, particularly Q/F ratio, grain size and CI content, indicates that the relatively mature Campos Basin deepwater sandstones were formed by the amalgamation of multiple depositional events. The well-defined petrographic oscillations observed in the mature turbidites formed beyond a wide platform, with moderate coastal relief, under downstream stratigraphic control, suggest that the sand supply to deepwater settings has been controlled by high-frequency climate changes of the Milankovitch band during 3rd order lowstands (Figs. 9,

20, and 22; Table 4). Following this interpretation, the internal growing-upwards trends of Q/F ratio and CI with constant or fining-upwards grain size (Albian – Fig. 9; Upper Oligocene – Fig. 20; Miocene – Fig. 22) are attributed to the rise of the base level at the end of 3rd order lowstands, with progressive restriction of the contribution of first-cycle sediments to deepwater settings.

In the case of immature deepwater sandstones formed under upstream stratigraphic control, the triggering of the turbidity currents was probably related to the association between the potential energy of the high coastal relief and by the kinetic energy of episodic events of enhanced rainfall flooding of coastal alluvial systems (Table 4). In the absence of a well developed shelf, immature, first-cycle alluvial and fluvial sediments were taken directly to deepwater settings during flooding events.

9. Conclusions

Two classes of deepwater sand-rich systems were defined in Campos Basin based on quantitative petrographic analysis (Fig. 25): (i) relatively mature turbidites, with alternating shelf-reworked and first-cycle contributions, and (ii) immature turbidites, with predominant first-cycle contribution. The geodynamic evolution of the continental margin has exerted the major control on the deposition of these deepwater systems. This control is determined by the interaction of three geodynamic processes (Fig. 40; Table 4): (i) escarpment retreat of the coastal relief, (ii) dynamic uplift and magmatic activity of the Trindade mantle plume, and (iii) tectonic reactivations of the major basement structures

The relatively mature deepwater sandstones were deposited beyond wide shelves or shallow ramps, during periods of escarpment retreat, with low to moderate coastal relief. Under such boundary conditions, the stratigraphic record was controlled by downstream factors, namely the 3rd order eustatic variations in the sea level and climate cyclicity of the Milankovitch band. However, it is important to notice that, in presence of a wide shelf, the downstream control can prevail even during phases of active tectonism (e.g. Cenomanian and Miocene systems; Fig. 40, Table 4).

The immature turbidite systems were formed during periods of high coastal relief and shelf degradation, caused by tectonic activity and by dynamic uplift. In such periods, the upstream stratigraphic control has prevailed and the deepwater sedimentation had been triggered exclusively by episodic rainfall flooding (Fig. 40, Table 4).

The two largest turbidite reservoir systems in Campos Basin are the Maastrichtian and the Upper Oligocene (black stars in Fig. 40). These systems were formed during periods of tectonic quiescence, just before the onset of the subsequent tectonic reactivation. This observation indicates that giant deepwater sand-rich systems can be formed in divergent margins as a consequence of tectonic rejuvenation followed by stable configuration of the source-basin system, independently of the type of stratigraphic control. In this situation, huge sand volumes can accumulate until the system happen to be aborted by a new tectonic pulse. Conversely, relatively more dispersed deepwater systems were formed when the physiography was unstable because of ongoing tectonic activity.

From a methodological point of view, the quantitative petrography of deepwater sandstones was revealed to be a powerful tool in the paleogeographic reconstruction of divergent margin settings, as it was emphatically confirmed for convergent margins. Particularly, the grain size and the quartz to feldspar ratio are very sensitive to the rejuvenation of the coastal relief, while the contents of intrabasinal carbonate grains, glaucony, and mud intraclasts are indicative of the evolution of the shelf-slope physiography. As the methodology is very simple, it can be easily applied in other divergent margin basins.

The integrated paleogeographic reconstruction presented in this work represents a significant change in the interpretation of the geodynamic and stratigraphic evolution of Campos Basin divergent margin phase. Particularly, the main controls on the formation of the Campos Basin giant turbidite reservoir systems were redefined as a complex interplay of tectonic, magmatic, eustatic and climatic aspects, contrasting with the conventional, sequence-stratigraphic models previously interpreted for these systems. This new approach will be of key importance to generate realistic models for the exploration of new turbidite reservoirs and for the optimized development of producing turbidite oilfields in such a world-class hydrocarbon province.

Acknowledgements

The present work was developed as part of a doctorate research project at the Graduate Program in Geosciences of Rio Grande do Sul Federal University (UFRGS – Porto Alegre, Brazil), sponsored by Petrobras. We acknowledge the discussions and the support of Cláudio Lima and Luci Arienti from Petrobras Research Center, and Carlos Rodrigues from Petrobras International. We also wish to thank Eliane de Freitas Ferreira from Petrobras Documentation Center. LFDR acknowledges the support by the National Council of Research - CNPq.

References

Almeida, F.F.M., Carneiro, C.D.R., and Mizusaki, A.M.P., 1996. Correlação do magmatismo das bacias da margem continental brasileira com o das áreas emersas adjacentes: Rev. Bras. Geoc. 26: 125-138.

Antunes, R.L., Shimabukuro, S., Oliveira, L.C.V., Rosa, A.L.Z., Costa, S.O., Cunha, A.A.S., and Lima, F.H.O., 2004. Towards a high resolution biostratigraphy: the Petrobras calcareous nannofossil zonation performance. Bol. Geoc. Petrobras 14: 125-131.

Arai, M., Lana, C.C., Araújo, C.V., and Menezes, T.R., 2005. The great Santonian fire - implications for the regional geology and petroleum exploration. Bol. Geoc. Petrobras 14: 125-131.

Assumpção, M., 1998. Seismicity and stresses in the Brazilian divergent margin: Bull. Seismol. Soc. Am. 88: 160-169.

Barroso, A.S., Mihaguti, M.K., Castro, D.D., Stank, C.V., Sarzenski, D.J., Adams, T., 2000. Roncador giant oil field: exploration and production from a heterogeneous Maastrichtian turbidite reservoir in ultra deep water Campos Basin, Brazil. AAPG Ann. Met., New Orleans, Louisiana, Abstr., AAPG Bull. 84:13.

Bezerra, F.H.R., and Vita-Finzi, C., 2000. How active is a divergent margin? Paleoseismicity in northeastern Brazil. Geology 28: 591-594.

Bruhn, C.H.L., Gomes, J.A.T., Del Luchese, C., and Johann, P.R.S., 2003. Campos Basin: reservoir characterization and management – historical overview and future challenges. OTC-Houston, paper OTC 15220, pp. 1-14.

Bruhn, C.H.L., Barroso, A.S., Lopes, M.R.F., Sarzenski, D.J., Abreu, C.J., Silva, C.M.A., 1998. High-resolution stratigraphy and reservoir heterogeneities of Upper Albian turbidite reservoirs of Albacora Field, Campos Basin, offshore Brazil. 1998 AAPG Ann. Conv., Salt Lake City, Utah, Ext. Abstr. 1:A95.

Bruhn, C.H.L., and Walker, R.G., 1995. High-resolution stratigraphy and sedimentary evolution of coarse-grained canyon-filling turbidites from the Upper-Cretaceous transgressive megasequence, Campos Basin, offshore Brazil. J. Sed. Res. 65: 426-442.

Burgess, P.M., and Hovius, N., 1998. Rates of delta progradation during highstands: consequences foe timing of deposition in deep-marine systems. J. Geol. Soc. London 155: 217-222.

Caddah, L.F.G., Alves, D.B., and Mizusaki, A.M.P., 1998, Turbidites associated with bentonites in the Upper-Cretaceous of the Campos Basin, offshore Brazil: Sed. Geol., v. 115, 175-184.

Campos Neto, M.C., 2000, Orogenic systems from southwestern Gondwana. In: U.G. Cordani, E.J. Milani, A. Thomaz Filho and D.A. Campos (Editors), Tectonic Evolution of South America. 31st Int. Geol. Congress, Rio de Janeiro, pp. 335-365.

Carvajal, C.R., and Steel, R.J., 2006. Thick turbidite succesions from supply-dominated shelves during sea-level highstand. Geology 34: 665-668.

Catuneanu, O., 2006. Principles of Sequence Stratigraphy. Elsevier, Amsterdam, 375 pp.

Chang, H.K., Kowsmann, R.O., Figueiredo, A.M.F., and Bender, A.A., 1992. Tectonics and stratigraphy of the East Brazil Rift system: an overview. Tectonophys. 213: 97-138.

Cibin, U., Spadafora, E., Zuffa, G.G., and Castellarin, A., 2001. Continental collision history from arenites of episutural basins in the Northern Apennines, Italy. GSA Bull. 113: 04-19.

Cobbold, P.R., Meisling, K.E., and Mount, S.V., 2001. Reactivation of an obliquely-rifted margin: Campos and Santos basins, SE Brazil. AAPG Bull. 85: 1925-1944.

Cobbold, P.R., and Szatmari, P., 1991. Radial gravitational gliding on divergent margins. Tectonophys. 188: 249-289.

Condie, K.C., 2001. Mantle Plumes and Their Record in Earth History. Cambridge University Press, Cambridge, 306 p.

Demercian, S., Szatmari, P., and Cobbold, P.R., 1993. Style and pattern of salt diapirs due to thin-skinned gravitational gliding, Campos and Santos basins, offshore Brazil. Tectonophys. 228: 393-433.

Dias, J.L., Scarton, J.C., Guardado, L.R., Esteves, F.R., and Carminatti, M., 1990. Aspectos da evolução tectono-sedimentar e da ocorrência de hidrocarbonetos na Bacia de Campos. In: G.P. Raja-Gabaglia, and E.J. Milani (Editors), Origem e Evolução de Bacias Sedimentares. Petrobras, Rio de Janeiro, pp. 333-360.

Dickinson, W.R., 1970. Interpreting detrital modes of greywacke and arkose. J. Sedim. Petrol. 40: 695-707.

Dickinson, W.R. and Suczec, C.A., 1979. Plate tectonics and sandsdtone compositions: AAPG Bull. 63: 2164-2182.

Dickinson, W.R., 1985. Interpreting provenance relations from detrital modes of sandstones. In: G.G. Zuffa (Editor), Provenance of arenites. D. Reidel Publ. Co.; NATO ASI Series, Math. Phys. Sci. 148, pp. 333-361.

Eisenstad, G., and Withjack, M.O., 1995. Estimating inversion: results from clay models. In: J.G. Buchanan and P.G. Buchanan (Editors), Basin Inversion. Geol. Soc. London Spec. Publ. 88, pp. 119-136.

Fetter, M., Lima, C.C., Silva, A.T., Machado, D., Castro, D.D., and Adams, T., 2002. Interaction between salt related extension and basement strike-slip reactivation in northern Campos Basin, deepwater Brazil. SEG 72nd Ann. Meet., Salt Lake City, Exp. Abstr., pp. 2413-2416.

Folk, R.L., 1968. Petrology of Sedimentary Rocks. Hemphill's Bookstore, Austin, 170 p.

Fontana, D., Zuffa, G.G., and Garzanti, E., 1989. The interaction of eustacy and tectonism from provenance studies of the Eocene Hecho Group turbidite complex (South-Central Pyrenees, Spain). Basin Res. 2: 223-237.

Ford, D., and Golonka, J., 2003. Phanerozoic paleogeography, paleoenviroment and lthofacies of the circum-Atlantic margins. Mar. Petrol. Geol. 20: 249-285.

Gallagher, K., and Brown, R., 1999. The Mesozoic denudation history of the Atlantic margins of southern Africa and southeast Brazil and the relationship to offshore sedimentation. In N.R. Cameron, R.H. Bate, and V.S. Clure (Editors), The Oil and Gas Habitats of the South Atlantic. Geol. Soc. London Spec. Publ. 153, pp. 41-53.

Gallagher, K., Hawkesworth, C.J., and Mantovani, M.S.M., 1995. Denudation, fission track analysis and the long-term evolution of divergent margin topography: application to southeast Brazilian margin. J. South Am. Earth Sci. 8: 65-77.

Galloway, W.E., 1989. Genetic stratigraphic sequences in basin analysis I: architecture and genesis of flooding-surface bounded depositional units. AAPG Bull. 73: 125-142.

Gazzi, P., 1966. Sulla determinazione microscopica della compozicione mineralogica e granulometrica delle rocce, in particolare delle arenarie e delle sabbie. Mineral. et Petrogr. Acta. 12: 61-68.

Gilchrist, A.R., and Summerfield, M.A., 1990. Differential denudation and flexural isostasy in the formation of rifted-margin upwarps. Nature 346: 739-742.

Griffiths, R.W., and Campbell, I.H., 1990. Stirring and structure in mantle starting plumes. Earth Planet. Sci. Lett. 99: 66-78.

Hawkesworth, C.J., Gallagher, K., Kelley, S., Mantovani, M., Peate, D.W., Regelous, M., and Rogers, N.W., 1992. Paraná magmatism and the opening of the South

Atlantic. In: B.C. Storey, T. Alabaster, and R.J. Pankhurst (Editors), Magmatism and the Causes of Continental Break-up. Geol. Soc. London Spec. Publ. 68, pp. 221-240.

Ingersoll R.V., Bullard T.F., Ford R.L., Grimm J.P., Pickle J.D., and Sares S.W., 1984. The effect of grain size on detrital modes: a test of the Gazzi-Dickinson point-counting method: J. Sedim. Petrol. 54: 103-116.

Karner, G.D., 2000. Rifts of the Campos and Santos Basins, southeastern Brazil: distribution and timing. In: M.R. Melo, and B.J. Katz (Editors), Petroleum Systems of South Atlantic Margins. AAPG Memoir 73, pp. 301-315.

Kolla, V., and Pelmutter, M.A., 1993. Timing of turbidite sedimentation on the Mississipi Fan: AAPG Bull. 77: 1129-1141.

Lima, C.C., 1999. Expressions topographiques et structurales de l´etat de compression généralisée au sein de la plaque Sud-Américaine. PhD Thesis, Univ. Rennes 1, France.

Mizusaki, A.M.P., and Mohriak, W.W., 1992. Sequências vulcano-sedimentares na região da plataforma continental de Cabo Frio (RJ). Anais 37^{o}. Congr. Soc. Bras. Geol., pp. 52-56.

Mizusaki, A.M.P., Petrini, R., Bellieni, G., Comin-Chiaramonti, P., Dias, J., De Min, A., and Piccirillo, E.M., 1992. Basalt magmatism along the passive continental margin of SE Brazil (Campos Basin). Contrib. Min. Petrol. 111: 143-160.

Mohriak, W.U., and Dewey, J.F., 1987. Deep seismic reflectors in the Campos Basin, offshore Brazil. Geophys. J. R. Astron. Soc. 89: 133-140.

Mutti, E., Davoli, G., Tinterri, R., and Zavala, C., 1996. The importance of fluvio-deltaic systems dominated by catastophic flooding in tectonically active basins. Mem. Sci. Geol. Padova 48: 233-291.

Mutti, E., Tinterri, R., Benevelli, G., di Biase, Davide, and Cavanna, G., 2003. Deltaic, mixed and turbidite sedimentation of ancient foreland basins. Mar. Petrol. Geol. 20: 733-755.

Normark, W.R., and Piper, D.J.W., 1991. Initiation processes and flow evolution of turbidity currents: implications for the depositional record. In: R.H. Osborne (Editor), From Shoreline to Abyss: Contributions in Marine Geology in Honor of Francis Parker Shepard. SEPM Spec. Publ. 46, pp. 207-230.

Ollier, C.D., 1985. Morphotectonics of continental margins with great escarpments. In: M. Morisawa and J.T. Hack (Editors), Tectonic Geomorphology. Allen & Unwin, Boston, pp. 3-25.

Perlmutter, M.A., and Azambuja, N.C., 2005. Cyclostratigraphy. In: E.A.M. Koutsoukos (Editor), Applied Stratigraphy. Springer Topics in Geobiology 23, pp. 301-338.

Pereira, M.J., 1994. Seqüências deposicionais de 2^{a}. e 3^{a}. ordens (50 a 2 Ma) e tectono-estratigrafia no Cretáceo de cinco bacias marginais do Brasil: comparações com outras áreas do globo e implicações geodinâmicas. PhD Thesis, Universidade Federal do Rio Grande do Sul, Porto Alegre, Brazil.

Peres, W.E., 1993. Shelf-fed turbidite system model and its application to the Oligocene deposits of the Campos Basin, Brazil. AAPG Bull. 77: 81-101.

Ponte, F.C., and Asmus, H.E., 1976. Brazilian marginal basins: current state of knowledge. Anais Acad. Bras. Ciênc. 48: 215-239.

Posamentier, H.W., Jervey, M.T., and Vail P.R., 1988. Eustatic controls on clastic deposition I: conceptual framework. In: C.K.. Wilgus, B.S. Hastings, C.G. st. C. Kendal, H.W. Posamentier, C.A. Ross, and J.C. Van Wagoner (Editors), Sea Level Changes: An Integrated Approach. SEPM Spec. Publ. 42, pp. 110-124.

Rabinowitz, P.D., and LaBrecque, J., 1979. The Mesozoic South Atlantic Ocean and evolution of its continental margins. J. Geophys. Res. 84: 5973-6002.

Saenz, C.A.T., Hackspacker, P.C., Hadler Neto, J.C., Iunes, P.J., Guedes, S., Ribeiro, L.F.B., and Paulo, S.R., 2003. Recognition of Cretaceous, Paleocene, and Neogene tectonic reactivation through apatite fission-track analysis in Precambriam areas of southeast Brazil: association with the opening of the south Atlantic ocean. J. South Am. Earth Sci. 15: 765-774.

Santos, P. R. S., Rangel, H. D., Quintaes, C. M. S. P., and Caixeta, J. M., 1999. Turbidite reservoir distribution in Roncador field, Campos Basin, Brazil. AAPG Int. Conf. Exhib., Birmingham, England, Ext. Abstr., pp. 530–531.

Scarton, J.C., 1993. Análise estratigráfica do Terciário Inferior da Bacia de Campos: Uma visão moderna (com ênfase na região dos campos petrolíferos de Corvina e Malhado). PhD Thesis, Universidade Federal do Rio Grande do Sul, Porto Alegre, Brazil.

Sibson, R.H., 1995. Selective fault reactivation during basin inversion - potential for fluid redistribution through fault-valve action. In: J.G. Buchanan and P.G. Buchanan (Editors), Basin Inversion. Geol. Soc. London Spec. Publ. 88, pp. 3-19.

Souza Cruz, C.E., 1995. Estratigrafia e sedimentação de águas profundas do Neogeno da Bacia de Campos, Estado do Rio de Janeiro, Brasil. PhD Thesis, Universidade Federal do Rio Grande do Sul, PortoAlegre, Brazil.

Spadini, A.R., Esteves, F.R., Dias-Brito, D., Azevedo, R.L.M., and Rodrigues, R., 1988. The Macaé Formation, Campos Basin, Brazil: its evolution in the context of the initial history of the South Atlantic. Rev. Bras. Geoc. 18: 261-272.

Stein, S., Cloetingh, S., Sleep, N.H., and Wortel, R., 1989. Divergent margin earthquakes, stresses, and rheology. In: S. Gregersen and P.W. Basham (Editors), Earthquakes at North-Atlantic Divergent Margins: Neotectonics and Post Glacial Rebound. Kluwer Academic, Dodrecht, pp. 231-259.

Thomaz Filho, A., de Cesaro, P., Mizusaki, A.M.P., and Leão, J.G., 2005. Hot spot volcanic tracks and their implications for South American plate motion, Campos Basin (Rio de Janeiro state), Brazil. J. South Am. Earth Sci. 18: 383-389.

Thompson, R.N., Gibson, S.A., Mitchell, J.G., Dickin, A.P., Leonardos, O.H., Brod, J.A., and Greenwood, J.C., 1998. Migrating Cretaceous-Eocene magmatism in the Serra do Mar alkaline province, SE Brazil: melts from the deflected Trindade mantle plume. J. Petrol. 39: 1493-1526.

Wilson, M., 1992. Magmatism and continental rifting during the opening of the South Atlantic Ocean: a consequence of Lower Cretaceous super-plume activity? In: B.C. Storey, T. Alabaster, and R.J. Pankhurst (Editors), Magmatism and the Causes of Continental Break-up. Geol. Soc. London Spec. Publ. 68, pp. 241-255.

Withjack, M.O., and Olsen, P.E., Schlische, R.W., 1995. Tectonic evolution of the Fundy rift basin, Canada: evidence of extension and shortening during divergent margin development. Tectonics 14: 390-405.

Woodcock, N.H., and Schubert, C., 1994. Continental strike-slip tectonics. In: P. Hancock (Editor), Continental Deformation. Oxford Pergamon Press, New York, pp. 251-263.

Zalán, P.V., and Oliveira, J.A.B., 2005. Origin and structural evolution of the Cenozoic Rift System of southeastern Brazil. Bol. Geoc. Petrobras 13: 269-300.

Ziegler, P.A., Cloetingh, S., and van Wees, J.D., 1995. Dynamics of intra-plate compressional deformation: the Alpine foreland and other examples. Tectonophys. 252: 7-59.

Zuffa, G.G., 1980. Hybrid arenites: their composition and classification. J. Sed. Petrol. 50: 21-29.

Zuffa, G.G., 1985. Optical analysis of arenites: influence of methodology on compositional results. In: G.G. Zuffa (Editor), Provenace of Arenites. D. Reidel Publ. Co, Dodrecht, pp. 165-189.

Zuffa, G.G., 1987. Unravelling hinterland and offshore paleogeography from deep-water arenites. In: J.K. Leggett and G.G. Zuffa (Editors), Marine Clastic Sedimentology. Graham & Trotman, London, pp. 39-61

Zuffa, G.G., 1991. On the use of turbidite arenites in provenance studies: critical remarks. In: A.C. Morton, S.P. Todd, and P.D.W. Haughton (Editors), Developments in Sedimentary Provenance Studies. Geol. Soc. London Spec. Publ. 57, pp. 23-29.

Zuffa, G.G., Cibin, U., and Di Giuglio, A., 1995. Arenite petrography in sequence stratigraphy. The J. of Geol. 103: 451-459.

Zuffa, G.G., Normark W.R., Serra, F., and Brunner, C.A., 2000. Turbidite megabeds in an ocean rift valley recording jökulhlaups of the Late Pleistocene lakes in the western United States. The J. of Geol. 108: 253-274.

Table Captions

Table 1 - Dataset used for the petrographic analysis of Campos Basin turbidite reservoirs, wells location is indicated in Figure 4. The average sample interval was around 8 m.

Table 2 - Average results of the quantitative petrographic analysis of the Campos Basin turbidite reservoirs. Q/F – quartz to feldspar ratio; VRF – volcanic rock fragment content; CI – carbonate intrabasinal content; Intracl – mud intraclasts content; Glauc – glaucony content; Mica –content of micaceous grains.

Table 3 - Basement reactivation events indicated by structural analysis of regional 3D seismic data during the divergent margin phase in Campos basin.

Table 4 - Maturity, internal petrographic pattern, main geodynamic and stratigraphic controls, and paleogeography of the deepwater sand-rich systems formed during the divergent margin phase of Campos Basin.

Figure Captions

Figure 1 - Location of Campos Basin in southeastern Brazilian coast. Observe the mantle plumes related to Campos Basin evolution. CFB – continental flood basalts of the Paraná Basin.

Figure 2 - Structural section through central Campos Basin. Observe the thick rift successions deposited during Lower Cretaceous, and the transgressive-regressive successions deposited from the Albian to the Neogene. Observe also the up to 2700 m high *Serra do Mar* mountains close to the basin border, the wide Neogene shelf, and the dominant detached structural style. The inserts show the location of the basin, and the position of the section in the basin.

Figure 3 - Integrated map of Campos Basin with the basement structure (to the right of the coast line) and the digital topographic model of the continental margin. The bathymetry is indicated in white contours (500 m interval). Observe the wide shelf formed by progradation during the Neogene (closed black dashed line), and the high mountains along the basin border. Observe also the main orientations of the Proterozoic basement fabrics (white dashed lines): Ribeira (NE-SW) and Vitória-Colatina (NNW-SSE).

Figure 4 - Location of the well cores used for quantitative petrographic analysis of the Campos Basin turbidite reservoirs (see Table 1 for details). The integrated map was composed with the basement elevation and the digital topographic model along the basin border.

Figure 5 - Compositional classification of the main Campos Basin turbidite reservoirs according to the classic compositional diagram for sandstones of Folk (1968). Observe that most of the samples plot in the arkose field, with a few samples in the lithic arkose field.

Figure 6 - High-hierarchy compositional classification of the Campos Basin turbidite reservoirs according to the major classes of grains (modified from Zuffa, 1980). Observe that most of the samples plot in the field of siliciclastic non-carbonate extrabasinal grains (NCE). The Albian turbidites show a departure towards the carbonate intrabasinal origin (CI). The Santonian and the Paleocene reservoirs show a departure towards the non-carbonate intrabasinal contribution (NCI). The Cenomanian, Upper Eocene and Miocene turbidites show a mixed departure to intrabasinal contribution (CI and NCI). The Upper Eocene includes one sample classified as a calcarenite.

Figure 7 - Compositional classification of the Campos Basin turbidite reservoirs according to the tectonic setting of the sediment-source area (Dickinson and Suczec, 1979; Dickinson, 1985). Observe that most of the samples plot in the field of uplifted basement blocks (rift basin and immature divergent margin). The Upper Oligocene reservoir shows a departure towards the transitional continent field (mature divergent margin), as well as a few Albian, Cenomanian and Miocene samples. The Maastrichtian reservoir shows a departure towards the field of volcanic contribution.

Figure 8 - Photomicrographs of the Albian reservoir (Well 01): Observe the widespread calcite cementation. (a) Well-sorted, sub-angular, fine-grained sandstone arkose; observe the foliated metamorphic rock fragment. (b) Well-sorted, subr-ounded, fine-grained sandstone arkose; observe the intrabasinal carbonate grains (oncoid, bioclasts). (c) Well-sorted, sub-rounded, fine-grained sandstone arkose; observe the significant content of micaceous grains. (d) Poorly-sorted, sub-rounded, fine-grained sandstone arkose; observe the coarse microcline and plagioclase grains. (e) Moderately-sorted, sub-angular, fine-grained sandstone arkose to hybrid arenite; observe the large carbonate bioclasts (mostly mollusks). (f) Well-sorted, sub-rounded, fine-grained sandstone arkose to hybrid arenite; observe the carbonate ooids.

Figure 9 - Petrographic parameters grain size, quartz to feldspar ratio (Q/F), and carbonate intrabasinal content (CI) of the Albian reservoir (Well 01). Observe constant fine grain size. Observe also that Q/F and CI show co-variant, high-frequency cyclicity, and growing upwards trend (dashed arrows).

Figure 10 - Photomicrographs of the Cenomanian reservoir (Well 02): Observe the widespread calcite cementation. (a) Moderately-sorted, sub-angular, fine-grained sandstone arkose; observe the carbonate bioclast. (b) Well-sorted, sub-angular, medium-grained sandstone arkose. (c) Moderately-sorted, sub-rounded, medium-grained sandstone arkose; observe the coarse plagioclase grain. (d) Moderately-sorted, sub-angular, fine-grained sandstone arkose; observe the high content of micaceous grains. (e) Poorly-sorted, sub-angular, fine-grained sandstone arkose; observe the pebble-size plutonic rock fragment. (f) Poorly-sorted, sub-angular, fine-grained sandstone arkose; observe the coarse microcline grain and the large mud intraclast.

Figure 11 - Photomicrographs of the Santonian reservoir (Well 03): (a) Moderately-sorted, sub-rounded, medium-grained sandstone, arkose; observe the pseudo-matrix (derived from compacted mud intraclasts) replaced by calcite (cc) and opaline silica (sc). (b) Poorly-sorted, sub-rounded, medium-grained sandstone, arkose; observe the pseudo-matrix (from compacted mud intraclasts) replaced by opaline silica (sc), containing bioclasts of nannofossils and planktonic foraminifera. (c) Poorly-sorted, sub-angular, medium-grained sandstone, arkose; observe the large compacted mud intraclast. (d) Poorly-sorted, sub-rounded, coarse-grained sandstone, arkose. (e) Very poorly-sorted, sub-rounded, medium-grained sandstone, arkose; observe the pebble-sized microcline grain. (f) Poorly-sorted, sub-angular, medium-grained sandstone, arkose; observe the coarse quartz and feldspar grains.

Figure 12 - Cross plot showing the internal correlation between grain size and quartz to feldspar ratio (Q/F) observed in the Santonian and in the Paleogene deepwater sand-rich systems of Campos Basin.

Figure 13 - Photomicrographs of the Campanian reservoir (Well 04): (a) Poorly-sorted, sub-angular, very coarse-grained sandstone arkose. (b) Poorly-sorted, sub-angular, fine-grained sandstone, arkose; observe the large mud intraclast with planktonic bioclasts. (c) Poorly-sorted, sub-angular, coarse-grained sandstone arkose. (d) Moderately-sorted, sub-rounded, fine-grained sandstone arkose; observe the volcanic rock fragment with trachytic texture. (e) Poorly-sorted, sub-angular, medium-grained sandstone arkose; observe the compacted volcanic rock fragment. (f) Moderately-sorted, sub-rounded, coarse-grained sandstone arkose. Observe the overall very low quartz to feldspar ratio.

Figure 14 - Photomicrographs of the Maastrichtian reservoir (Well 05): (a) Poorly-sorted, sub-angular, medium-grained sandstone, lithic arkose; observe the volcanic rock fragments. (b) Very poorly-sorted, sub-angular, medium-grained sandstone, arkose; observe the pebble-sized feldspar grains. (c) Poorly-sorted, sub-angular, coarse-grained sandstone, arkose; observe the pebble-size feldspar grains. (d) Moderately-sorted, sub-angular, fine-grained sandstone, arkose; observe the high content of micaceous grains and of black carbonaceous fragments of burned wood. (e) Detail of the compacted carbonaceous fragments and micas. (f) Moderately-sorted, sub-angular, fine-grained sandstone, lithic arkose; observe the volcanic rock fragment.

Figure 15 - Photomicrographs of the Paleocene reservoir (Well 06): (a) Poorly-sorted, sub-rounded, coarse-grained sandstone, arkose. (b) Moderately-sorted, sub-angular, medium-grained sandstone, arkose; observe the volcanic rock fragments. (c) Moderately-sorted, sub-angular, medium sand arkose; observe the volcanic rock fragment. (d) Poorly-sorted, sub-angular, medium-grained sandstone, arkose; observe the mollusk bioclast (lower-left), the compacted mud intraclast (upper-right), and the glaucony grain (G). (e) Poorly-sorted, sub-angular, fine-grained sandstone, arkose; observe the planktonic foraminifer bioclasts, and the volcanic rock fragment. (f) Poorly-sorted, sub-rounded, coarse sand arkose; observe the large glauconitic intraclast (G).

Figure 16 - Photomicrographs of the Middle Eocene reservoir (Well 06): (a) Moderately-sorted, sub-angular, fine-grained sandstone, arkose; observe the compacted glaucony grain (G). (b) Moderately-sorted, sub-rounded, medium-grained sandstone, arkose; observe the high feldspar content. (c) Poorly-sorted, sub-angular, coarse-grained sandstone, arkose. (d) Poorly-sorted, sub-angular, fine-grained sandstone, arkose; observe the large argillaceous fragment with "silky" texture characteristic of soils (SF). (e) Large, laminated microbialite fragment. (f) Poorly-sorted, sub-rounded, fine-grained sandstone, arkose; observe the large intraclast (lower left), and the very coarse plutonic rock fragment and microcline grains.

Figure 17 - Photomicrographs of the Upper Eocene reservoir (Well 06): (a) Poorly-sorted, sub-angular, medium-grained sandstone, arkose; observe the large red algae bioclast (RA). (b) Moderately-sorted, sub-angular, medium-grained sandstone, arkose; observe the moderately compacted mica grain. (c) Poorly-sorted, medium-grained calcarenite; observe the glaucony grains (G), the macroforaminifer bioclast (FF), and the intense calcite cementation. (d) Poorly-sorted, sub-angular, coarse-grained sandstone, arkose. (e) Moderately-sorted, sub-angular, medium-grained hybrid arenite; observe the foraminifer bioclasts. (f) Poorly-sorted, sub-angular, medium-grained sandstone, arkose; observe the carbonate bioclasts, and the glaucony grains (G).

Figure 18 - Photomicrographs of the Lower Oligocene reservoir (Well 07): (a) Well-sorted, sub-angular, fine-grained sandstone, arkose; observe the carbonate bioclasts; "coatings" around the grains are effect of defective impregnation. (b) Poorly-sorted, sub-rounded, fine-grained sandstone, arkose; observe the very coarse sand grains. (c) Moderately-sorted, sub-angular, fine-grained sandstone, arkose; observe the large, compacted mud intraclast with planktonic bioclasts. (d) Moderately-sorted, sub-angular, medium-grained sandstone, arkose. (e) Poorly-sorted, subangular fine-grained sandstone, arkose; observe the large bryozoan bioclast. (f) Well-sorted, sub-angular, fine-grained sandstone, arkose.

Figure 19 - Photomicrographs of the Upper Oligocene reservoir (Wells 08/09): (a) Poorly-sorted, sub-angular, fine-grained sandstone, arkose; observe the coarse feldspar grains. (b) Poorly-sorted, sub-angular, fine-grained sandstone, arkose; observe the large bryozoan bioclast. (c) Poorly-sorted, sub-rounded, fine-grained sandstone, arkose. (d) Moderately-sorted, sub-rounded, fine-grained sandstone, arkose; observe the foraminifer bioclast. (e) Well-sorted, sub-rounded fine-grained sandstone, arkose; observe the planktonic foraminifer bioclasts, and the large mud intraclast (lower right) with carbonaceous fragments (black). (f) Well-sorted, sub-angular, fine–grained sandstone, arkose.

Figure 20 - Petrographic parameters of the Upper Oligocene reservoir (Wells 08/09): grain size and quartz to feldspar ratio (Q/F). Observe the almost constant fine grain size. Observe also that the Q/F ratio shows a growing-upwards trend (dashed arrow), a well-defined step with higher quartz content in the upper-half of the cored section, and a superimposed high-frequency cyclicity.

Figure 21 - Photomicrographs of the Miocene reservoir (Well 10): (a) Well-sorted, sub-angular, fine-grained sandstone, arkose; observe the foraminifer bioclast. (b) Well-sorted, sub-rounded, fine-grained sandstone, arkose; observe the foraminifer bioclasts. (c) Well-sorted, sub-rounded, fine-grained sandstone, arkose; observe the carbonate bioclasts. (d) Moderately-sorted, sub-angular, fine-grained sandstone, arkose; observe the carbonate bioclasts, and the glaucony grains (G). (e) Well-sorted, sub-rounded fine-grained sandstone, arkose; observe the glaucony grain (G). (f) Poorly-sorted, sub-angular, medium-grained sandstone, arkose; observe the very coarse microcline grain.

Figure 22 - Petrographic parameters grain size and quartz to feldspar ratio (Q/F) of the Miocene reservoir (Well 10): Observe the fining-upwards trend from medium to very fine sand grain size. Observe also that the Q/F ratio shows a well-defined growing-upwards trend (dashed arrow).

Figure 23 - Average quartz to feldspar ratio (Q/F) of the main Campos Basin deepwater sand-rich systems. The Q/F trend shows a linear drop from 1.00 in the Albian and the Cenomanian to 0.75 in the Upper Cretaceous and the Paleogene; then there is an exponential increase to 1.40 in the Upper Oligocene, and an equally strong drop to 0.90 in the Miocene.

Figure 24 - Grain size trend of the main Campos Basin deepwater sand-rich systems. The average grain size changed from fine sand during the Albian and Cenomanian, to medium sand from Santonian to Upper Eocene, and returned to fine sand from Lower Oligocene to Miocene.

Figure 25 - Cross-plot between the petrographic parameters grain size and quartz to feldspar ratio (Q/F) of the main Campos Basin turbidite reservoirs. Observe that two types of deepwater sand-rich systems can be defined by the compositional-textural character: (i) mature, fine sand systems (average Q/F = 1.00), and (ii) immature, medium sand systems (average Q/F = 0.75).

Figure 26 - Average amounts of volcanic rock fragments (VRF) in the main Campos Basin deepwater sand-rich systems. VRF content shows a background around 1%, and a peak close to 9% in the Maastrichtian, with amounts above 3% in the Campanian and in the Paleocene.

Figure 27 - Average contribution of carbonate intrabasinal grains (CI) in the main Campos Basin deepwater sand-rich systems. The CI content shows strong oscillations, with peaks in the Albian and Upper Eocene, and troughs around zero at the end of the Cretaceous and during the Middle Eocene. CI contribution is around 5% in the Cenomanian, the Paleocene, and the Oligocene turbidite systems; it grows slightly in the Miocene (7.5%).

Figure 28 - Average content of mud intraclasts in the main Campos Basin deepwater sand-rich systems. Mud intraclast contribution was very low during the Albian. There is a step of average intraclast content around 10% from Cenomanian to Lower Oligocene. During the Upper Oligocene and the Miocene the intraclast contribution dropped to around 5%.

Figure 29 - Average content of glaucony in the main Campos Basin turbidite reservoirs. The background glaucony content is very low (below 0.5%), but there are significant peaks in the Paleocene, Upper Eocene and Miocene (above 2%).

Figure 30 - Average content of micaceous grains in the main Campos Basin deepwater sand-rich systems. Observe the oscillation in the amount of micaceous grains between 1% and 3%, and the overall trend of decrease (dashed arrow) from 3.5% in the Albian to 0.5% in the Miocene.

Figure 31 - Location of the seismic sections used in the structural analysis of basement reactivations (sections A, B, C, D, E, F, G, and H). The map was composed with the basement structure, in the offshore portion to the right of the coast line, and the digital topographic model of the continental margin, to the left of the coast line.

Figure 32 - (a) Seismic attribute map of Barremian horizon and insert with kinematical interpretation. (b) 3D perspective with seismic section and attribute map of Barremian horizon. (c) Depth-converted seismic section (see the regional position of section A in Fig. 31). Observe Lower-Cretaceous strata folded at Albian-Cenomanian transition. Fold axes are indicated by darker high maximum curvature trends. The structure is interpreted as a result of transpression related to left-lateral strike-slip reactivation of NE-SW basement fabric. SHmax is the maximum horizontal stress. Observe also the Paleogene volcanic structure.

Figure 33 - (a) Dip map of Albian horizon and insert with kinematic interpretation. Observe mixed S and Z sinuous pattern of *en-echelon* fold axes at Albian strata. The structure can be interpreted as a change from right-lateral to left-lateral reactivation of NNW-SSE basement fabric associated with rotation of regional loading stresses. (b) 3D perspective with seismic section and attribute map of Albian horizon. Observe that low Dip values define very well the fold axes at Albian successions of the early divergent margin phase. (c) Depth-converted seismic section (see the regional position of section B in Fig. 31). Observe that pre-Aptian strata of the rift phase are also faulted and folded. Observe possible buttress effect of the basement high. SHmax is the maximum horizontal stress.

Figure 34 - (a) Structural map of Albian horizon and insert with kinematic interpretation. Observe the pattern of *en-echelon* fold axes at Albian strata. The structure can be interpreted as a right-lateral reactivation of NE-SW basement fabric. (b) 3D perspective with seismic section and structural map of Albian horizon. Observe folding of Albian and Upper Cretaceous strata. (c) Depth-converted seismic section (see the regional position of section C in Fig. 31). Observe that only pre-Maastrichtian strata are folded. SHmax is the maximum horizontal stress.

Figure 35 - (a) Structural map of Santonian horizon showing an anticline trending NE-SW and plunging to NE. (b) 3D perspective of the anticline. (c) Depth-converted seismic section showing a large fold with 3 km half-wavelength, and around 300 m amplitude (see the regional position of section D in Fig. 31). Up to 2700 m of Upper Cretaceous and Paleogene strata were folded during the Eocene. The main deformation phase is indicated by onlap and section growth in the Eocene. The structure is interpreted as a fault propagation fold associated with inversion of Albian listric normal faults. Inversion was caused by transpression along NW-SE basement fabric at northeastern Campos Basin. The structure is contiguous to the folded area of Figure 32.

Figure 36 - (a) Semblance map of Maastrichtian horizon showing a NNE-SSW fault system. (b) Depth-converted seismic section of the fault system (see the regional position of section E in Fig. 31). Observe fault activity and section growth during the Paleogene indicated by black bars. (c) Stereonet contour plot of the faults mapped in the area showing a quite dispersed distribution (188 fault poles). Faulting is interpreted as a negative flower structure associated with transtension caused by reactivation of NE-SW basement fabric.

Figure 37 - (a) Structural map of Lower Miocene horizon showing an anticline trending NE-SW. (b) 3D perspective of the structure. (c) Depth-converted seismic sections showing an inversion fold (see the regional position of sections F and G in Fig. 31). Observe that Paleogene depocenters (indicated by black bars) were inverted during Neogene. Fold axial plane is vertical and oriented at N40E. Folding was probably caused by transpression related to reactivation of basement fabric at the observed structural high.

Figure 38 - (a) Structural map of Oligocene horizon showing an anticline trending N-S, and plunging to the north. (b) 3D perspective of the structure. (c) Depth-converted seismic section showing an inverted grabben (see the regional position of section H in Fig. 31). Observe the constant isopach of the Paleogene, between Oligocene and Maastrichtian (pre-kinematic). The inversion of the Cretaceous depocenter in the Neogene is indicated by the sin-kinematic onlap pattern (dashed circle). The inversion was probably caused by transpression related to reactivation of the basement highs.

Figure 39 - Correlation between the drift of the South-American plate above the Trindade mantle plume and the evolution of the petrographic parameters of the deepwater sandstones in Campos Basin. Observe that the passage of the Campos Basin above the plume is associated with a consistent trend of increasing compositional and textural immaturity with average lower quartz to feldspar ratio (Q/F) and coarser grain size from the Santonian to the Eocene. Observe also that the average high contribution of volcanic rock fragments (VRF) corresponds to a shorter time interval from the Campanian to the Paleocene, when the plume was at the basin margin.

Figure 40 - Correlation between the main petrographic parameters of the deepwater sandstones and the geodynamic processes during the divergent margin phase in Campos Basin. Plume effects include dynamic uplift and magmatism. Observe that the two major deepwater sand-rich systems in Campos Basin (Bruhn et al., 2003), indicated with black stars, were formed at the end of periods of tectonic quiescence.

Well	Age	Age (Ma BP)	Core (m)	Thin Sections
Well 10	Miocene	16.5	110	10
Well 08/Well 09	Upper Oligocene	23.5	190	18
Well 07	Lower Oligocene	31	100	8
Well 06	Upper Eocene	41	20	6
Well 06	Middle Eocene	47	30	10
Well 06	Paleocene	58	50	8
Well 05	Maastrichtian	65	80	10
Well 04	Campanian	72	30	10
Well 03	Santonian	84	100	10
Well 02	Cenomanian	94	140	14
Well 01	Albian	98	140	17
		Total	990	121

Table 1

Reservoir	Q/F	Grain Size	VRF (%)	CI (%)	Intracl (%)	Glauc (%)	Mica (%)
Miocene	0.91	Fine sand	0.40	7.85	5.03	2.02	0.33
Upper Oligocene	1.40	Fine sand	1.29	3.87	4.66	0.17	0.35
Lower Oligocene	0.82	Fine sand	0.08	5.65	11.10	0.06	1.21
Upper Eocene	0.71	Medium sand	0.72	18.15	9.74	4.80	2.94
Middle Eocene	0.77	Medium sand	1.39	0.54	12.75	0.54	1.00
Paleocene	0.75	Medium sand	4.54	5.76	13.44	2.41	1.75
Maastrichtian	0.65	Medium sand	8.67	0.00	7.90	0.04	3.47
Campanian	0.69	Medium sand	3.10	0.30	11.46	0.00	3.23
Santonian	0.88	Medium sand	0.03	1.52	13.75	0.31	1.00
Cenomanian	1.00	Fine sand	0.62	5.43	11.10	0.30	2.95
Albian	1.02	Fine sand	0.78	13.42	0.82	0.12	3.53

Table 2

Age	Structural Style	Kinematics	Position in the basin
Neogene	Inversion fold; inverted grabben	Transpression or compression	Center; Northeastern
Paleogene	Fault-propagation fold; negative flower	Transpression; transtension	Northeastern; Center
Santonian	Regular folds with sinuous axes	Transpression	Northeastern
Albian-Cenomanian	Regular folds with sinuous axes	Transpression	South; Northeastern

Table 3

Deepwater system	Petrography	Internal pattern	Geodynamic Control	Stratigraphic Control	Relief	Shelf
Miocene	Relativ. Mature	Trend	Tectonic reactivation	Downstream	Moderate	Wide
Upper Oligocene	Relativ. Mature	Cyclic/Trend	Escarpment retreat	Downstream	Low	Wide
Lower Oligocene	Relativ. Mature	Episodic	Escarpment retreat	Downstream	Moderate	Short
Upper Eocene	Immature	Episodic	Tectonic reactivation	Upstream	High	Short
Middle Eocene	Immature	Episodic	Tectonic reactivation	Upstream	High	Short
Paleocene	Immature	Episodic	Tectonic reactivation	Upstream	High	Short
Maastrichtian	Immature	Episodic	Dynamic uplift	Upstream	High	Null
Campanian	Immature	Episodic	Dynamic uplift	Upstream	High	Null
Santonian	Immature	Episodic	Tectonic reactivation	Upstream	High	Null
Cenomanian	Relativ. Mature	Episodic	Escarpment retreat	Downstream	Moderate	Short
Albian	Relativ. Mature	Cyclic/Trend	Escarpment retreat	Downstream	Low	Wide

Table 4

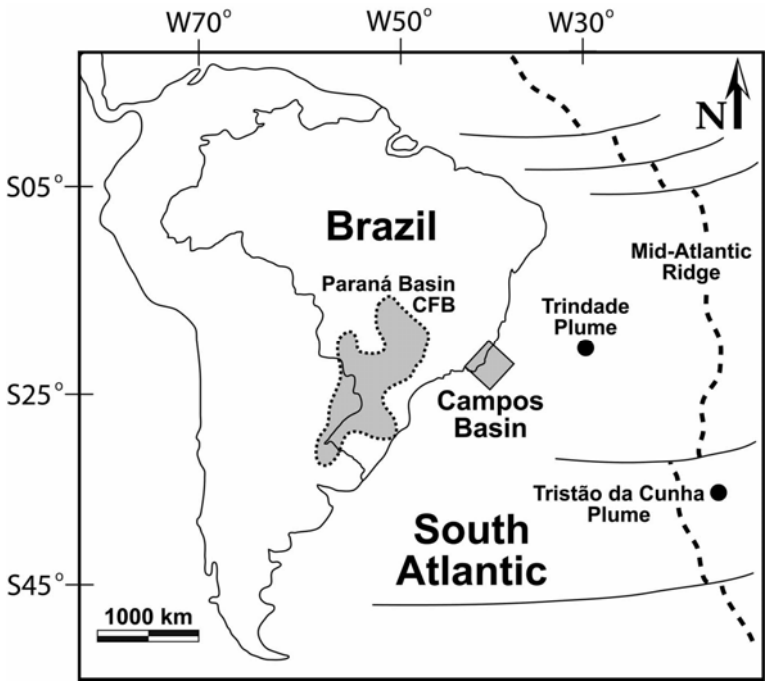

Figure 1

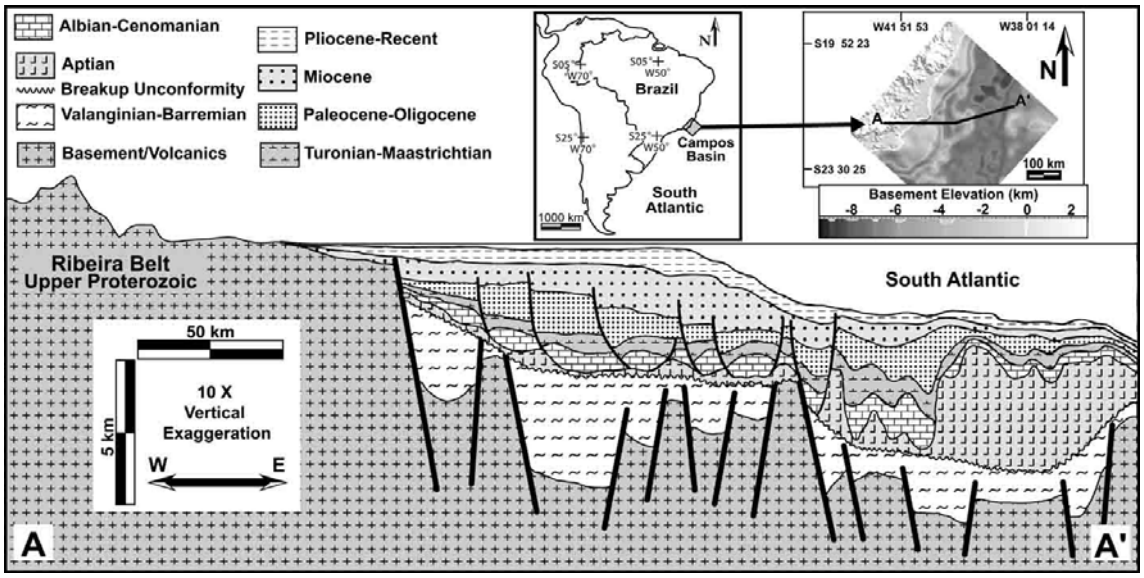

Figure 2

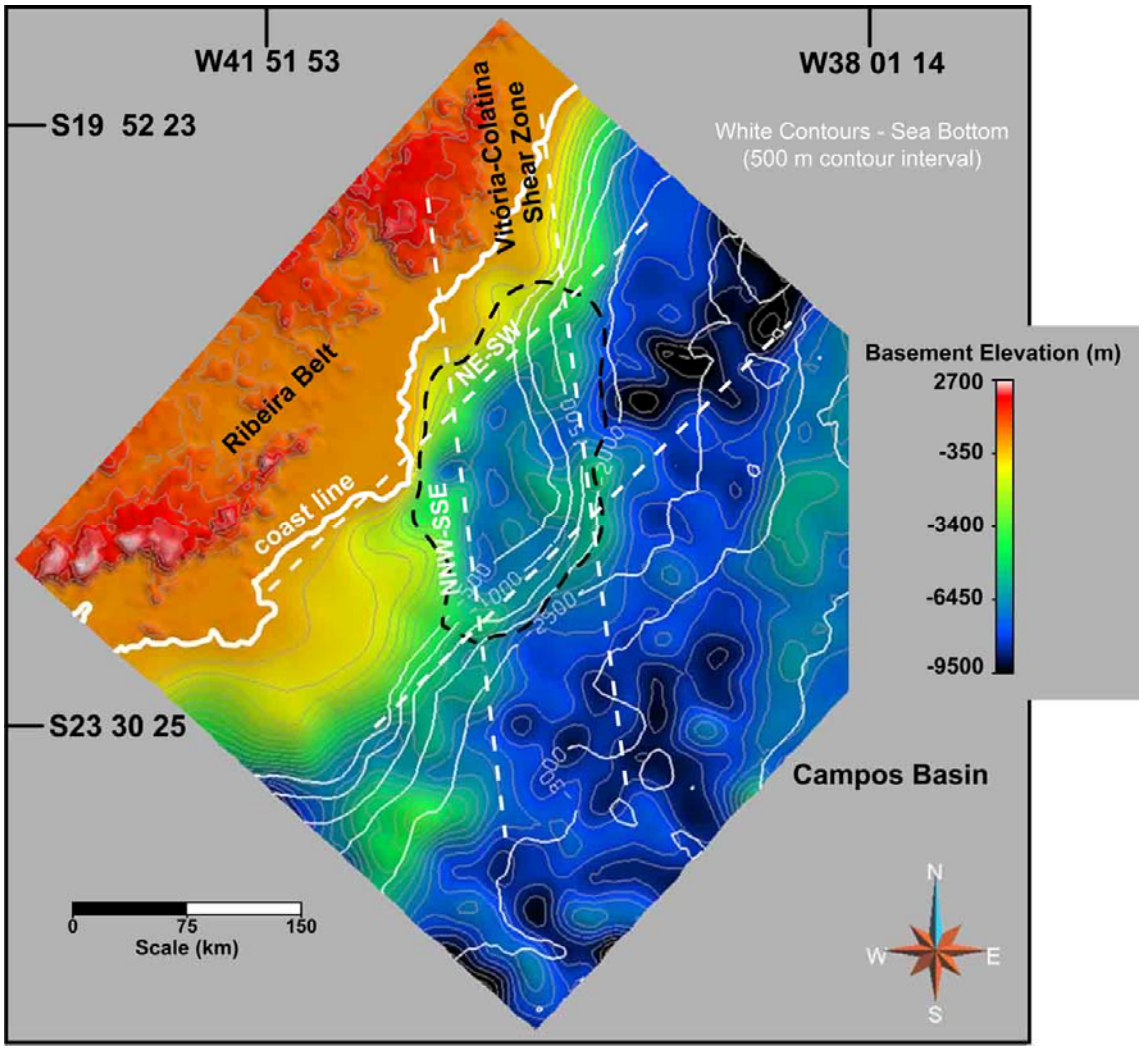
W41 51 53
W38 01 14
S19 52 23
S23 30 25
White Contours - Sea Bottom
(500 m contour interval)
Vitória-Colatina
Shear Zone
NE-SW
NNW-SSE
Ribeira Belt
coast line
Basement Elevation (m)
2700
-350
-3400
-6450
-9500
Campos Basin
0
75
150
Scale (km)
N
W
E
S

Figure 3

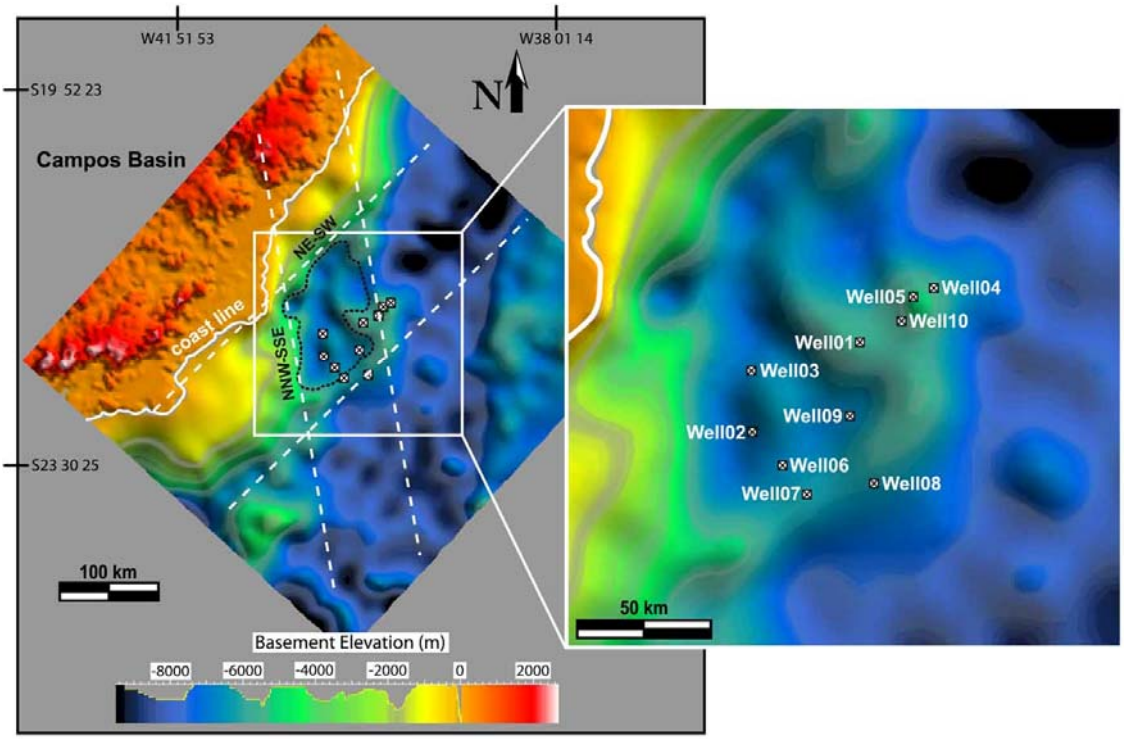

Figure 4

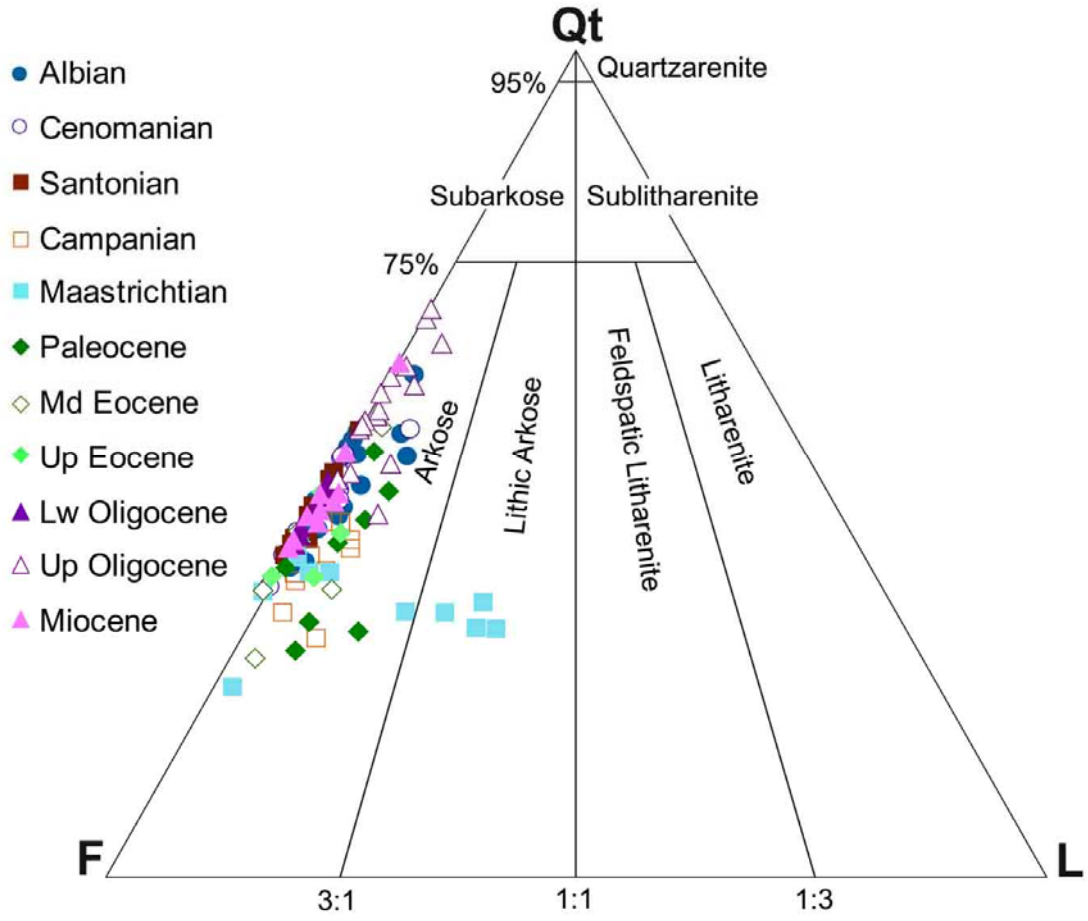

Figure 5

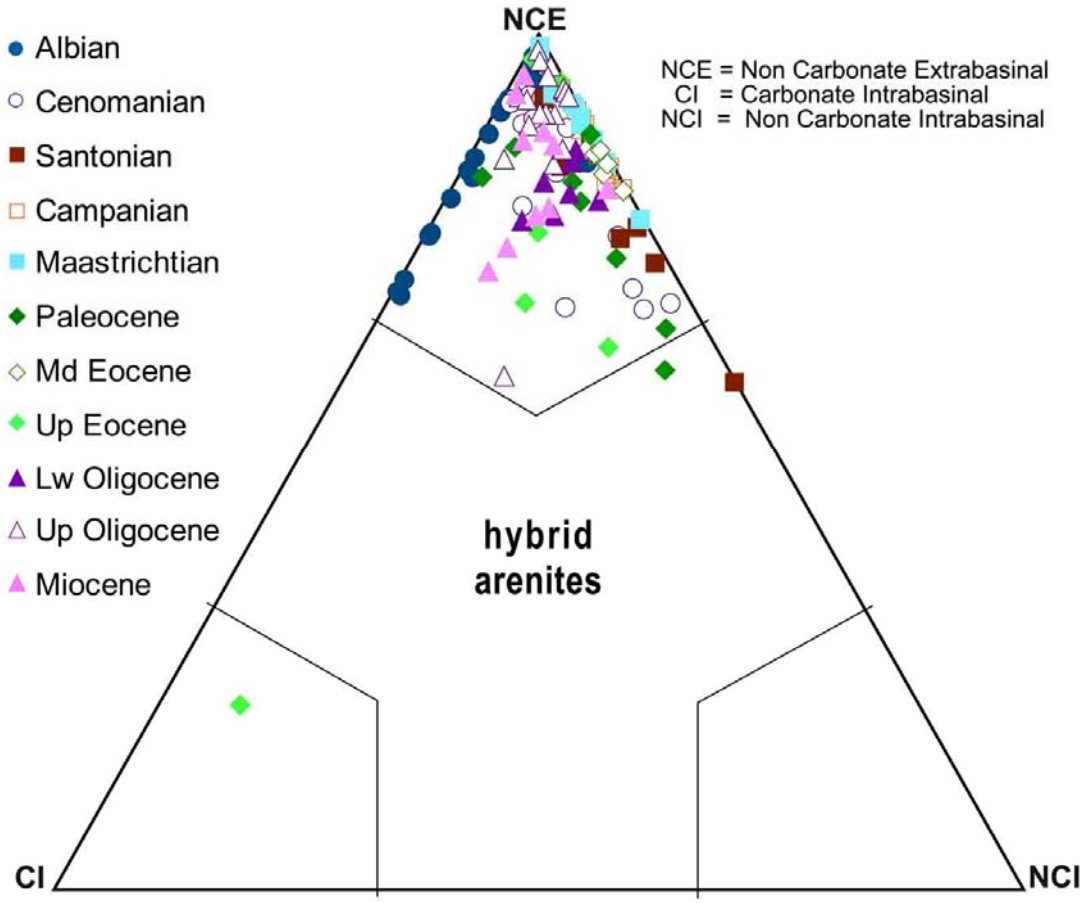

Figure 6

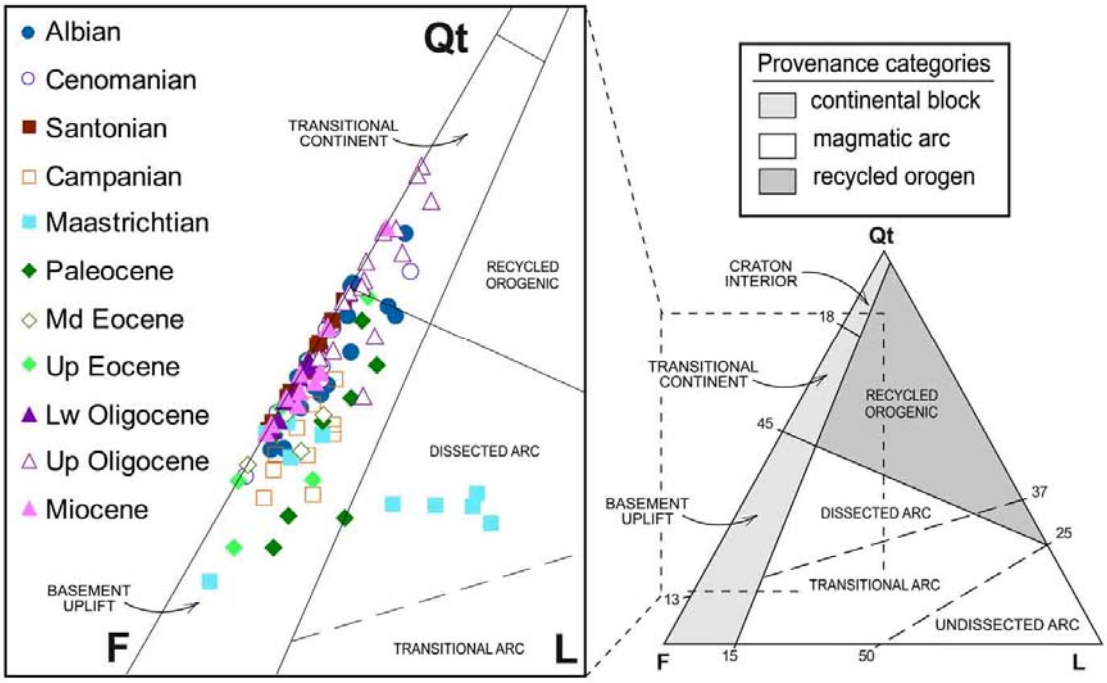

Figure 7

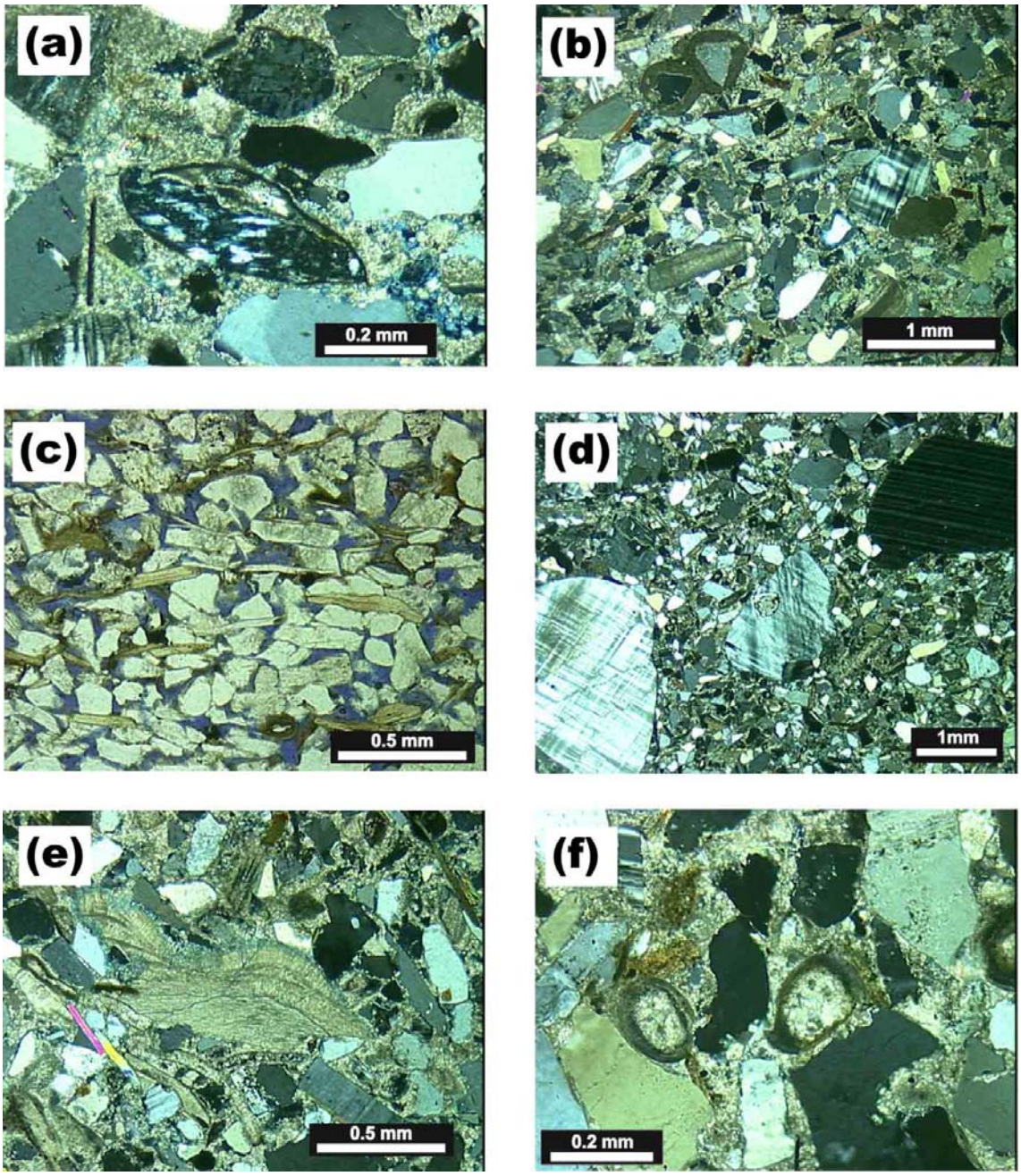

Figure 8

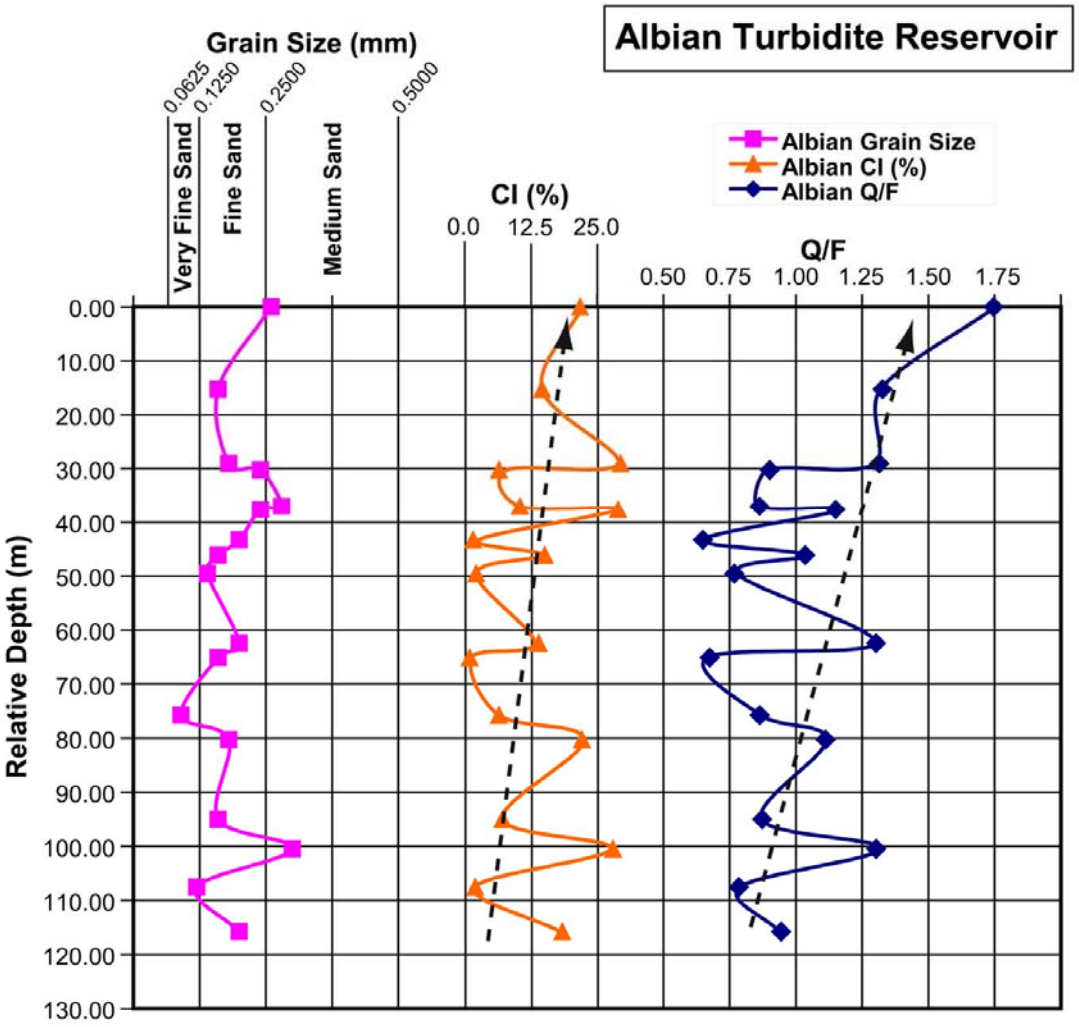
Albian Turbidite Reservoir
Grain Size (mm)
0.0625
0.1250
0.2500
0.5000
Very Fine Sand
Fine Sand
Medium Sand
Albian Grain Size
Albian Cl (%)
Albian Q/F
Cl (%)
0.0 12.5 25.0
Q/F
0.50 0.75 1.00 1.25 1.50 1.75
Relative Depth (m)
0.00
10.00
20.00
30.00
40.00
50.00
60.00
70.00
80.00
90.00
100.00
110.00
120.00
130.00

Figure 9

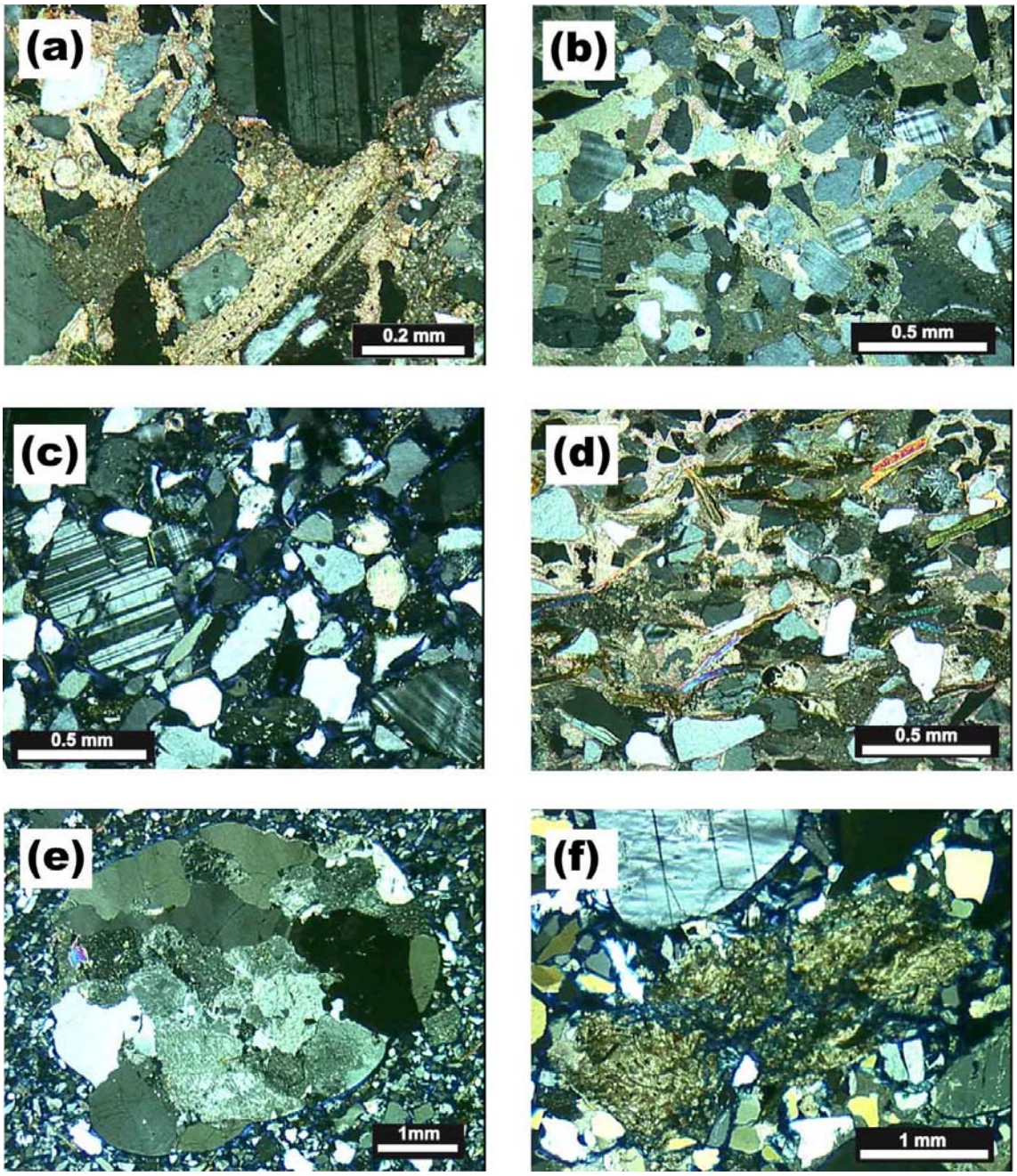

Figure 10

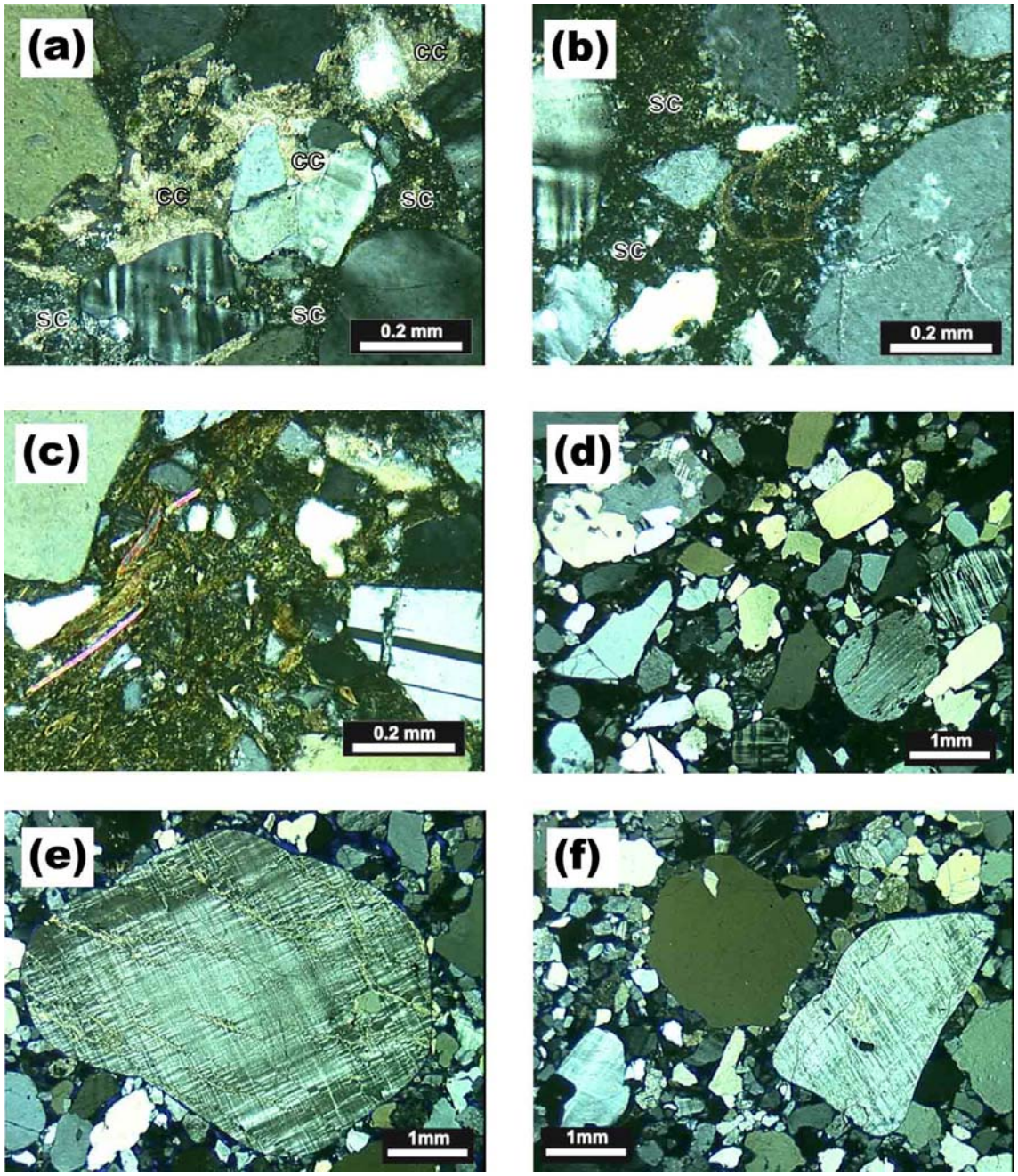

Figure 11

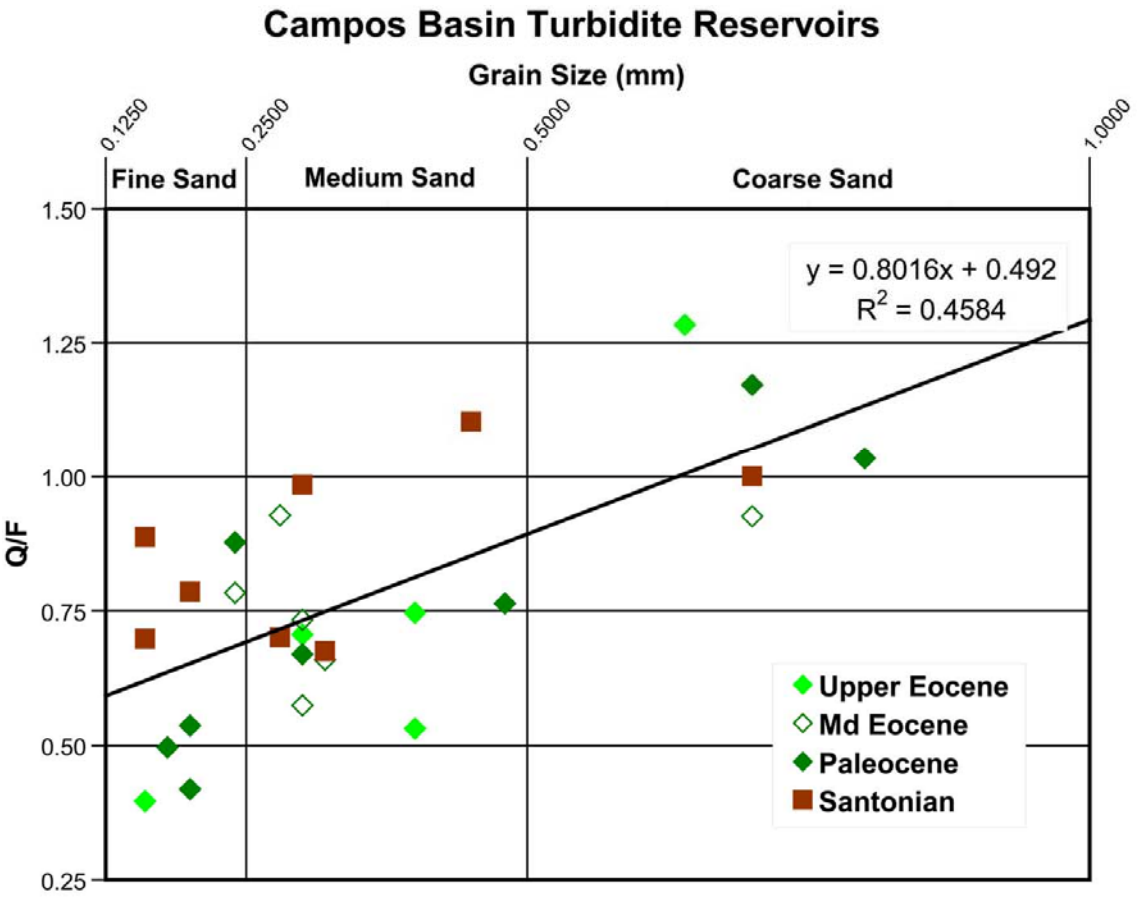
Campos Basin Turbidite Reservoirs
Grain Size (mm)
0.1250
0.2500
0.5000
1.0000
Fine Sand
Medium Sand
Coarse Sand
1.50
1.25
1.00
0.75
0.50
0.25
Q/F
y = 0.8016x + 0.492
R2 = 0.4584
Upper Eocene
Md Eocene
Paleocene
Santonian

Figure 12

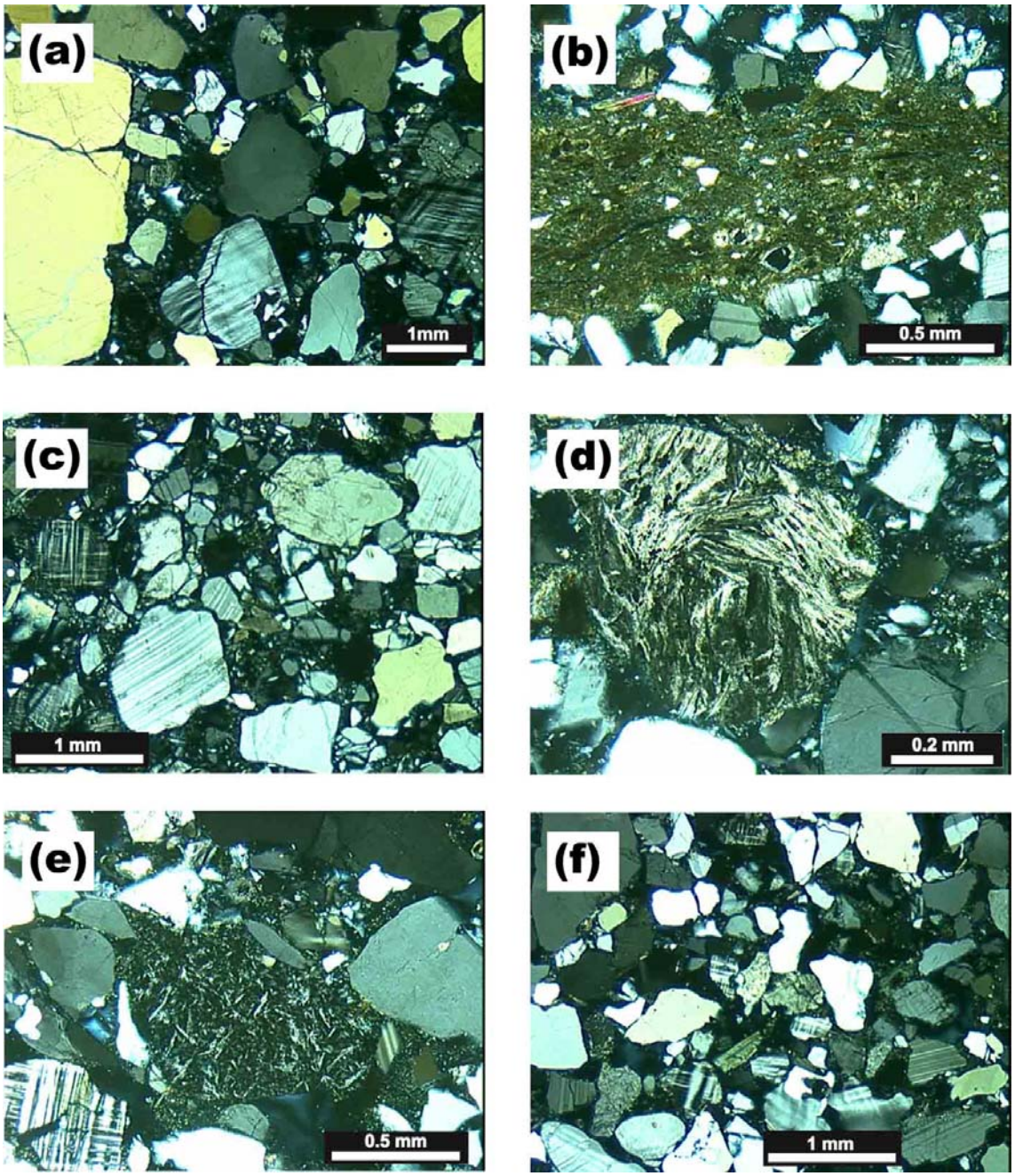

Figure 13

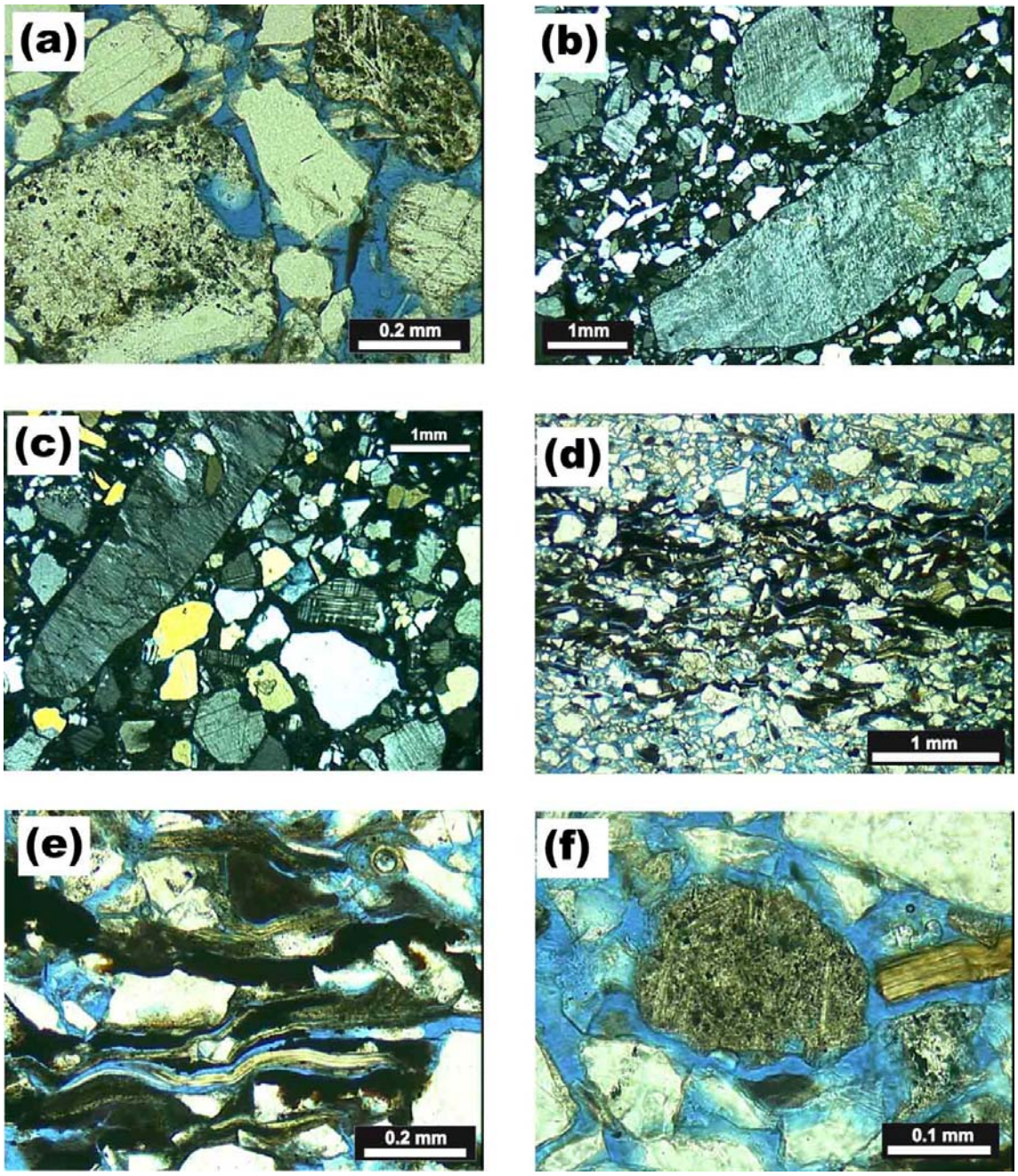

Figure 14

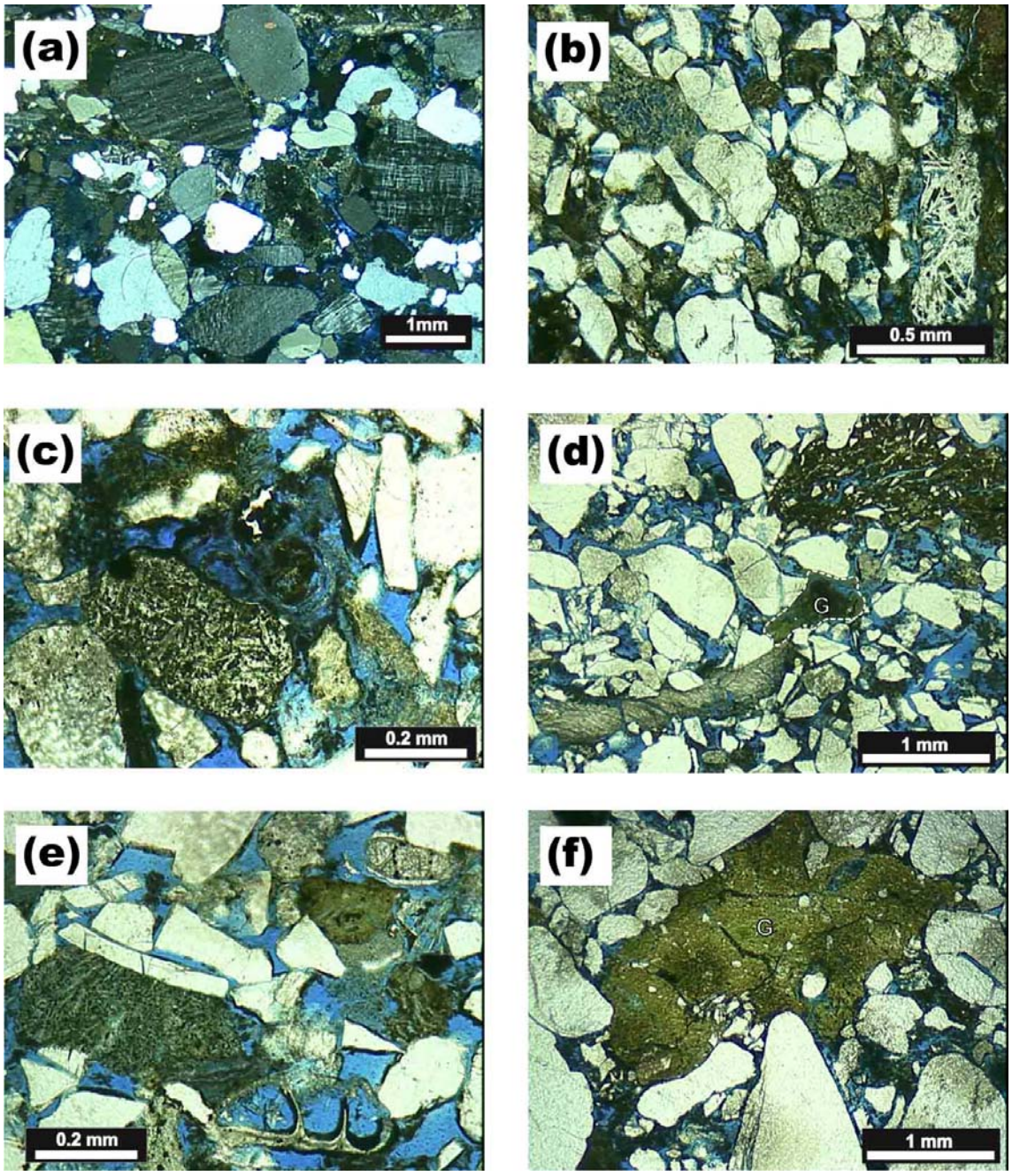

Figure 15

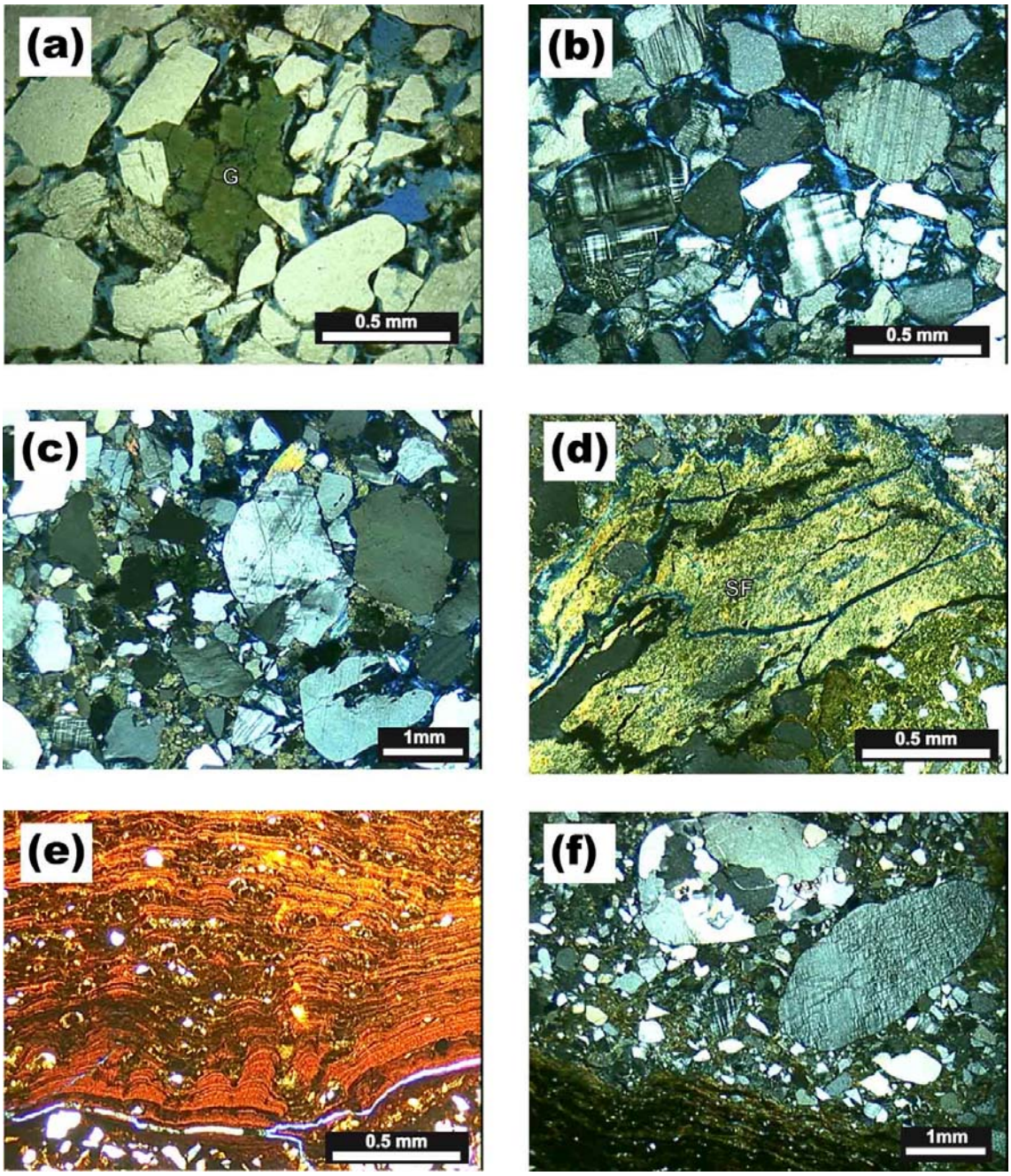

Figure 16

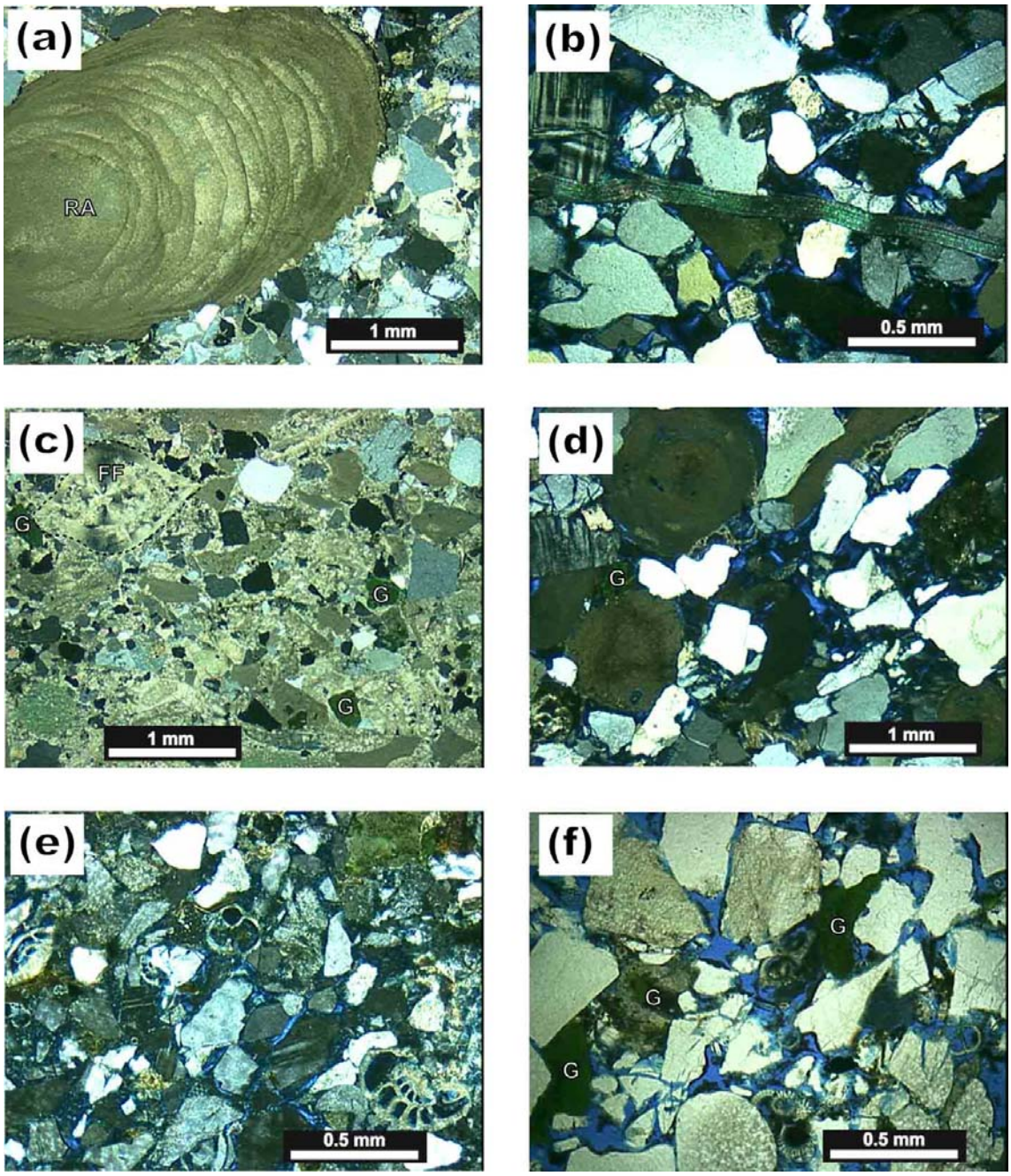

Figure 17

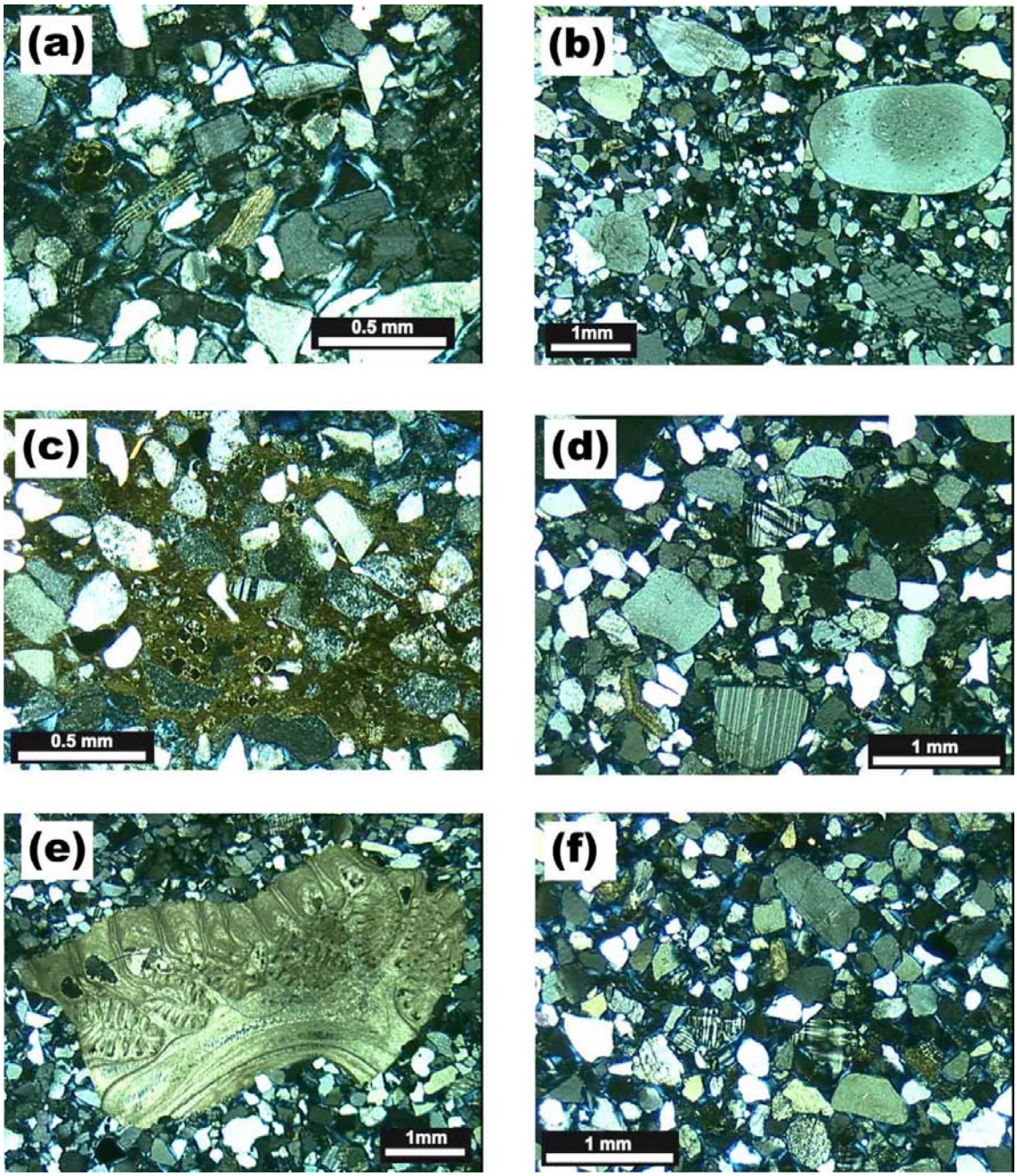

Figure 18

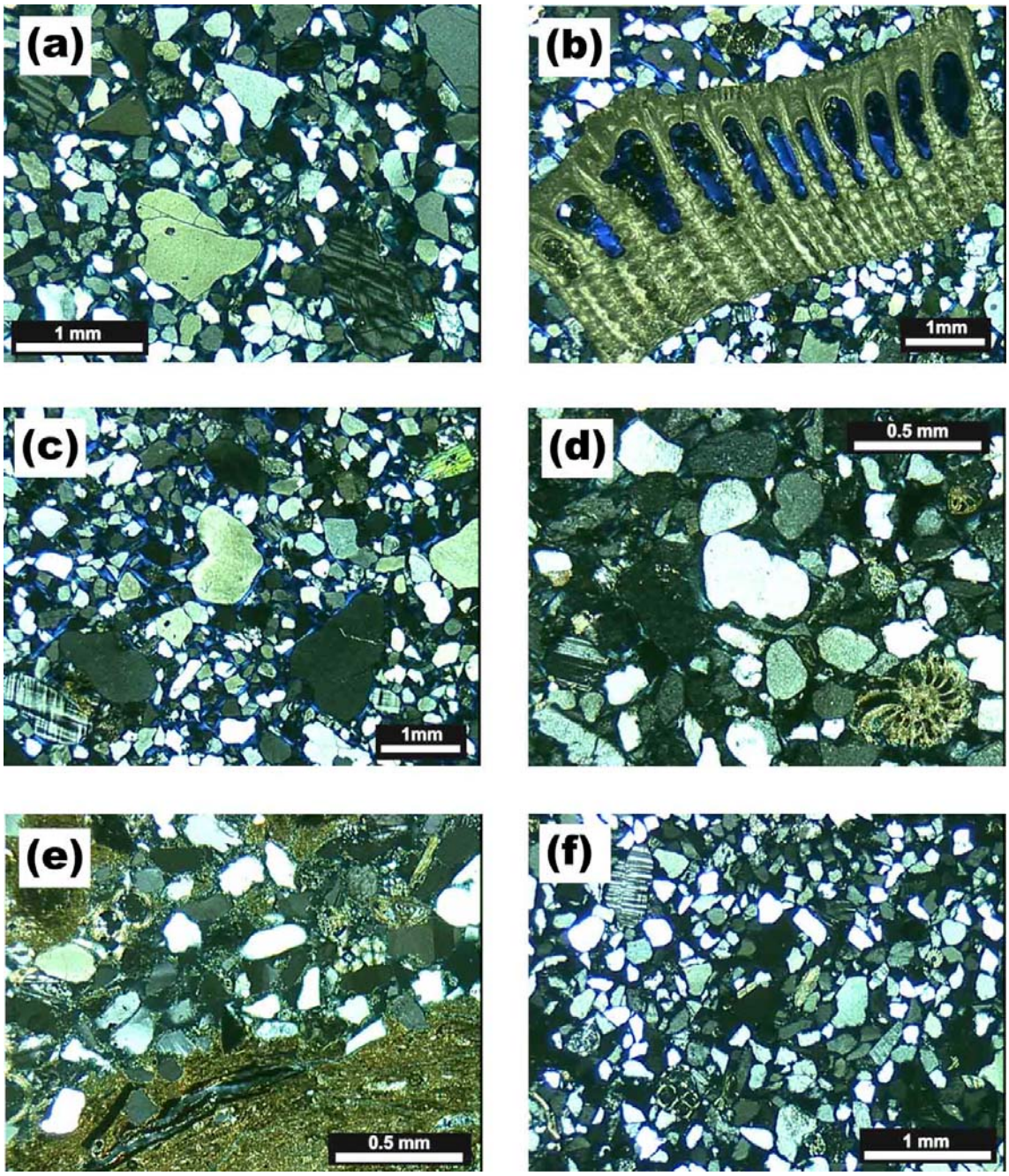

Figure 19

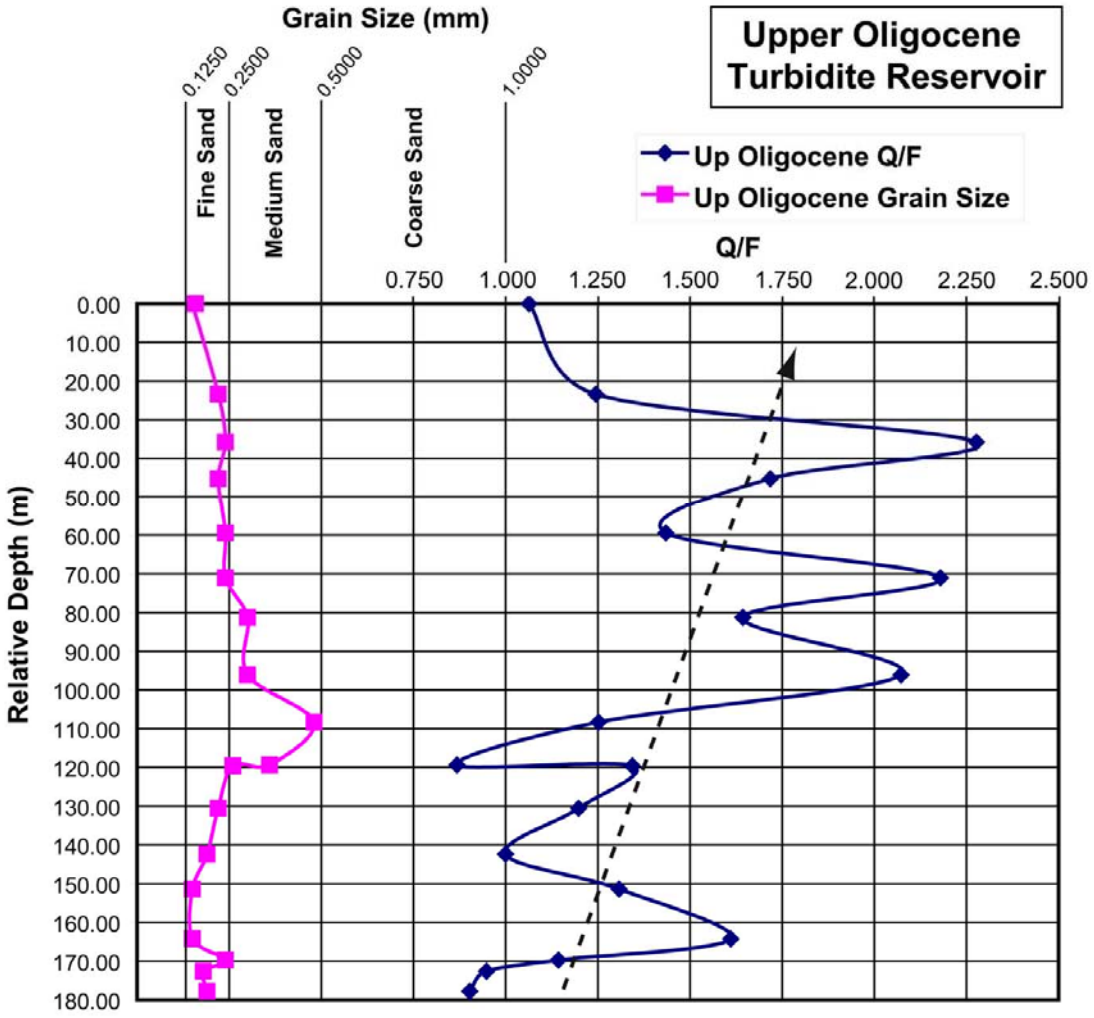
Grain Size (mm)
0.1250
0.2500
0.5000
1.0000
Fine Sand
Medium Sand
Coarse Sand
Upper Oligocene
Turbidite Reservoir
Up Oligocene Q/F
Up Oligocene Grain Size
Q/F
0.750
1.000
1.250
1.500
1.750
2.000
2.250
2.500
Relative Depth (m)
0.00
10.00
20.00
30.00
40.00
50.00
60.00
70.00
80.00
90.00
100.00
110.00
120.00
130.00
140.00
150.00
160.00
170.00
180.00

Figure 20

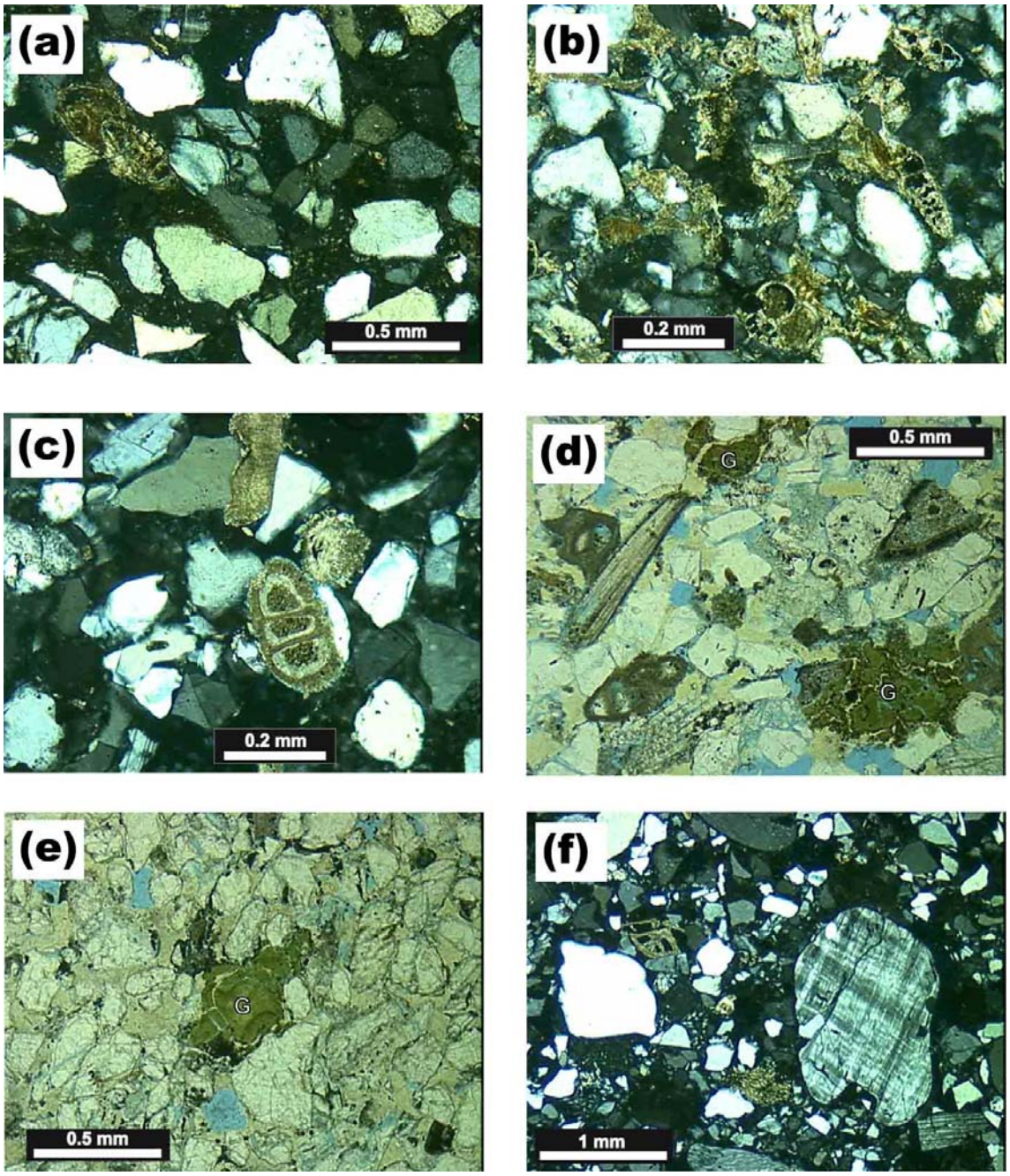

Figure 21

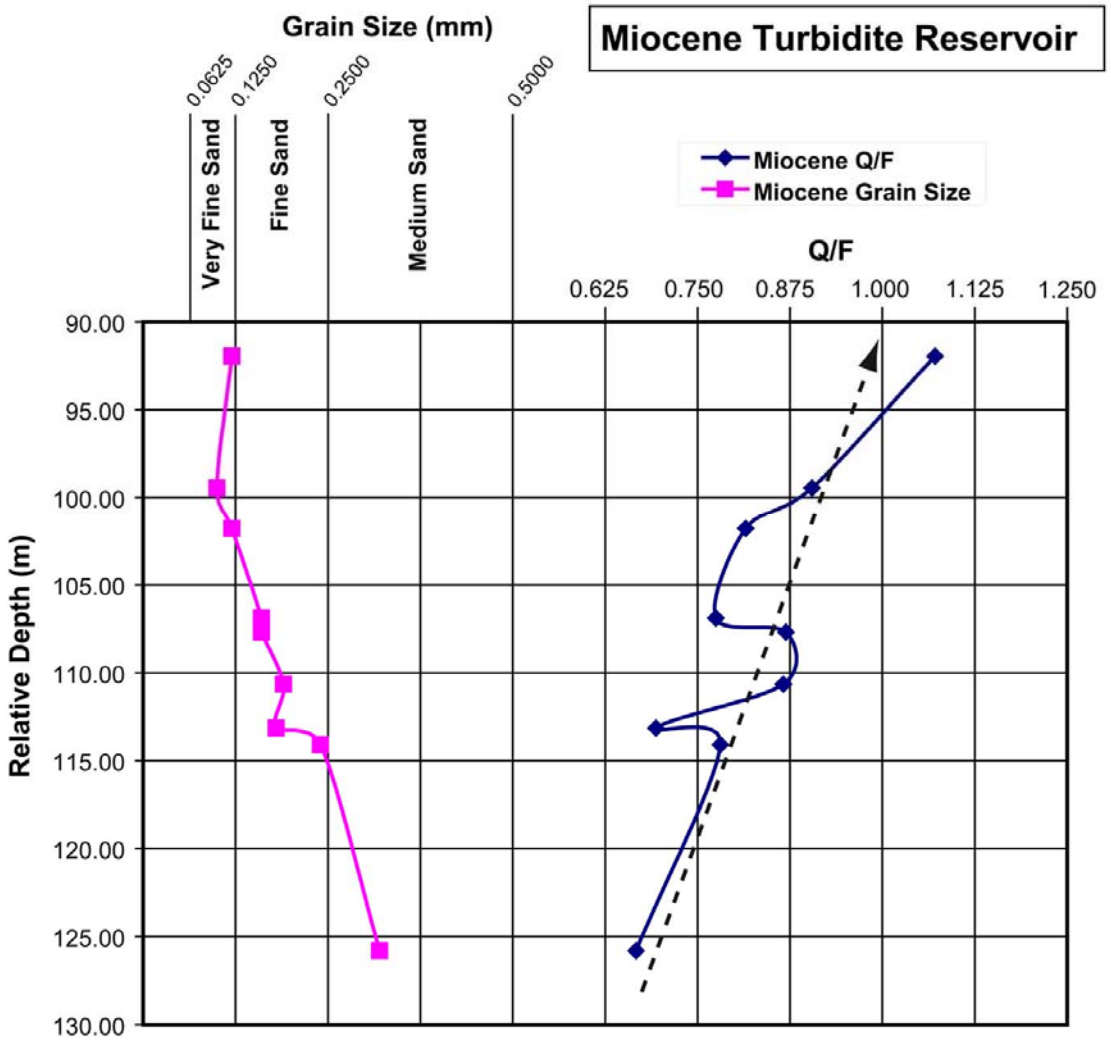
Miocene Turbidite Reservoir
Grain Size (mm)
0.0625
0.1250
0.2500
0.5000
Very Fine Sand
Fine Sand
Medium Sand
Miocene Q/F
Miocene Grain Size
Q/F
0.625
0.750
0.875
1.000
1.125
1.250
Relative Depth (m)
90.00
95.00
100.00
105.00
110.00
115.00
120.00
125.00
130.00

Figure 22

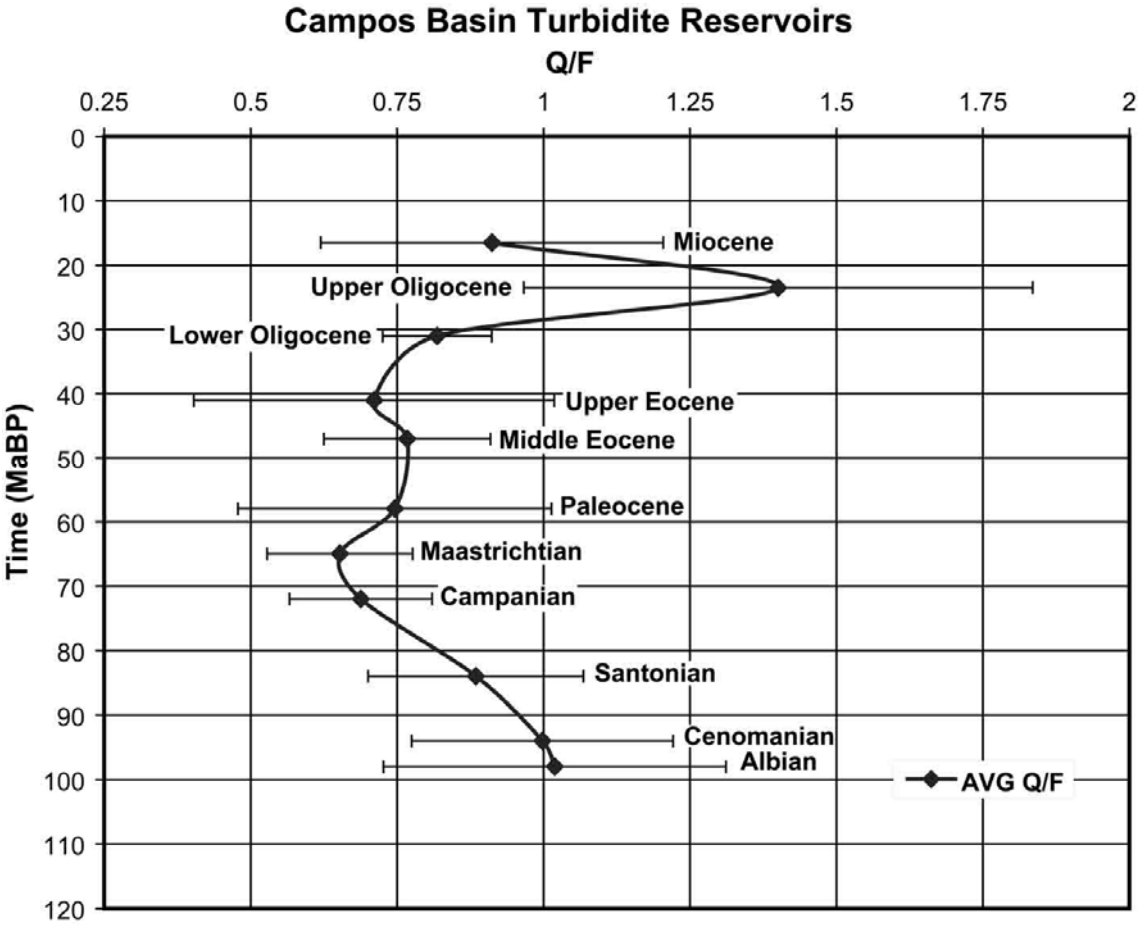
Campos Basin Turbidite Reservoirs
Q/F
0.25
0.5
0.75
1
1.25
1.5
1.75
2
Time (MaBP)
0
10
20
30
40
50
60
70
80
90
100
110
120
Miocene
Upper Oligocene
Lower Oligocene
Upper Eocene
Middle Eocene
Paleocene
Maastrichtian
Campanian
Santonian
Cenomanian
Albian
AVG Q/F

Figure 23

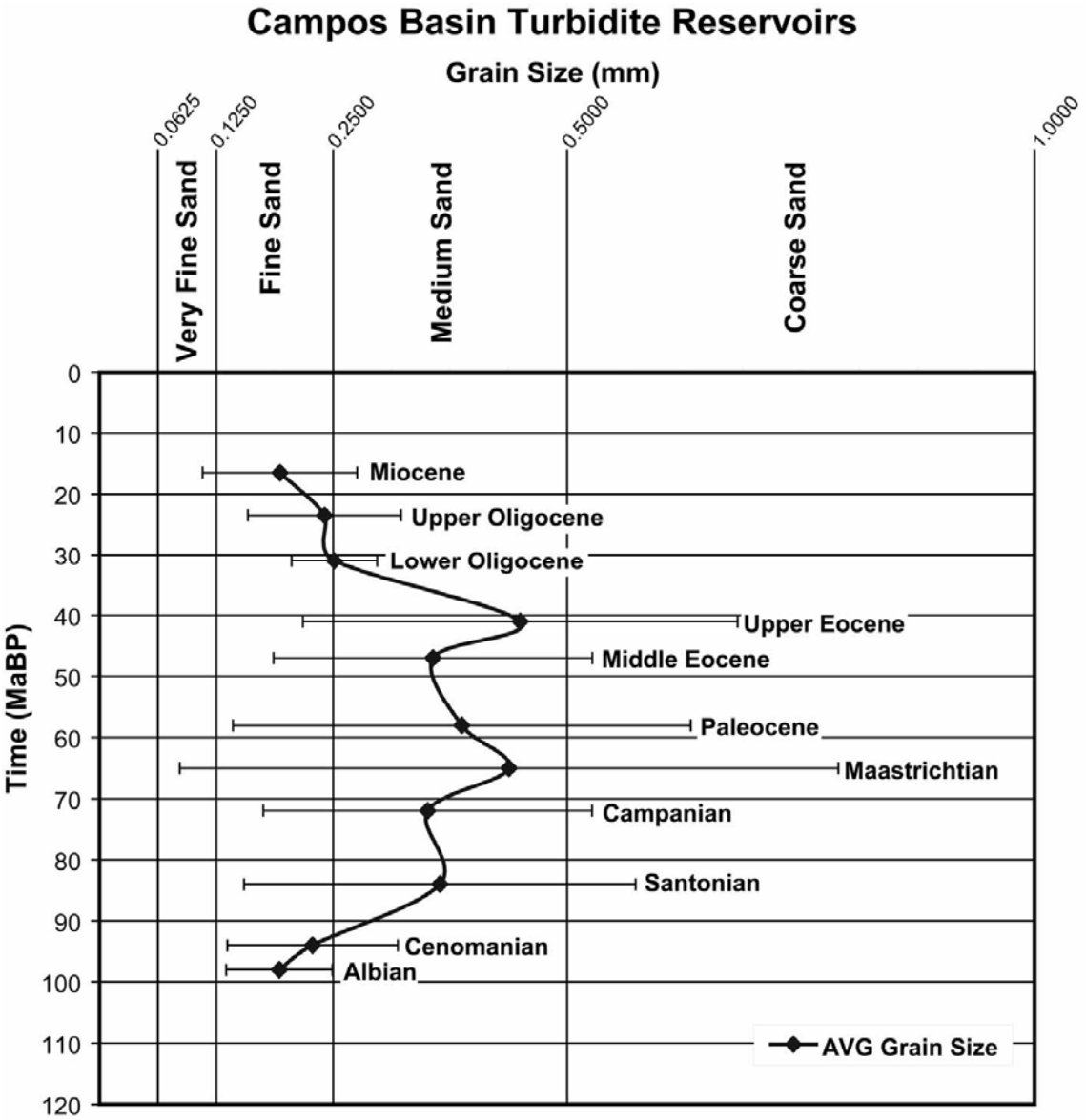
Campos Basin Turbidite Reservoirs
Grain Size (mm)
0.0625
0.1250
0.2500
0.5000
1.0000
Very Fine Sand
Fine Sand
Medium Sand
Coarse Sand
Time (MaBP)
0
10
20
30
40
50
60
70
80
90
100
110
120
Miocene
Upper Oligocene
Lower Oligocene
Upper Eocene
Middle Eocene
Paleocene
Maastrichtian
Campanian
Santonian
Cenomanian
Albian
AVG Grain Size

Figure 24

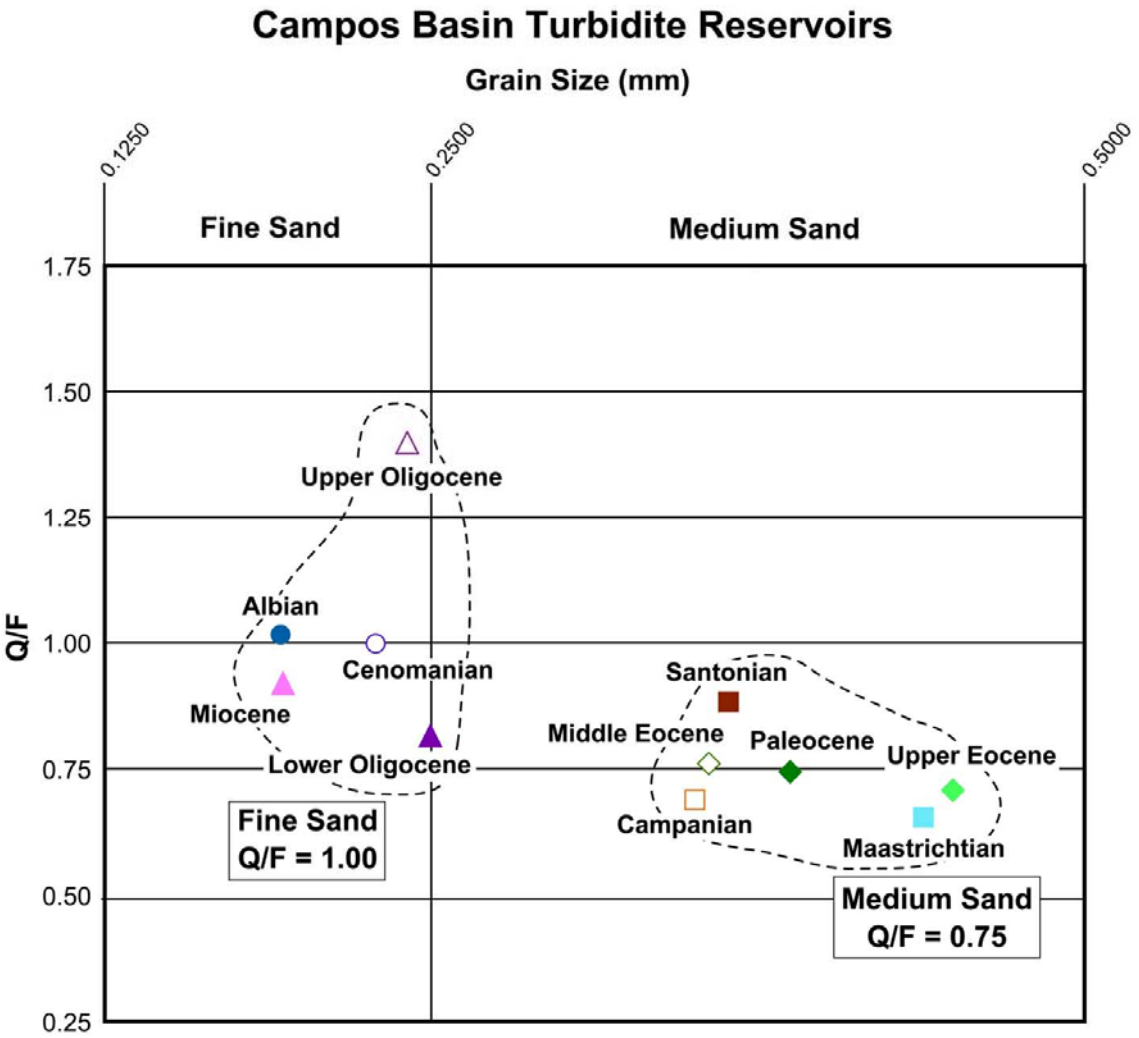
Campos Basin Turbidite Reservoirs
Grain Size (mm)
0.1250
0.2500
0.5000
Fine Sand
Medium Sand
Q/F
1.75
1.50
1.25
1.00
0.75
0.50
0.25
Upper Oligocene
Albian
Cenomanian
Miocene
Lower Oligocene
Fine Sand
Q/F = 1.00
Santonian
Middle Eocene
Paleocene
Upper Eocene
Campanian
Maastrichtian
Medium Sand
Q/F = 0.75

Figure 25

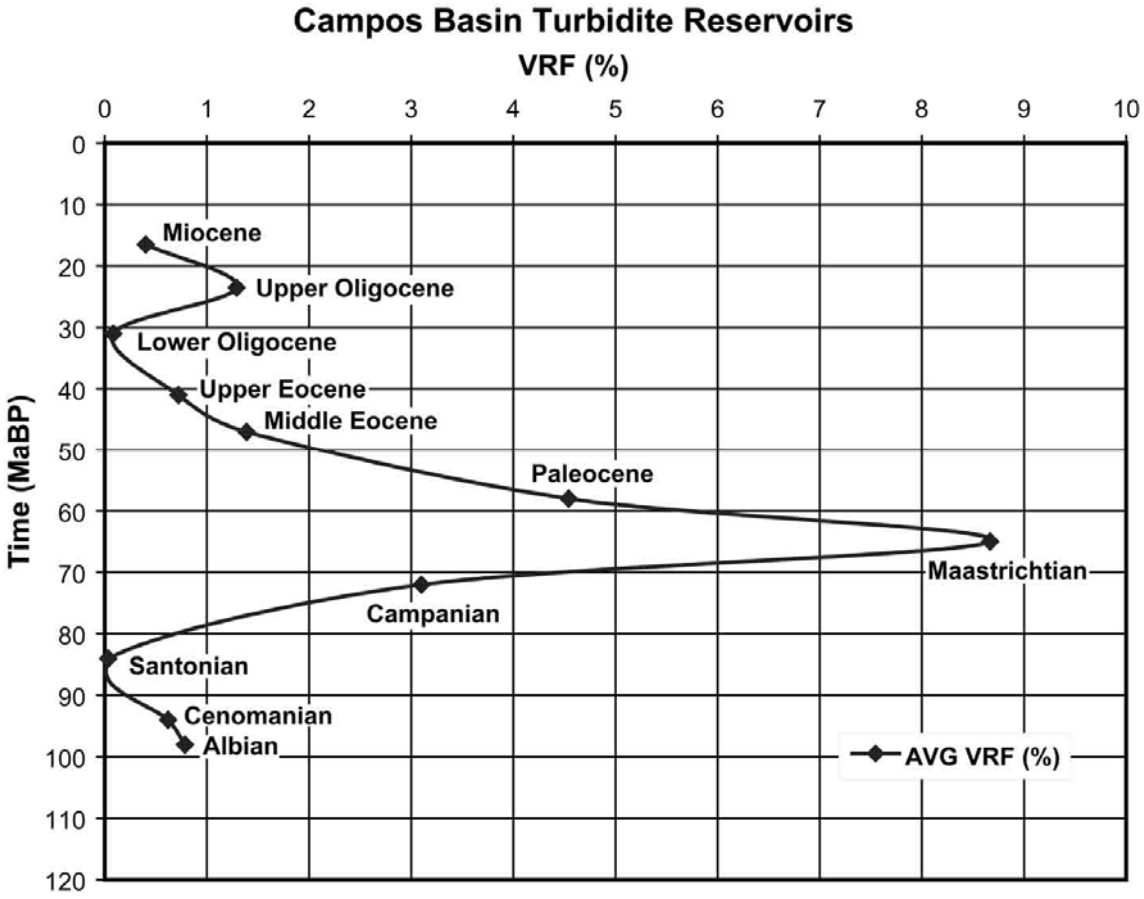
Campos Basin Turbidite Reservoirs
VRF (%)
0
1
2
3
4
5
6
7
8
9
10
Time (MaBP)
0
10
20
30
40
50
60
70
80
90
100
110
120
Miocene
Upper Oligocene
Lower Oligocene
Upper Eocene
Middle Eocene
Paleocene
Maastrichtian
Campanian
Santonian
Cenomanian
Albian
AVG VRF (%)

Figure 26

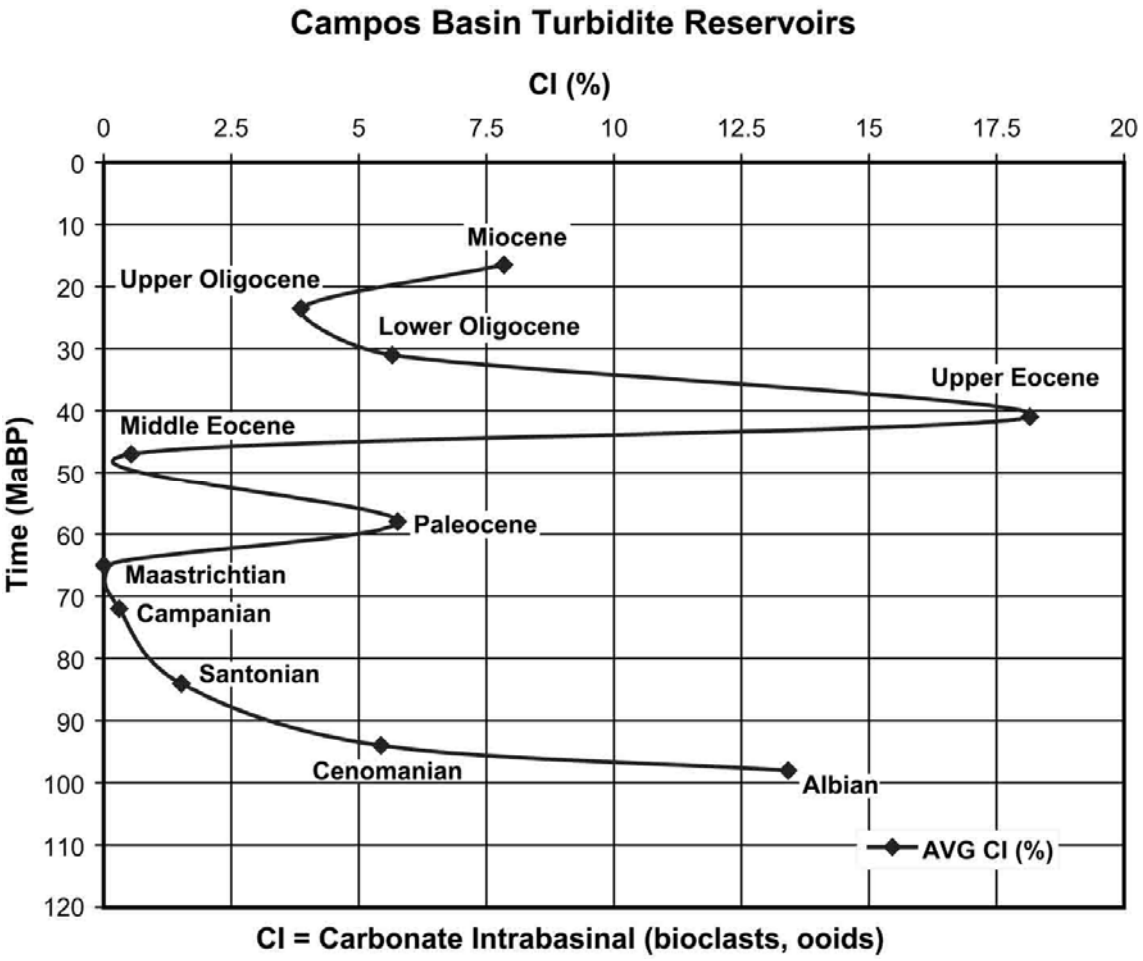
Campos Basin Turbidite Reservoirs
CI (%)
0
2.5
5
7.5
10
12.5
15
17.5
20
Time (MaBP)
0
10
20
30
40
50
60
70
80
90
100
110
120
Miocene
Upper Oligocene
Lower Oligocene
Upper Eocene
Middle Eocene
Paleocene
Maastrichtian
Campanian
Santonian
Cenomanian
Albian
AVG CI (%)
CI = Carbonate Intrabasinal (bioclasts, ooids)

Figure 27

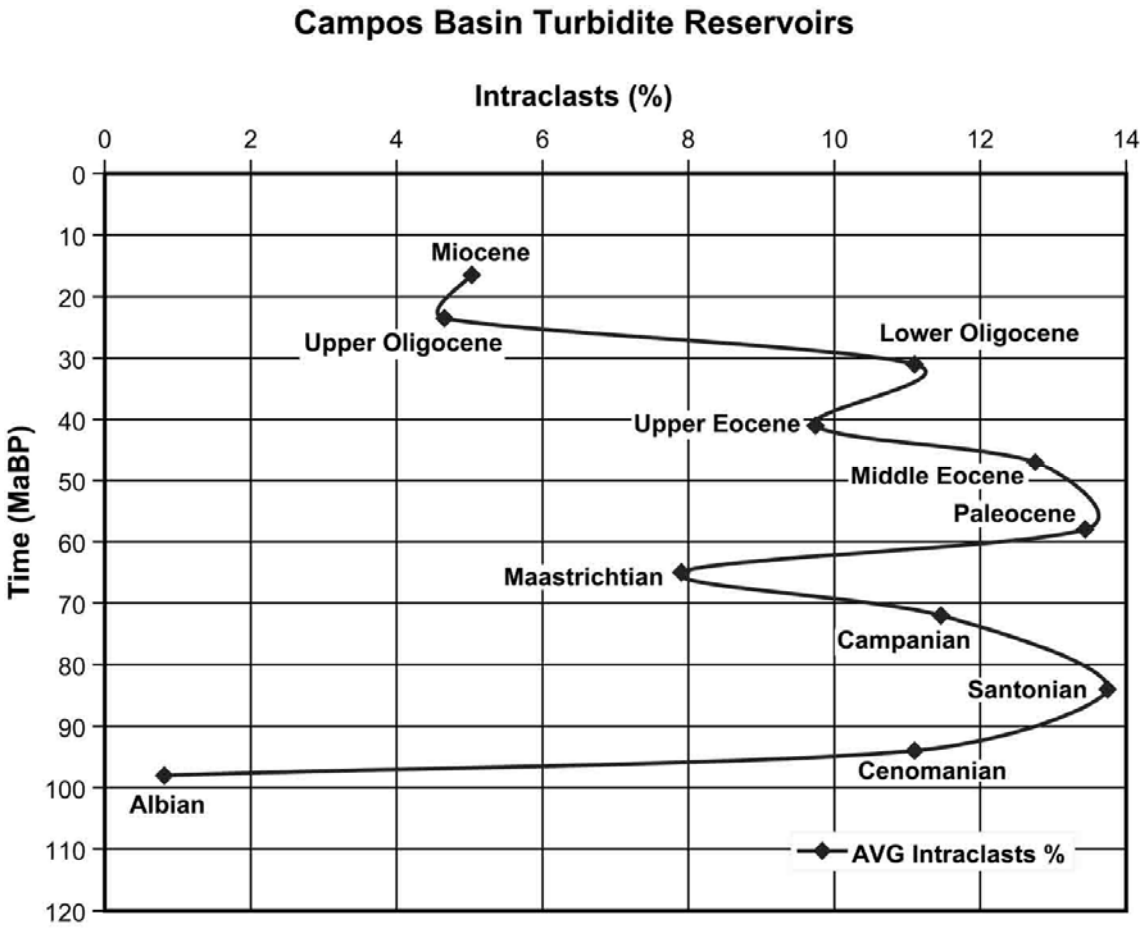
Campos Basin Turbidite Reservoirs
Intraclasts (%)
0
2
4
6
8
10
12
14
Time (MaBP)
0
10
20
30
40
50
60
70
80
90
100
110
120
Miocene
Upper Oligocene
Lower Oligocene
Upper Eocene
Middle Eocene
Paleocene
Maastrichtian
Campanian
Santonian
Cenomanian
Albian
AVG Intraclasts %

Figure 28

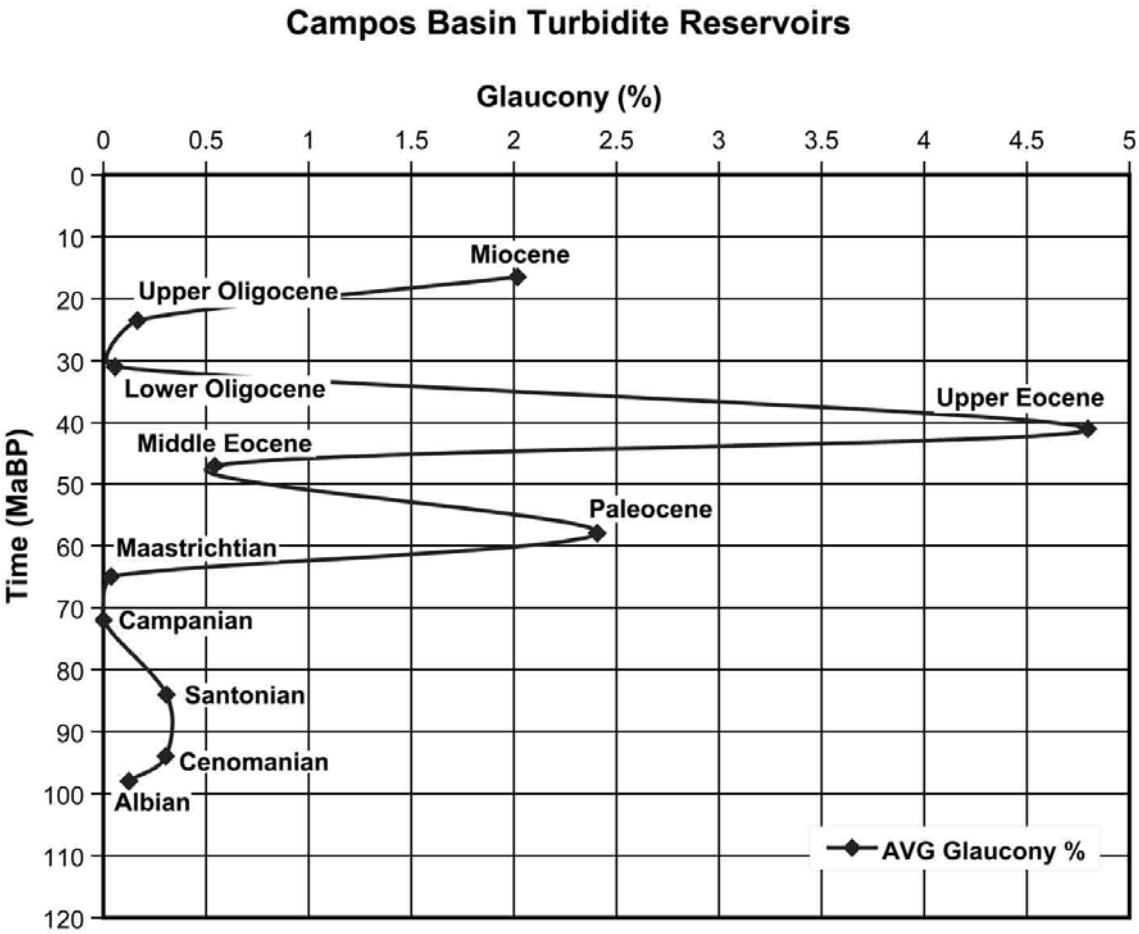
Campos Basin Turbidite Reservoirs
Glaucony (%)
0
0.5
1
1.5
2
2.5
3
3.5
4
4.5
5
Time (MaBP)
0
10
20
30
40
50
60
70
80
90
100
110
120
Miocene
Upper Oligocene
Lower Oligocene
Upper Eocene
Middle Eocene
Paleocene
Maastrichtian
Campanian
Santonian
Cenomanian
Albian
AVG Glaucony %

Figure 29

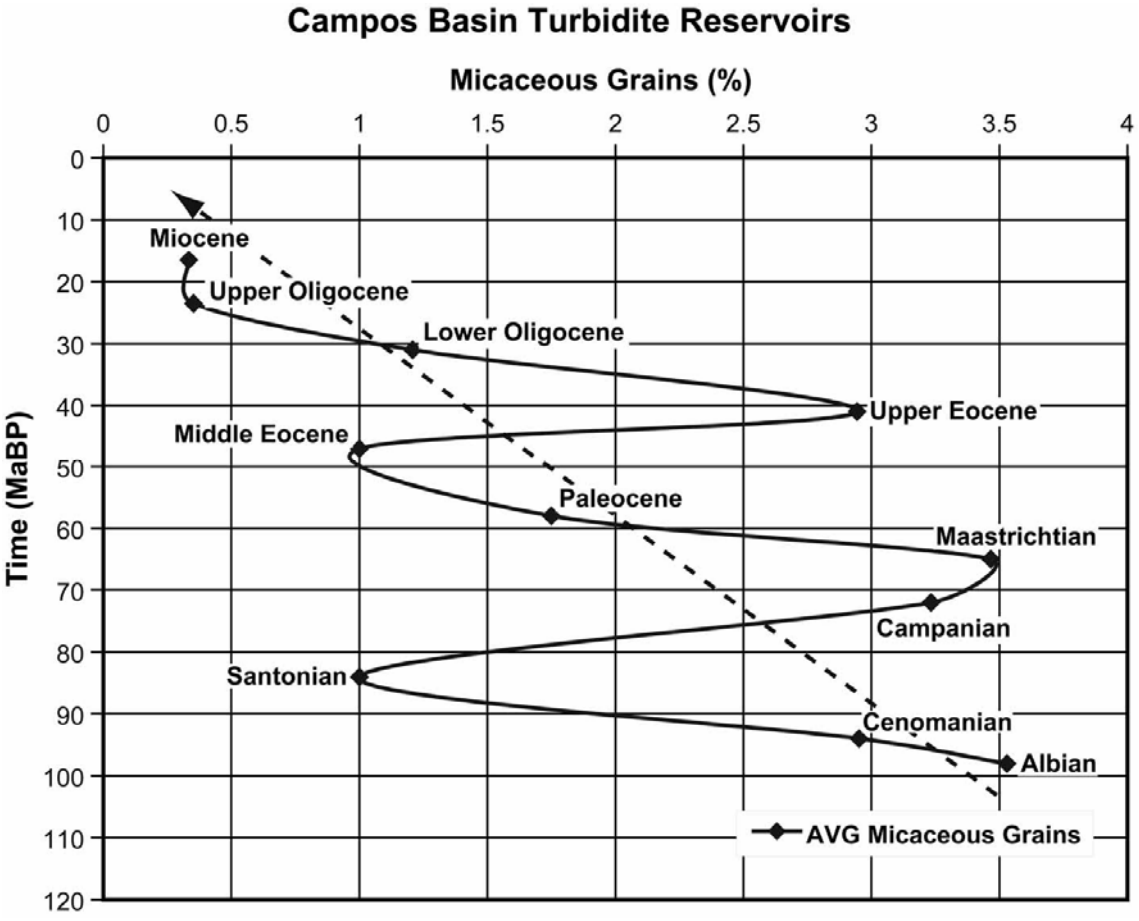

Figure 30

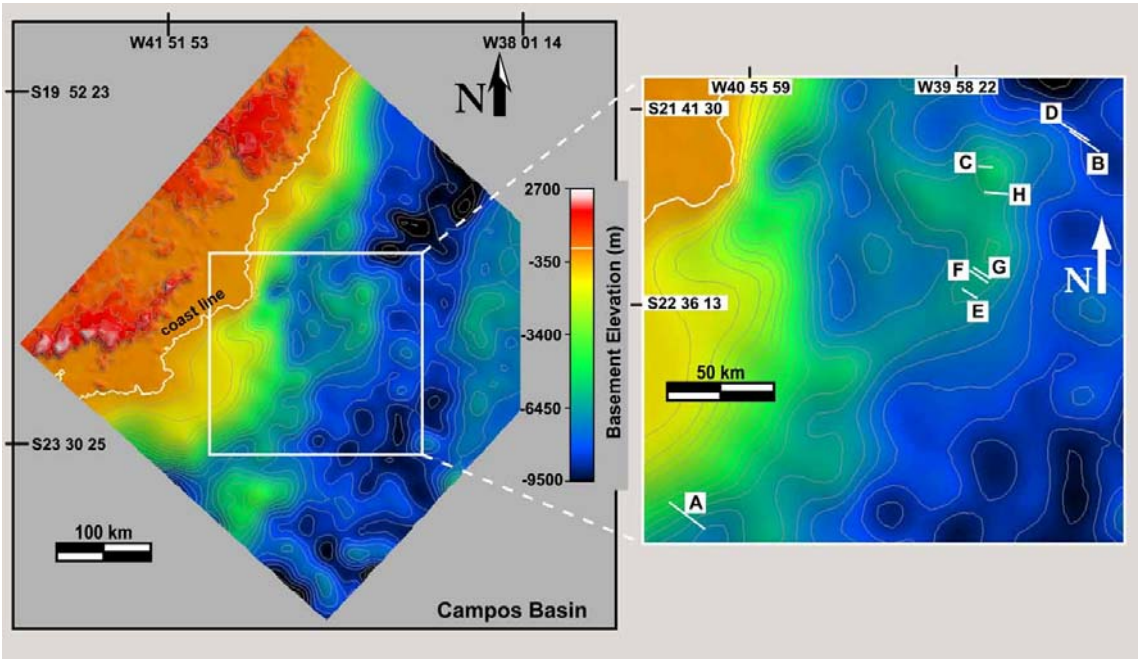

Figure 31

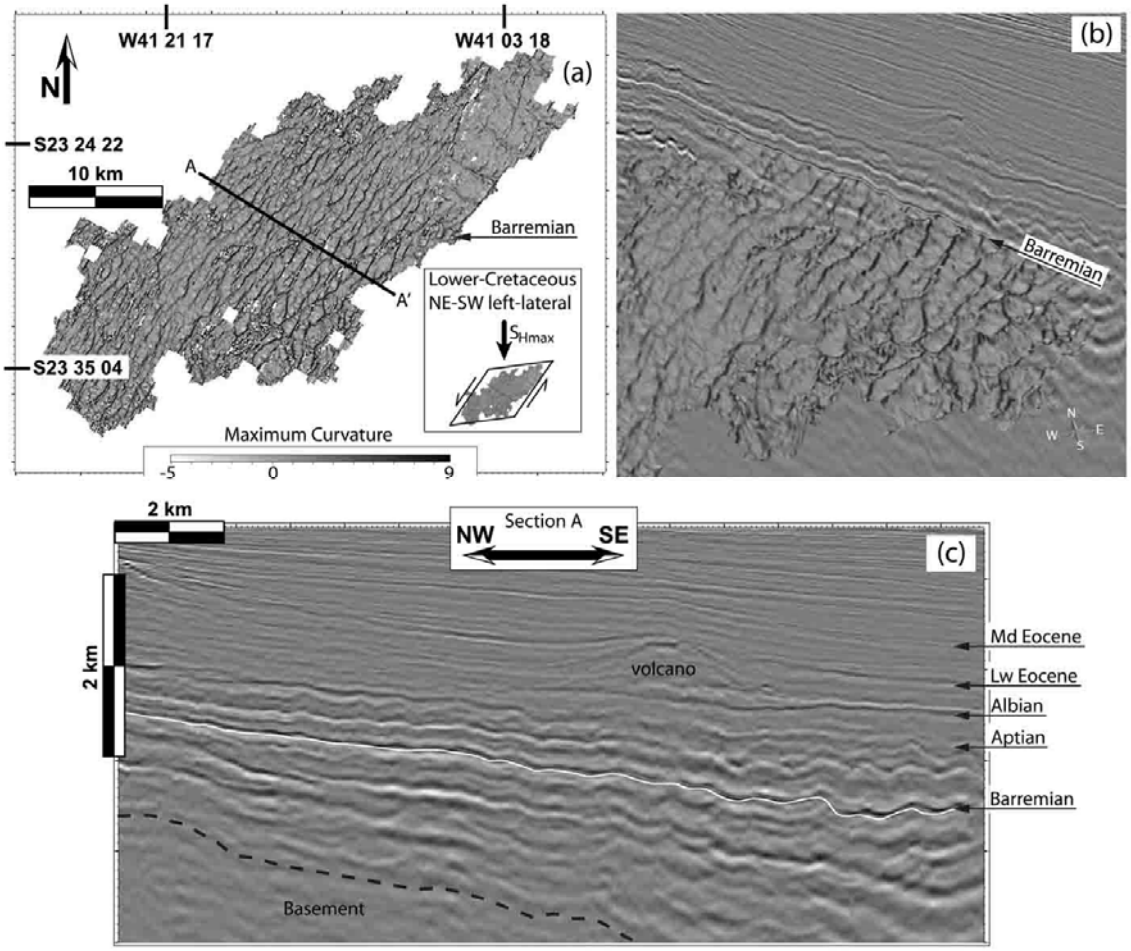
W41 21 17
W41 03 18
(a)
N
S23 24 22
10 km
A
A'
Barremian
Lower-Cretaceous
NE-SW left-lateral
S_{Hmax}
S23 35 04
Maximum Curvature
-5
0
9
(b)
Barremian
N
W
E
S
2 km
NW
Section A
SE
(c)
2 km
volcano
Md Eocene
Lw Eocene
Albian
Aptian
Barremian
Basement

Figure 32

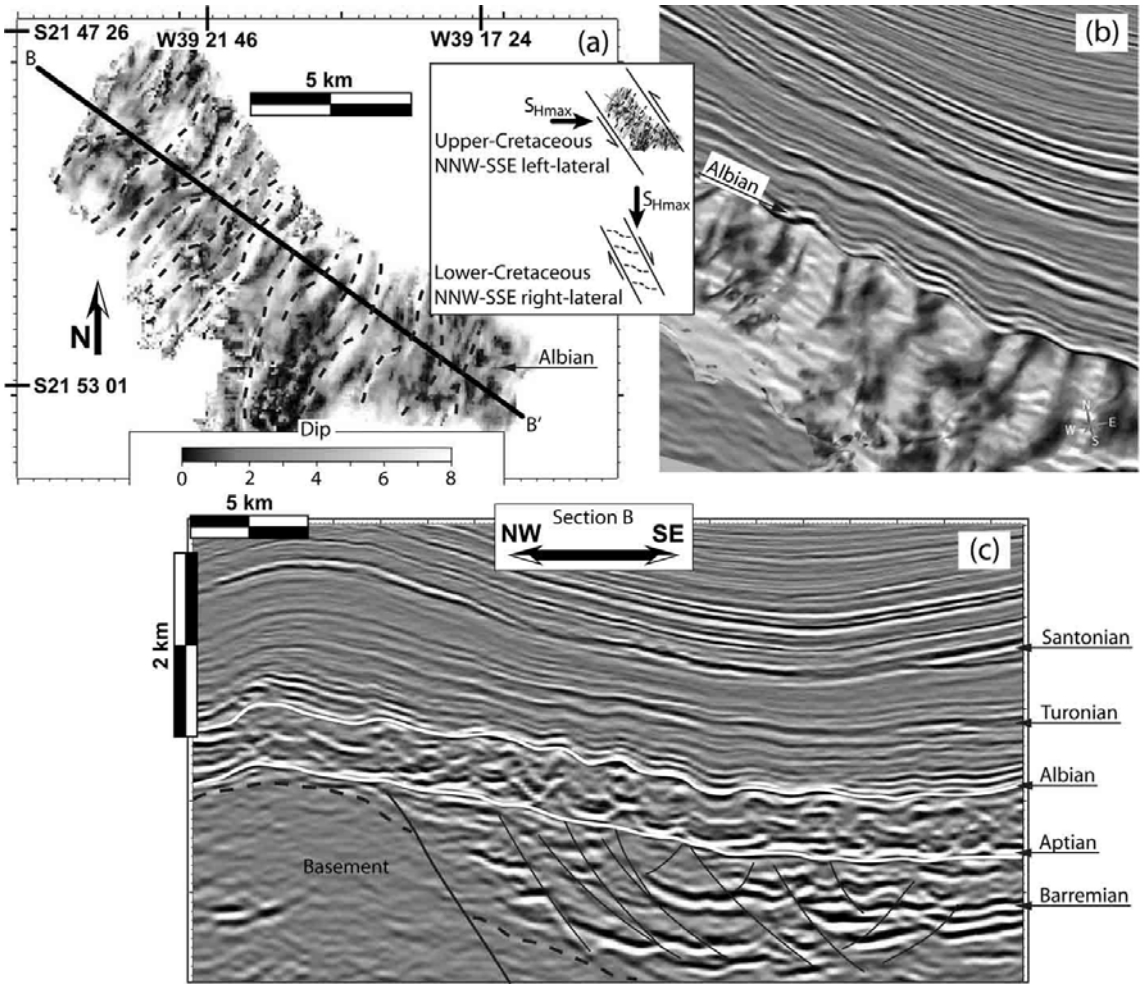
S21 47 26
W39 21 46
W39 17 24
(a)
B
5 km
N
S21 53 01
B'
Albian
Dip
0 2 4 6 8
SHmax
Upper-Cretaceous
NNW-SSE left-lateral
SHmax
Lower-Cretaceous
NNW-SSE right-lateral
(b)
Albian
5 km
Section B
NW
SE
(c)
2 km
Santonian
Turonian
Albian
Aptian
Barremian
Basement

Figure 33

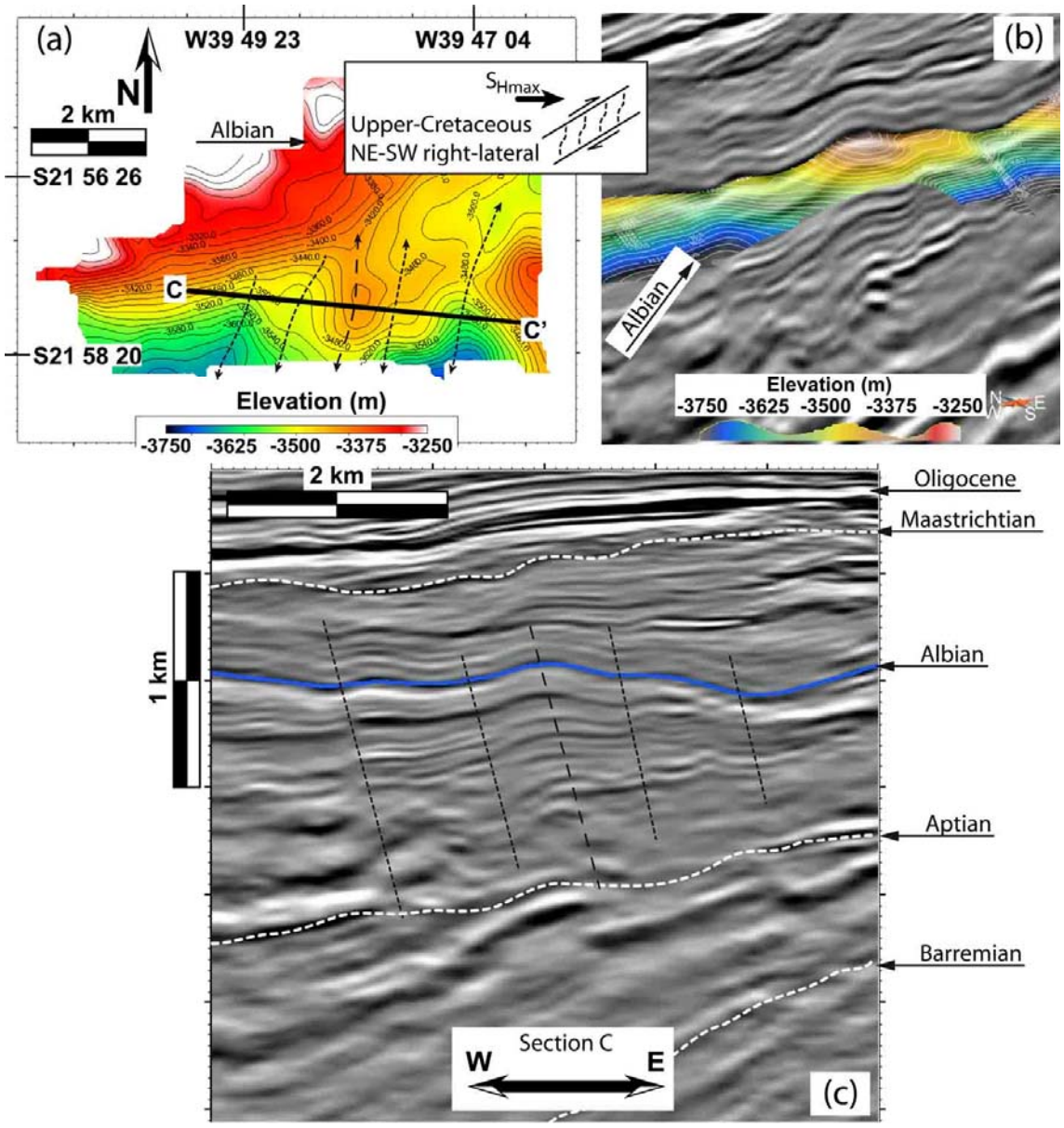
(a)
W39 49 23
W39 47 04
N
2 km
S21 56 26
S21 58 20
Albian
S_{Hmax}
Upper-Cretaceous
NE-SW right-lateral
C
C'
Elevation (m)
-3750 -3625 -3500 -3375 -3250
(b)
Albian
Elevation (m)
-3750 -3625 -3500 -3375 -3250
2 km
1 km
Oligocene
Maastrichtian
Albian
Aptian
Barremian
Section C
W
E
(c)

Figure 34

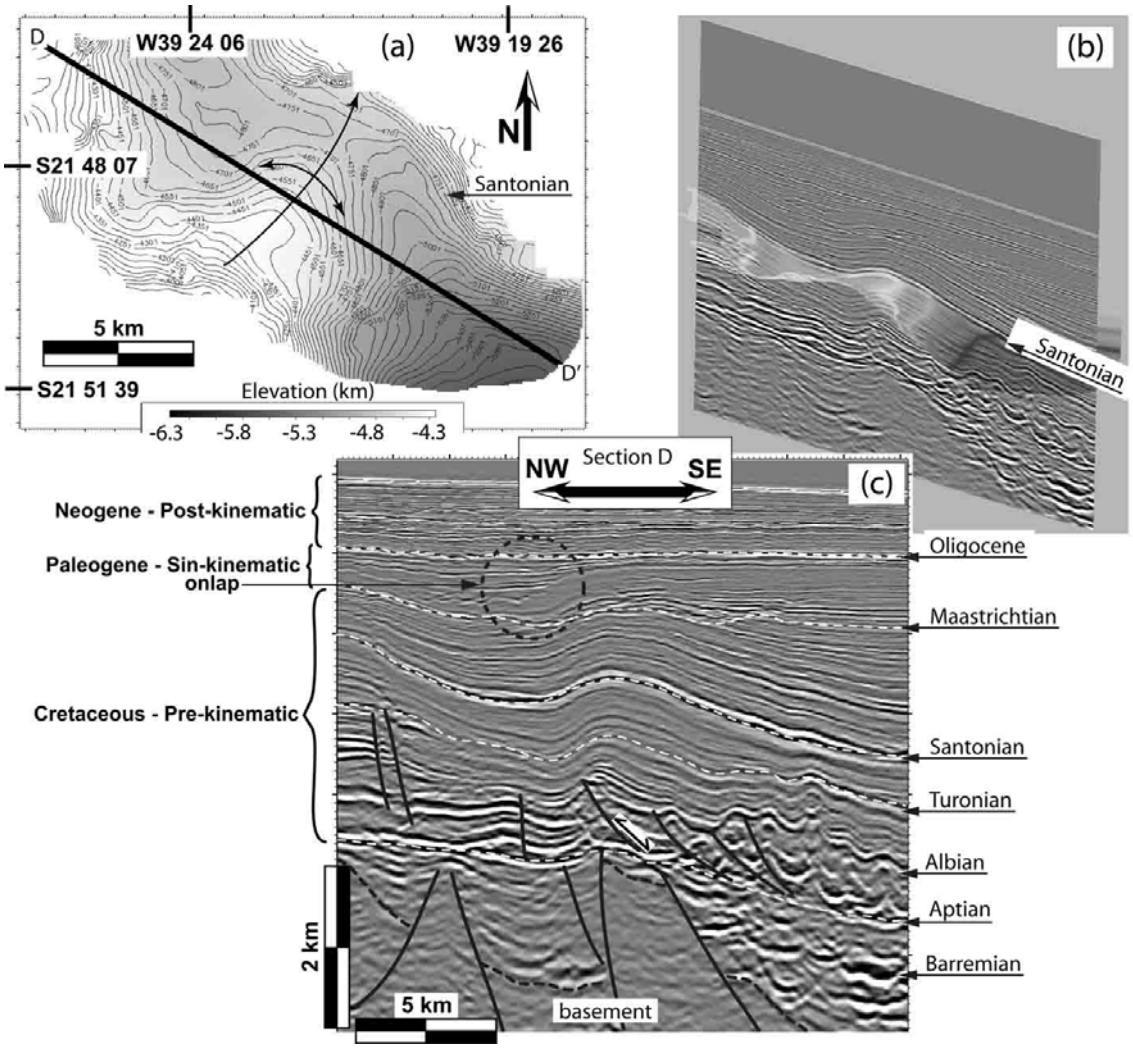
D
W39 24 06
(a)
W39 19 26
N
S21 48 07
Santonian
5 km
S21 51 39
D'
Elevation (km)
-6.3
-5.8
-5.3
-4.8
-4.3
(b)
Santonian
NW
Section D
SE
(c)
Neogene - Post-kinematic
Paleogene - Sin-kinematic onlap
Cretaceous - Pre-kinematic
Oligocene
Maastrichtian
Santonian
Turonian
Albian
Aptian
Barremian
2 km
5 km
basement

Figure 35

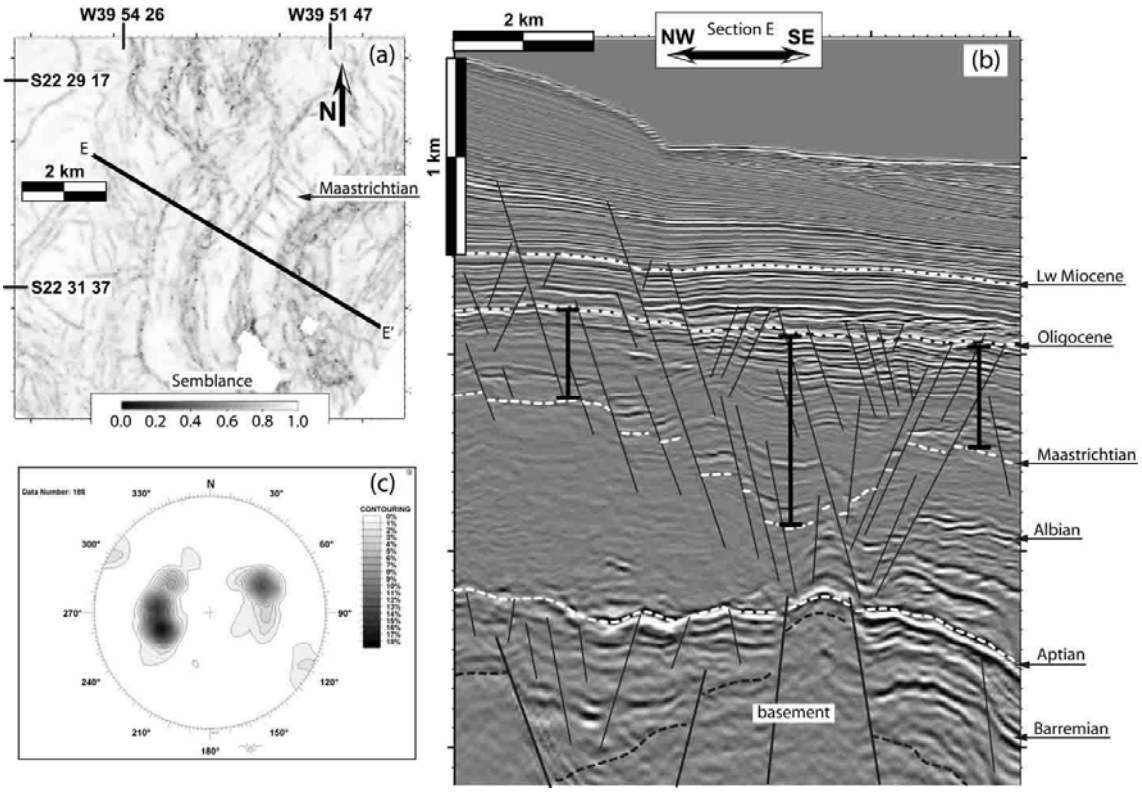

Figure 36

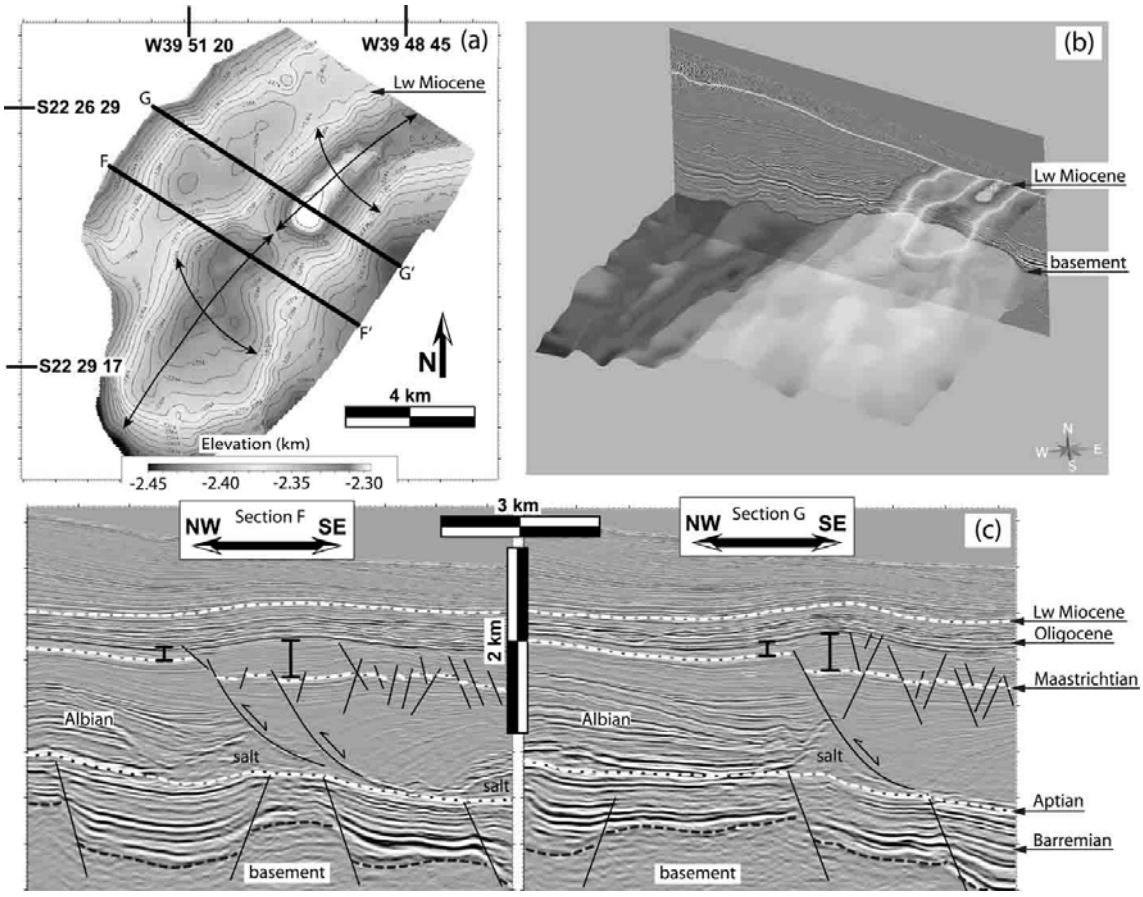

Figure 37

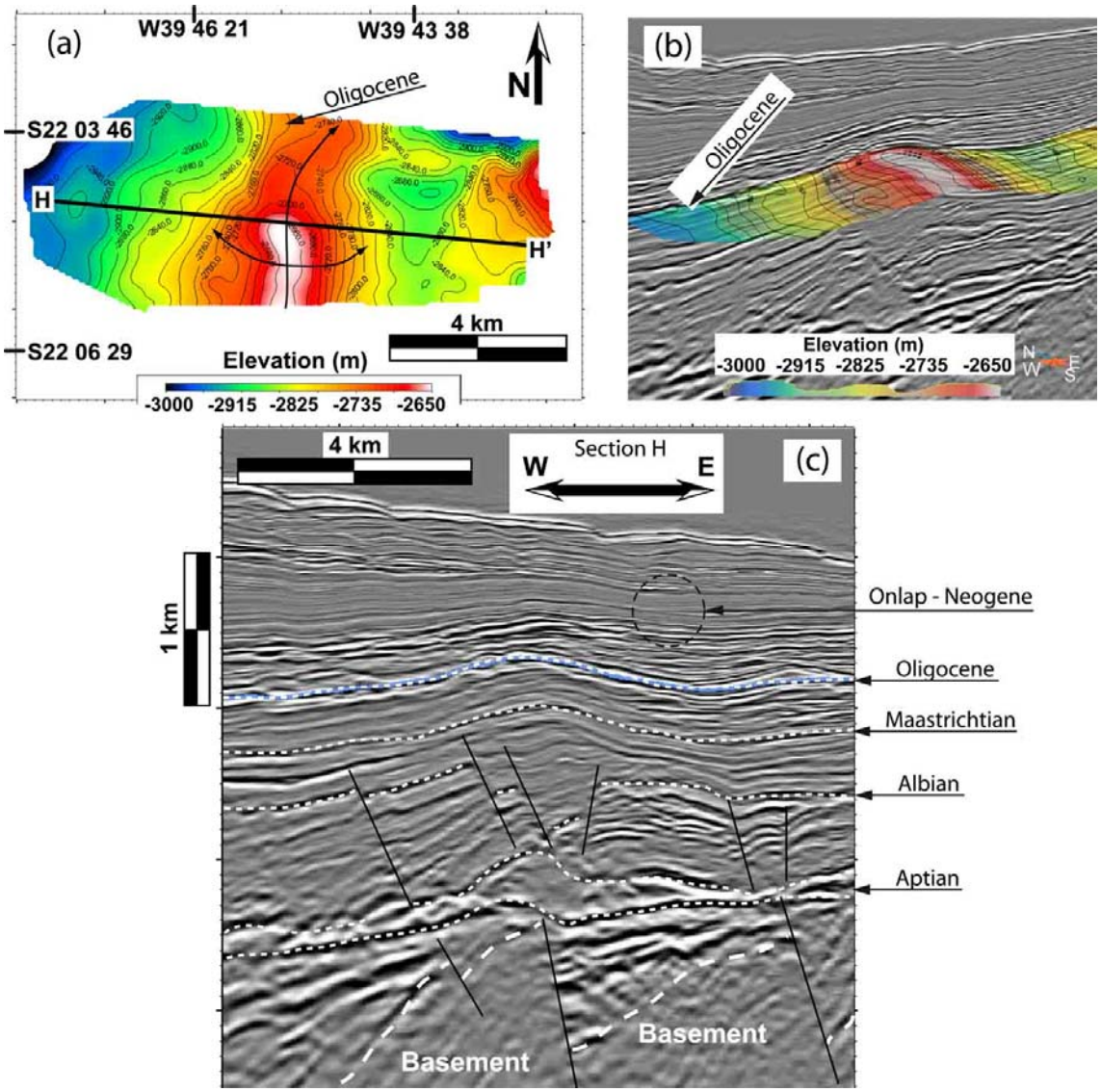
(a)
W39 46 21
W39 43 38
N
Oligocene
S22 03 46
H
H'
4 km
S22 06 29
Elevation (m)
-3000 -2915 -2825 -2735 -2650
(b)
Oligocene
Elevation (m)
-3000 -2915 -2825 -2735 -2650
4 km
Section H
W
E
(c)
1 km
Onlap - Neogene
Oligocene
Maastrichtian
Albian
Aptian
Basement
Basement

Figure 38

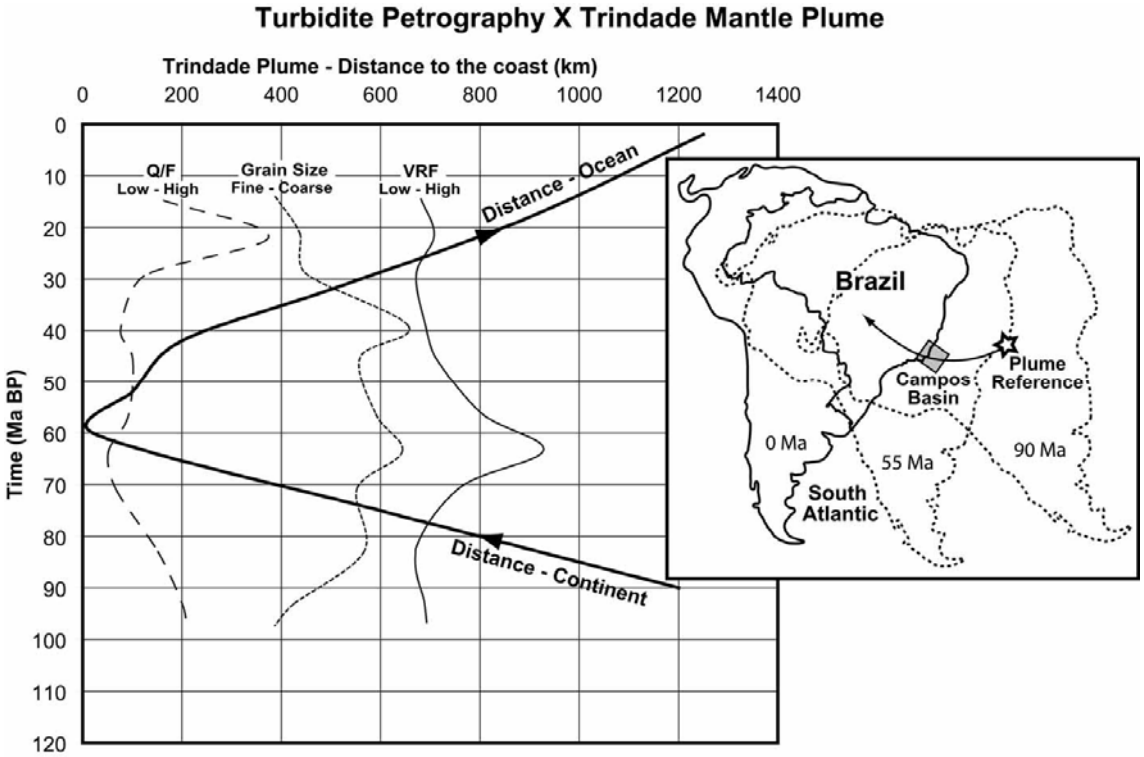

Figure 39

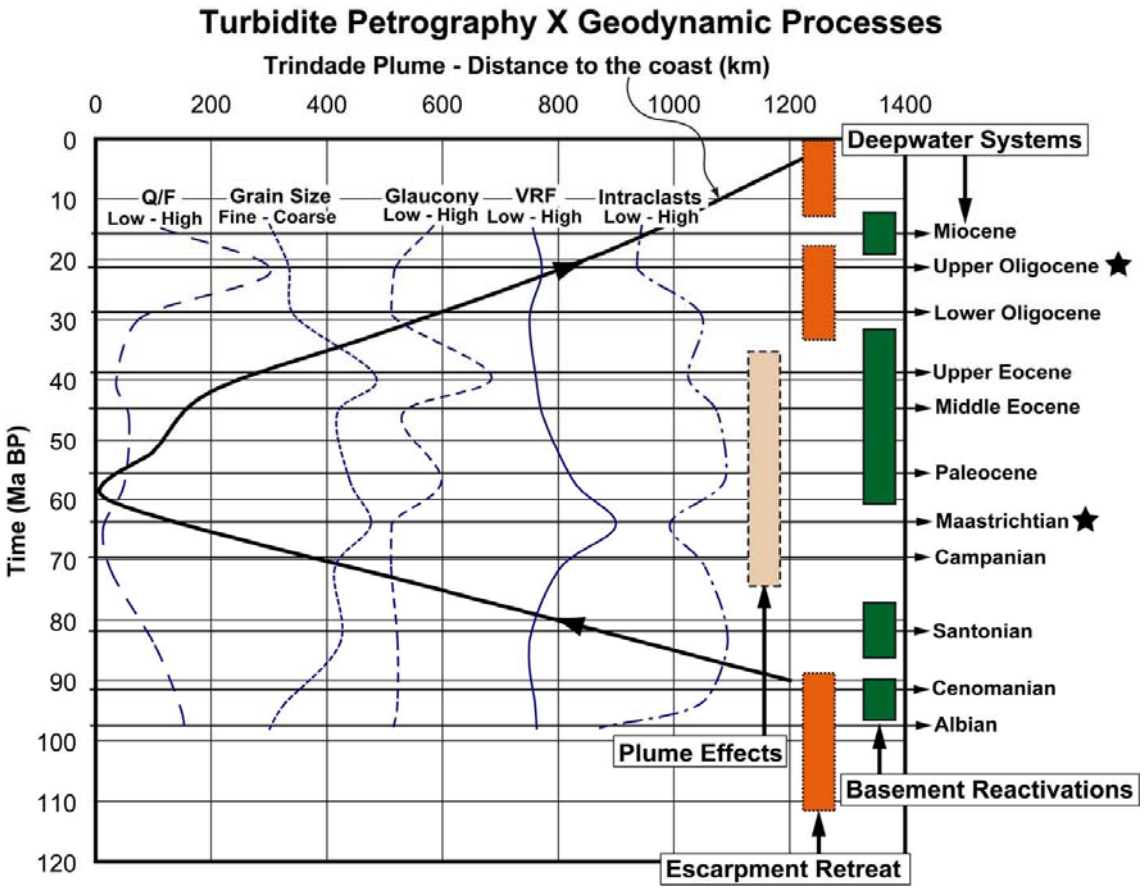

Figure 40

Anexos

Anexo A

Comprovantes de Recebimento dos Artigos Submetidos

Anexo B

CD com Planilhas de Descrição Petrográfica

Livros Grátis

(http://www.livrosgratis.com.br)

Milhares de Livros para Download:

Baixar livros de Literatura
Baixar livros de Literatura de Cordel
Baixar livros de Literatura Infantil
Baixar livros de Matemática
Baixar livros de Medicina
Baixar livros de Medicina Veterinária
Baixar livros de Meio Ambiente
Baixar livros de Meteorologia
Baixar Monografias e TCC
Baixar livros Multidisciplinar
Baixar livros de Música
Baixar livros de Psicologia
Baixar livros de Química
Baixar livros de Saúde Coletiva
Baixar livros de Serviço Social
Baixar livros de Sociologia
Baixar livros de Teologia
Baixar livros de Trabalho
Baixar livros de Turismo